T.R.
GEBZE TECHNICAL UNIVERSITY
GRADUATE SCHOOL OF NATURAL AND APPLIED SCIENCES

DEVELOPMENT OF STRETCHABLE PZT-BASED ELASTIC COMPOSITE STRUCTURES AND THEIR ELECTROMECHANICAL CHARACTERIZATION

EMRE CANANOĞLU

A THESIS SUBMITTED FOR THE DEGREE OF
MASTER OF SCIENCE
DEPARTMENT OF MATERIAL SCIENCE AND ENGINEERING

GEBZE
2023

T.R.
GEBZE TECHNICAL UNIVERSITY
GRADUATE SCHOOL OF NATURAL AND APPLIED SCIENCES

DEVELOPMENT OF STRETCHABLE PZT-BASED ELASTIC COMPOSITE STRUCTURES AND THEIR ELECTROMECHANICAL CHARACTERIZATION

EMRE CANANOĞLU

A THESIS SUBMITTED FOR THE DEGREE OF
MASTER OF SCIENCE
DEPARTMENT OF MATERIAL SCIENCE AND ENGINEERING

THESIS SUPERVISOR
PROF. DR. EBRU MENŞUR ALKOY

GEBZE
2023

T.C.

GEBZE TEKNİK ÜNİVERSİTESİ

FEN BİLİMLERİ ENSTİTÜSÜ

GERİLEBİLİR PZT TABANLI ELASTİK KOMPOZİT YAPILARIN GELİŞTİRİLMESİ VE ELEKTROMEKANİK KARAKTERİZASYONU

EMRE CANANOĞLU

YÜKSEK LİSANS TEZİ

MALZEME BİLİMİ VE MÜHENDİSLİĞİ ANABİLİM DALI

TEZ DANIŞMANI

PROF. DR. EBRU MENŞUR ALKOY

GEBZE

2023

GEBZE TEKNİK ÜNİVERSİTESİ	**YÜKSEK LİSANS JÜRİ ONAY FORMU**

GTÜ Fen Bilimleri Enstitüsü Yönetim Kurulu'nun 01/12/2022 tarih ve 2022/63 sayılı kararıyla oluşturulan jüri tarafından 23/12/2022 tarihinde tez savunma sınavı yapılan Emre CANANOĞLU'nun tez çalışması Malzeme Bilimi ve Mühendisliği Anabilim Dalında YÜKSEK LİSANS tezi olarak kabul edilmiştir.

JÜRİ

ÜYE
(TEZ DANIŞMANI) : Prof. Dr. Ebru MENŞUR-ALKOY

ÜYE : Doç. Dr. Neslihan TAMSÜ SELLİ

ÜYE : Dr. Öğr. Üyesi Ayşe BERKSOY YAVUZ

ONAY

Gebze Teknik Üniversitesi ………….. Enstitüsü Yönetim Kurulu'nun
……../……../………. tarih ve ………./…….. sayılı kararı.

İMZA/MÜHÜR

SUMMARY

In this thesis, commercial lead zirconate titanate (PZT5A) and 67.5 lead manganese niobate - 32.5 lead titanate (67.5PMN-32.5PT) ceramic powders used with poly-di-methyl siloxane (PDMS) and polyurethane (PU) to fabricate flexible polymer matrix ceramic composite structures. The main idea behind constructing the composites was eliminating weaknesses of the bulk piezo-ceramics such as unavailability to apply on non-flat surfaces like human-body or intricate geometries and instant cracking of the samples. Electromechanical characterization was done on the samples to be a scientific foresight for further futuristic studies i.e., tactile sensors, body implants, ultrasonic devices, etc. Dielectric constant, hysteresis of the samples, d_{33} coefficient and energy harvesting performances were recorded. For the sake of the comparison of electromechanical behaviors of composites and bulk ceramics, PMN-PT ceramic pellets were produced. After this work, a general understanding of piezo-composites is believed to be a mile-stone for studies to come.

Key Words: Lead Zirconate Titanate, PMN-PT, Poly-Di-Methyl Siloxane (PDMS), Polyurethane (PU), Piezocomposite, Tactile Sensor.

ÖZET

Bu tezde, ticari kurşun zirkonat titanat (PZT5A) ve 67.5 kurşun manganez niyobat - 32.5 kurşun titanat (67.5PMN-32.5PT) seramik tozları, poli-di-metil siloksan (PDMS) ve poliüretan (PU) ile birlikte kullanılarak esnek polimer matrisli seramik kompozit yapılar üretildi. Kompozitleri oluşturmanın arkasındaki ana fikir, insan vücudu veya karmaşık geometriler gibi düz olmayan yüzeylere uygulanamama ve numunelerin anında çatlaması gibi bulk piezo-seramiklerin zayıflıklarını ortadan kaldırmaktı. Dokunsal sensörler, vücut implantları, ultrasonik cihazlar gibi fütüristik çalışmalar için bilimsel bir öngörü olması amacıyla numunelere elektromekanik karakterizasyon yapıldı. Dielektrik sabiti, histerezis ile d_{33} katsayısı ve enerji hasadı performansları kaydedildi. Kompozitlerle elektromekanik davranışlarının karşılaştırılması adına bulk PMN-PT seramik peletler üretildi. Bu çalışmadan sonra, piezo-kompozitler için genel bir anlayışın, gelecek çalışmalar için bir kilometre taşı olacağına inanılmaktadır.

Anahtar Kelimeler: **Kurşun Zirkonat Titanat (PZT5A), PMN-PT, Poli-Di-Metil Siloksan (PDMS), Poliüretan (PU), Piezo-kompozit, Dokunsal Sensör.**

ACKNOWLEDGEMENTS

First of all, I would like to express my gratitude to those who had been a part of my thesis. I exclusively thank my dear supervisor Prof. Dr. Ebru Menşur-ALKOY who has always been with me until the end of my master's program.

I want to send my special thanks to the Air Force Office of Scientific Research (AFOSR) European Office and Prof. Dr. Ali Sayır for their funding.

Also, Dr. Ayşe Berksoy-Yavuz and Prof. Dr. Sedat Alkoy will have a private place in my heart for they never turned me down for my hundreds of questions and assisted my studies.

I especially wish to thank my family and my forever best friends for they never left me and helped when I needed it most. Along this journey, laboratories and our office has been the place of the best moments that we shared.

Before concluding, I send my regards to Adem Şen and Ahmet Nazım for their share in my thesis.

Best wishes...

TABLE OF CONTENTS

LIST OF ABBREVIATIONS AND ACRONYMS

Abbreviations and Acronyms		**Explanations**
°	:	Celcius Degree
%	:	Percent
cm	:	Centimeter
cm^2	:	Centimeter Square
C	:	Coulomb
C	:	Celcius Degree
E	:	Electric Field
E_c		Coercive Field
ε_r	:	Dielectric Constant
ECE	:	Electrocaloric Effect
E_c	:	Coersive Field
F	:	Farad
kHz	:	Kilo Hertz
LCR	:	Inductance Capacitance Resistance
m	:	Meter
MHz	:	Mega Hertz
MPa	:	Mega Pascal
MPB	:	Moprhotrophic Phase Boundary
nm	:	Nanometer
N	:	Newton
PMN-PT	:	Lead Manganese Niobate-Lead Titanate
PZT5A	:	Lead Zirconate Titanate
PU	:	Polyurethane
PDMS	:	Poly Di-Methyl Siloxane
P_{max}	:	Maximum Polarization
P_r	:	Remnant Polarization
P_s	:	Saturation Polarization

SEM	:	Scanning Electron Microscope
T	:	Temperature
T_{Curie}	:	Curie Temperature
$\tan\delta$	:	Dielectric Loss
μ	:	Micron
μm	:	Micron Meter
$\mu m/cm^2$	:	Microcoulomb/Centimeter Square
V	:	Volt
XRD	:	X-Ray Diffraction
X	:	Mechanical Stress
x	:	Mechanical Strain

LIST OF FIGURES

LIST OF TABLES

1. INTRODUCTION

1.1. Scope of the Thesis

Piezoelectricity is a phenomenon where electricity and strain are generated as a result of external applied electric field or stress. Piezoelectric materials consist of ceramics and polymers. Ceramics are categorized due to the their content of the chemical compositions. While lead zirconate titanate (PZT), and lead manganese niobate-lead titanate (PMN-PT) are lead-based ceramics, barium zirconate titanate (BZT), barium calcium zirconate titanate (BCZT), potasium sodium niobate(KNN), and barium titanate (BTO) are lead-free ceramics. Considering these, chemical composition, microstructure, fabrication and poling conditions, dielectric properties, etc. are fundamental factors that affect piezoelectric performance of the devices.

Recently, there have been studies on combining polymers and ceramics to generate a new group of materials called piezo composites with different micro geometries such as 0-3, 1-3, 2-2, 3-3, etc. Each geometry has unique behavior as a result of polymer-ceramic interactions. In these ceramics, ceramic-polymer interface, particle size, and the ratio of the contents with respect to each other are important. The ease of fabrication, flexibility, low density, and piezoelectricity has led to the design of sensors, energy harvesters, and much more. In the near future, with the development and potential studies in this field, there will be improvements that contribute to both science and technology.

In the light of the information above, this thesis can be chosen as a guide to gain the fundamentals in an easy way as it requires no pre-information about the topic. The experimental studies were accomplished on bulk ceramics and piezo composites of 67.5PMN-PT. Furthermore, PZT5A powder was utilized in order to compare the electrical properties of piezo composites that consist of different powders. Additionally, PU and PDMS matrix was preferred to observe the effect of the matrix on the properties. At the end of the study, an example of an energy harvester was designed and characterized to obtain proof of its applicability.

2. LITERATURE REVIEW

2.1 Basic Concepts

This introductory chapter basically explains the fundamental theory behind the ferroelectricity, piezoelectricity and dielectricity of materials.

2.1.1. Ferroelectricity

Ferroelectricity is a term that is very much similar to ferromagnetics where ceramics exhibit dipole moments that are spontaneously present in the crystal structure. Dipoles can be exerted and reoriented by the application of an electric field. There are examples that are famous and widely studied. Lead zirconate titanate ($Pb(Zr_xTi_{1-x})O_3$) and barium titanate ($BaTiO_3$) are two major ferroelectric ceramics that are being frequently inspected. In a more detailed observation of the crystal, the $BaTiO_3$ tetragonal phase structure is an example of how the lattice reorients according to the applied electric field as shown in Figure 2.1.

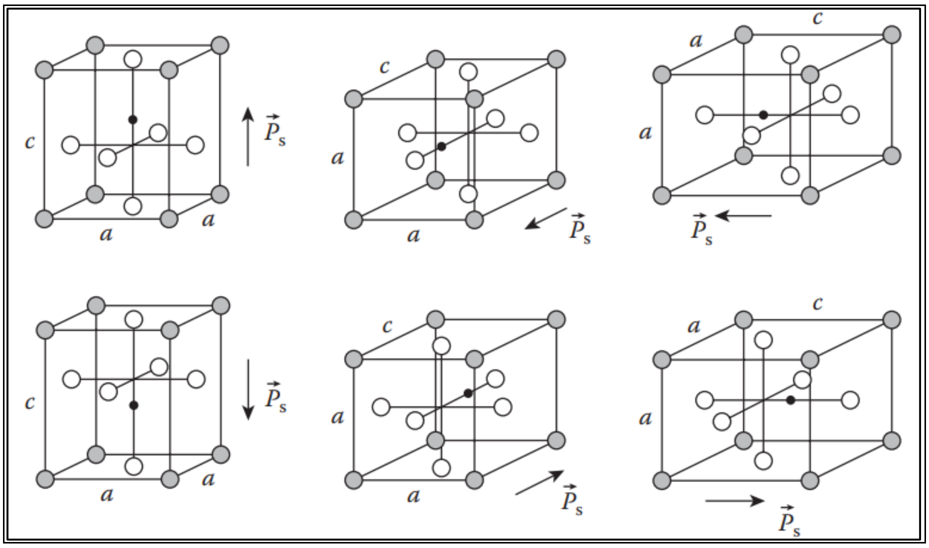

Figure 2.1: Six spontaneous polarization states and three spontaneous strain states in the tetragonal phase of barium titanate ($BaTiO_3$).

The lattice contains O^{2-} ions in the corners with Ba^{2+} ions on the faces and Ti^{4+} ion at the center. The shape and the size of the lattice change following the direction of the electric field. The motion of the Ti^{4+} ion with the applied field causes distortion in the shape of the lattice thus, aligning dipoles that were pre-existing but randomly oriented. The ionic motion within the lattice is observable in Figure 2.2. The negatively charged oxygen lattice moves against the positively charged Ba and Ti ions.

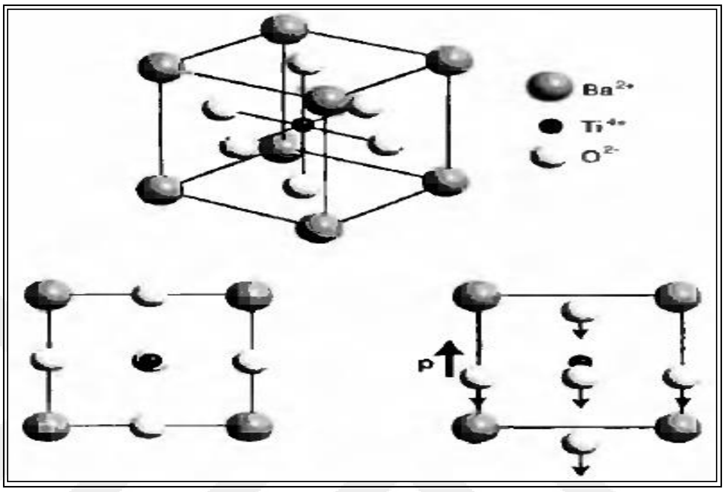

Figure 2.2: In the ferroelectric state, sub-lattice of oxygen ions and sub-lattice of Ba and Ti ions.

The crystal structure of these ceramics is not constricted to the tetragonal phase. While examining the phase diagram of the ($Pb(Zr_xTi_{1-x})O_3$), there are some points that need to be clarified.

At relatively low temperatures and $PbTiO_3$ concentrations, the orthorhombic phase is formed. By just increasing the concentration of the $PbTiO_3$, the low and high-temperature forms of the rhombohedral phase occur. The morphotropic phase boundary separates the tetragonal phase from the orthorhombic and rhombohedral. Closer to the MPB the superior electromechanical performance is reached. MPB is a temperature-dependent compositional range over which there is a mixture of monoclinic and tetragonal phases. At the higher region of the diagram, there is a horizontal line which is called Curie temperature, which must not be crossed, after that point, cubic crystal structure forms, and the polarization is lost.

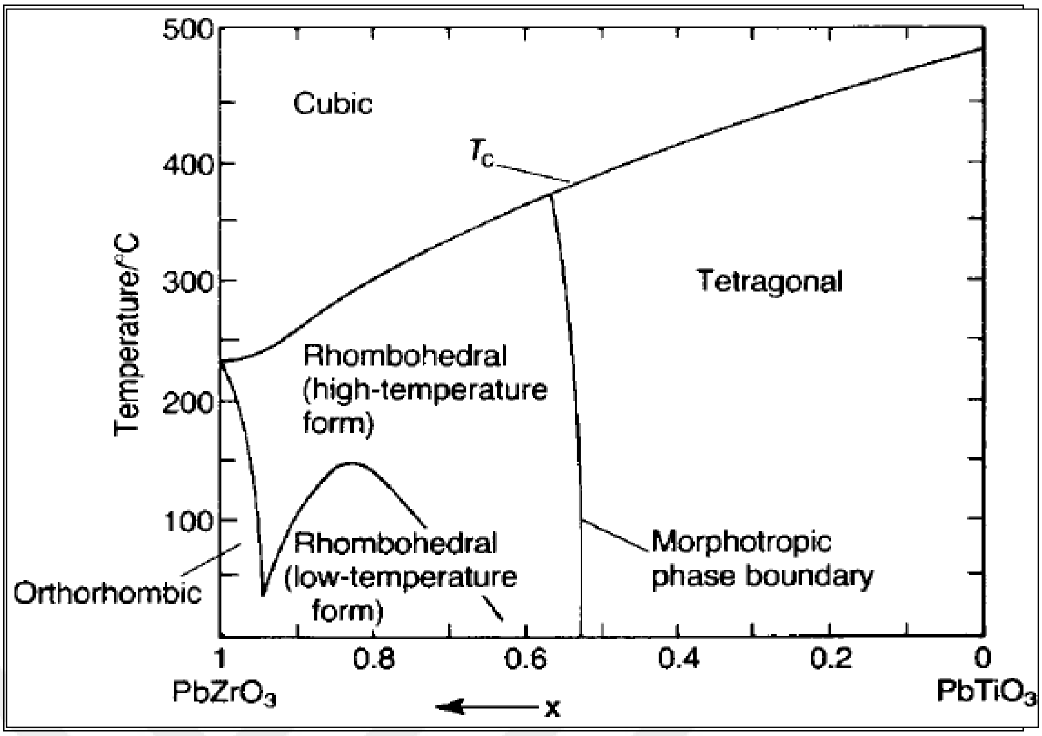

Figure 2.3: Diagram of stable phases of PZT.

As mentioned earlier, when the electric field is applied dipoles orient by the field. These dipoles are assumed and named as domains. The application of a sufficiently strong field will orient the 180^o domains in the field direction. The field will also have an orienting effect on 90^o domains in tetragonal material and on 71^o and 109^o domains in the rhombohedral form with a limited response due to the strain situation. Domain wall motions and hysteresis curve is strongly related because it shows the effect of the applied field versus the polarization. The curve below is a basic example showing the hysteresis behavior of PVDF film which is one of the most utilized ferroelectric polymers.

On this curve, there are points of interest that indicate the characteristics of the ferroelectric sample. The maximum polarization of a sample can be seen from the sharp edges of the curve at the far end. The points where the curve intercepts with the y-axis are called remnant polarization which shows the polarization after the cut-off of the electric field. The coercive field is determined from the intercepts of the curve with the x-axis. This field is strongly dependent upon the crystal structure while maximum polarization is not.

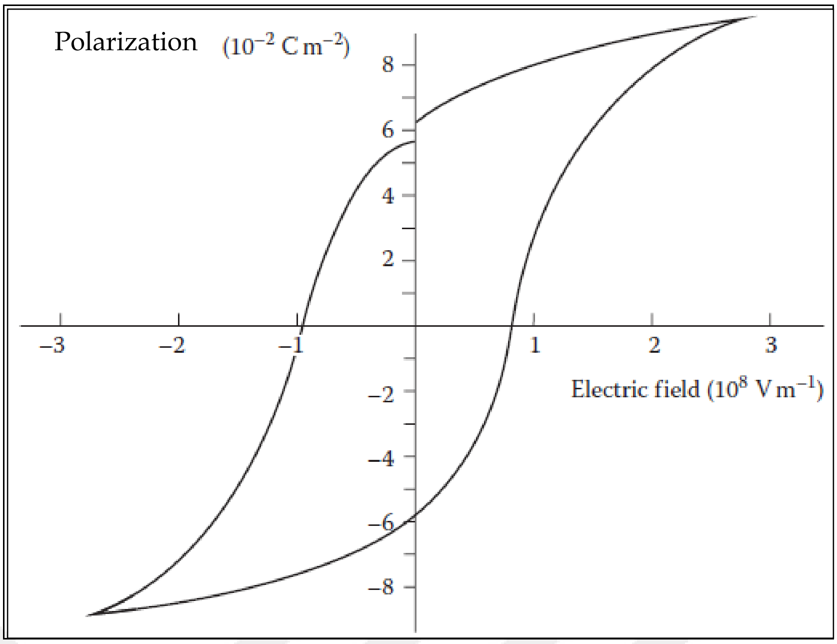

Figure 2.4: Hysteresis loop for a polyvinylidene fluoride (PVDF) film.

2.1.2. Piezoelectricity

The piezoelectric effect is present in ferroelectrics but not restricted to only this group of materials ZnO and SiO_2 are examples that exhibit piezoelectricity although, both of them are not ferroelectrics. Basically, the process starts with poling of a ferroelectric material to cause a net polarization. If we assume a PZT material as an example, positively charged Ti and Zr ions move towards the negative side of the field in the asymmetric crystal structure. Although, there will be no current flow because, in order to allow current flow, compressive stress is required to change polarization by affecting the dipole moment. After that, if there is a sufficient amount of surface charges, transient current flow happens. To obtain the voltage, stress is needed but not limited to compressive stress. Tensile stress perpendicular to the polarization direction gives the same polarity. Figure 2.5. represents the nature of the piezoelectricity in which the phenomenon works both ways namely, direct and converse.

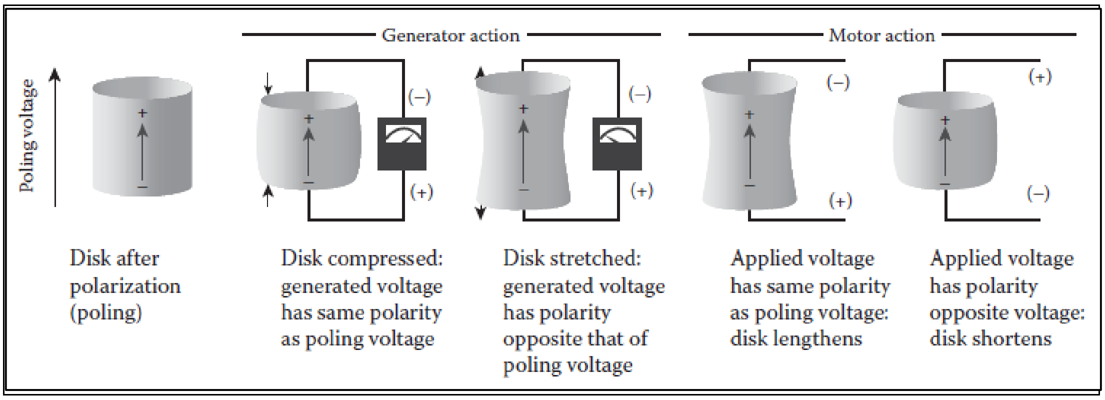

Figure 2.5: Representation of direct and converse piezoelectric effect.

The subjection of the poled material to either compressive or tensile stresses generates a voltage across the dielectric material by developing net charges on the surfaces by the direct piezoelectric effect. As opposed to that, the application of an electric field causes strain, which leads to the observation of motor effect. For practical applications, strain vs electric field and polarization vs electric field loops have to be described. Figure 2.6. show the basic so-called butterfly and P-E loops.

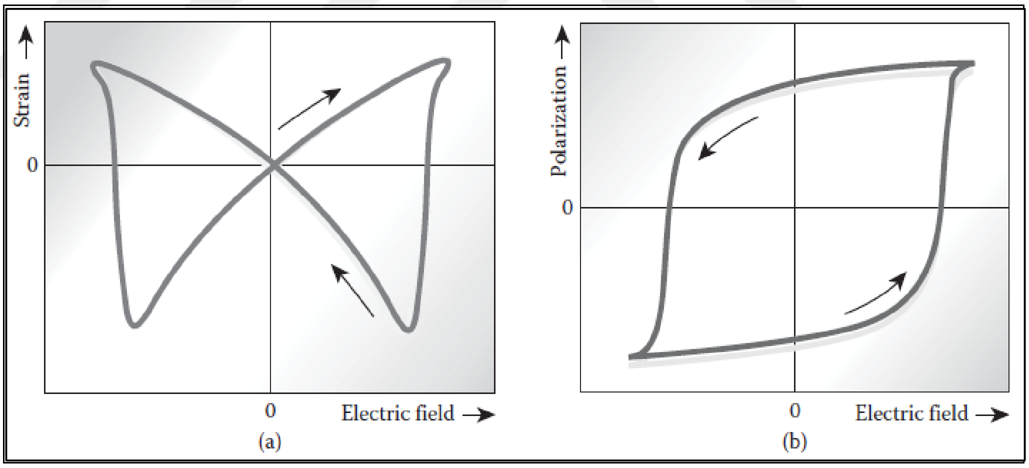

Figure 2.6: *x*-E and P-E loops of ferroelectrics.

Piezoelectric properties are expressed with several parameters that are D, E, X, and *x*. While D stands for direct piezoelectric effect, E, X, and *x* are electric field, stress, and strain, respectively.

Direct piezoelectric effect can be written in terms of strain:

$$D=e^{*}x \qquad (2.1)$$

The converse piezoelectric effect is represented by the given relation below:

$$x=d^{*}E \qquad (2.2)$$

The piezoelectric coefficients e, h, g^* , d^* are tensors and their values depend on the directions of E, D, X, x. Additionally, these tensors are called electrostriction coefficients. The electrostrictive effect is highly important as it defines the resultant strain which is proportional to the square of the field. The relation is expressed in the formula (3).

$$X=Q^{*}P^{2} \qquad (2.3)$$

In general, the relationship between these tensors can be given as in Figure 2.7. according to thermodynamics.

$$\left(\frac{\partial D}{\partial X}\right)_{E,T} = \left(\frac{\partial x}{\partial E}\right)_{X,T} = d$$

$$-\left(\frac{\partial E}{\partial X}\right)_{D,T} = \left(\frac{\partial x}{\partial D}\right)_{X,T} = g$$

$$\left(\frac{\partial D}{\partial x}\right)_{E,T} = -\left(\frac{\partial X}{\partial E}\right)_{x,T} = e$$

$$\left(\frac{\partial E}{\partial x}\right)_{D,T} = \left(\frac{\partial X}{\partial D}\right)_{x,T} = -h$$

Figure 2.7: Summarization of the relationship between tensors.

Piezoelectricity is the effect that has the ability to transform two forms of energy into one another. This has been the basis of some practical applications as mentioned earlier and fields of application areas are shown in Figure 2.8.

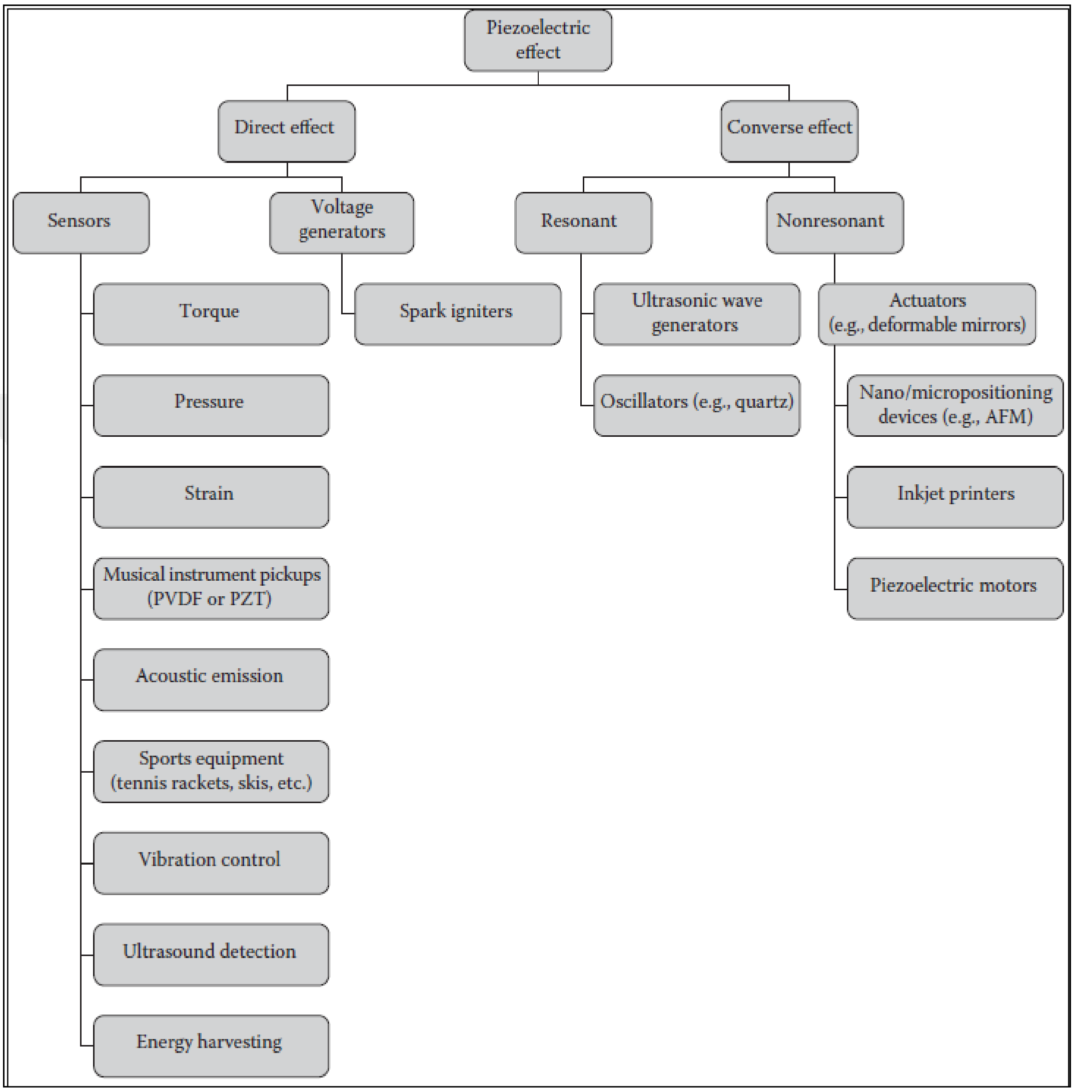

Figure 2.8: Direct and converse piezoelectric effect applications areas, in detail.

Apart from the PZT, there are other ceramics that many studies have been done as such BT-based, KNN-based, NBT-based, BZT, and BCZT lead-free ceramics. Interestingly, β-PVDF, Teflon and show piezoelectric behavior, as well. Figure 2.9. is representing some of the ceramic's d_{33} coefficient with respect to the Curie temperature.

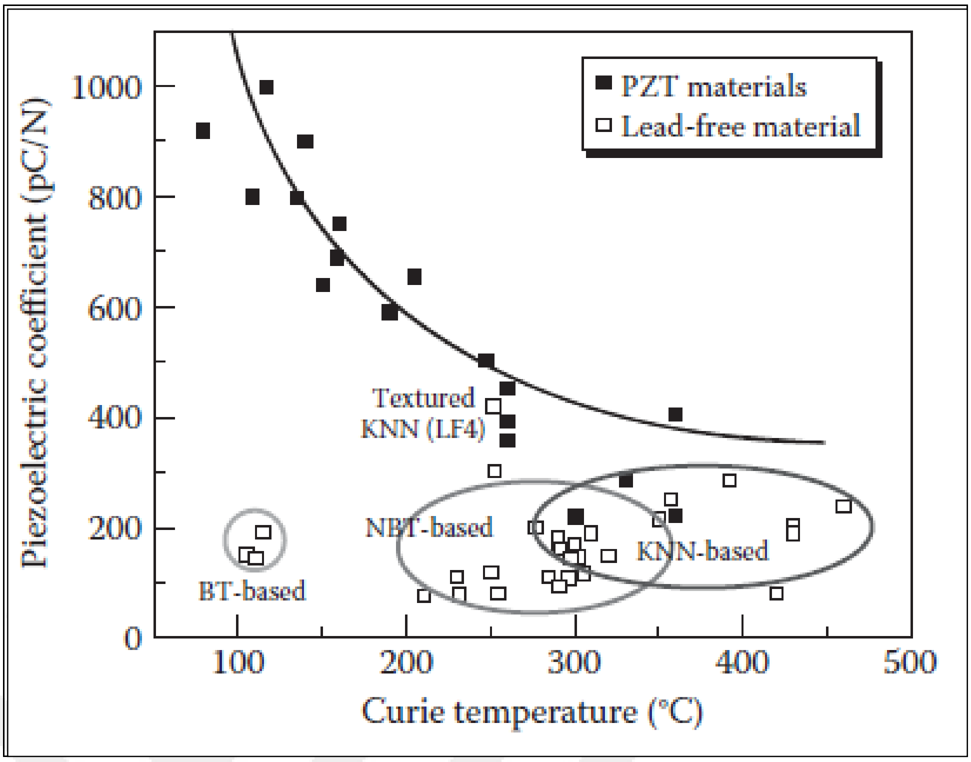

Figure 2.9: Room-temperature values of the piezoelectric coefficient d_{33} as a function of the Curie temperature for PZT materials and lead-free piezoceramics.

2.1.3. Dielectrics

Large bandgap ($E_g > 4eV$) and high resistivity (ρ) are dielectric materials' typical aspects and they do not conduct electricity by any of the charges (ions, electrons, and so on). Under specific situations (changes in the composition or microstructure or exposure to very high electric fields), semiconductivity or metallic behavior is observed. The electrostatic induction concept can be expressed by bound and free charges to figure out the mechanism behind the dielectrics. The generation of negative charges on the conductor is simply called electrostatic induction. These charges are induced by the charged insulator and are named bound charges. If the ground connection of the conductor is satisfied, the flow of electrons is possible, they make up for positive charges on the conductor and these positive charges are free charges Conversely, dielectric materials do not generate induced charge due to the lack of charge carriers.

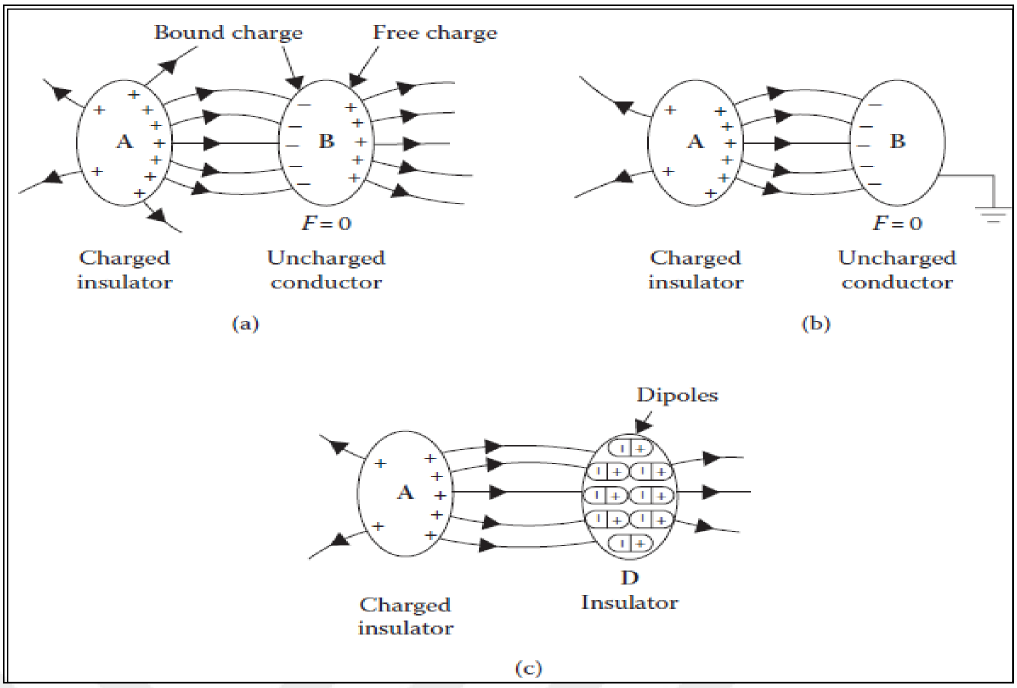

Figure 2.10: Illustration of bound and free charges with electrostatic induction, where A is the charged insulator, B is the conductor, and D is dielectric. (a) Isolated, (b) grounded, and (c) induction with an insulator.

The macroscopic approach to the dielectrics can be viewed by the given formula:

$$P = X_r \varepsilon_0 E \tag{2.4}$$

Here, X_r stands for electric susceptibility, ε_0 is the permittivity of the vacuum and E is the electric field. A standard approach to electric polarization is the plane plate capacitor. For an empty capacitor, a constant value of $|E| = \sigma / \varepsilon_0$ is satisfied where σ is the surface charge density on the plates, then a simple $C = \varepsilon_0 A/d$ rule can be applied. Placing a dielectric in between two parallel plates leads to a macroscopic polarization which is shown by P. With that, the electric dipole term emerges, which can be represented by the formula where α is the dipole moment.

$$P = \alpha E \tag{2.5}$$

Inspection of the dielectrics phenomena by the means of the microscopic approach is also necessary and this polarization is strongly related to the frequency. At all frequencies, electronic polarization exists. Some molecules, especially polar molecules, feel the torque and align themselves in the direction of the applied electric field and this process is called orientational polarization. Also, ionic molecules follow the electric field but in a slower manner because ions are heavy as compared to electrons and atoms. Lastly, interfacial polarization or surface charge polarization happens at lower frequencies.

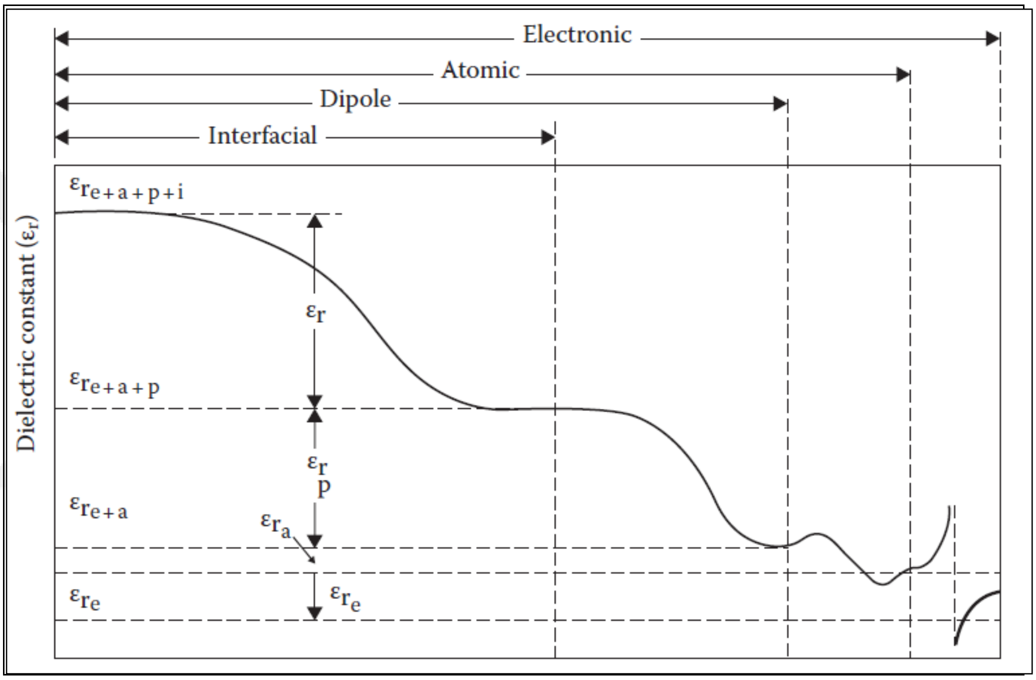

Figure 2.11: Dielectric constant-frequency graph with different polarization mechanisms.

Table 2.1: Approximate room temperature dielectric constants for some dielectric materials or classes of materials (Frequency 1kHz-1MHz).

Material	Dielectric Constant (ε_r)
Vacuum	
Oxygen (O_2) gas	1.000494
Argon (Ar) gas	1.000517
Mineral oil	2.25
Water (H_2O)	78
Polymers	~2–9
Teflon	2.1
Polyethylene	2.2
Silicon (Si)	11
Linear dielectric ceramics (SiO_2, TiO_2, Al_2O_3, and so on)	~4–200
Silica (SiO_2)	3.8–4.0
Alumina (Al_2O_3)	9.9
96% Al_2O_3 thick film	9.5
Magnesium oxide (MgO)	20
Nonlinear dielectrics or ferroelectrics	10–10,000
Polyvinylidene fluoride (a piezoelectric and ferroelectric polymer)	12–13
Barium titanate ($BaTiO_3$; a ferroelectric ceramic)	~2000–5000

The term dielectric constant (ε_r) or relative dielectric permittivity is the ratio of E_0 / E and represents the electric field existing in a capacitor filled with a dielectric material. In table 2.1, some dielectric materials are given [1]-[3].

2.2. Stretchable & Flexible Polymer Matrices

2.2.1. Poly Di-Methyl Siloxane (PDMS)

Poly di-methyl siloxane or PDMS is simply an organosilicon compound that belongs to a group named silicones. Its chemical formula is $CH_3[Si(CH_3)_2O]nSi(CH_3)_3$, where n is the number of repeating monomer $[SiO(CH_3)_2]$ units. It has found various workspace since its biocompatible, resistant to chemicals, low-cost, optically transparent, non-flammable, and thermally stable.

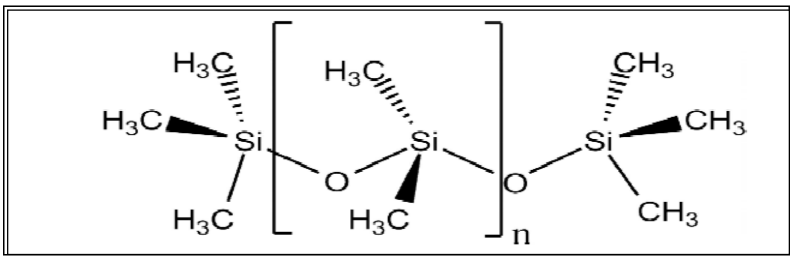

Figure 2.12: The chemical structure of the PDMS polymer.

After the curing of the PDMS, it becomes hydrophobic and can be shaped and sized as desired. PDMS with longer chains is a viscoelastic material and its mechanical properties should be taken into account at different rates of impact. Key applications of the PDMS are the creation of lab-on-chip devices and microfluidics. Cross-linking is a crucial factor since it allows the polymer to adapt to mechanical changes in the surrounding environment. Due to this adaptation, PDMS is a emerging candidate which may be used in the near future tissue engineering and flexible medical devices.

As previously discussed, optical transparency is an advantage along with the stretchability because various futuristic gadgets might be developed such as suspended particle devices for smart window applications. Defoamers, water-repellent coatings, contact lenses, cosmetics, lubricants, and many others are promising applications where PDMS is involved. Interestingly, Gecko-inspired structures like polymeric brushes and gloves having the ability of adhesion were designed and utilized.

Table 2.2: The adhesion force of PDMS/ZnO/toluene, PDMS/ZnO and PDMS from down to top.

Sample	Adhesion force (nN)
PDMS	9.33
PDMS/ZnO	7.91
PDMS/ZnO/toluene	10.57

Future technology, especially, flexible devices more specifically flexible sensors rely on the composite of polymers and advanced ceramics. In environments such as human tissue, water, and other organic materials these polymers exhibit low acoustic impedance, which is favorable. The combination of the dielectric constant and high piezoelectric charge coefficient of piezo ceramics with the low density and flexibility of polymers perfectly matched for sensing technology [4],[5].

2.2.2. Polyurethane (PU)

Polyurethanes are versatile polymers with their physical, mechanical, chemical, and, biological properties. Via the use of advanced characterization techniques and/or change in the production process, PUs can be modified for specific applications such as paints, liquid coatings, elastomers, insulators, elastic fibers, foams, and integral skins, etc.

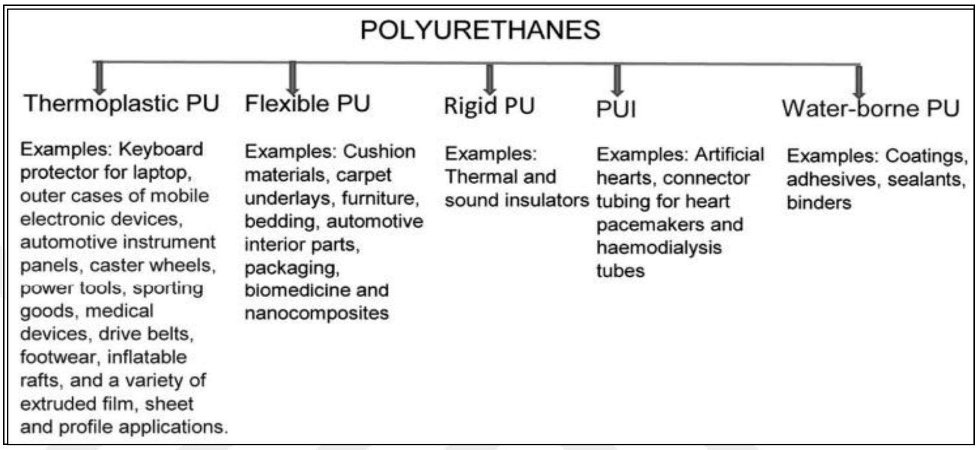

Figure 2.13: Common examples of PUs and their types.

Synthesis of PU is performed in several ways, but the reaction between a polyol and a diisocyanate is an important and useful method. Additives including flame retardants, pigments, cross-linkers, fillers, blowing agents, surfactants, and catalysts may incorporate through the process. A variety of density and hardness can be achieved by alternating the ratio of polyol, diisocyanate, and additives.

PU is a great choice in areas including construction, automotive, marine, coating, medical, apparel, flooring, and, packaging technologies since the latest advances in the PU production satisfied the needs of the industry by the means of high performance, light weight, ease to installation, durability, and versatility. Additionally, advanced electronics like energy harvesters require flexibility, versatility, and durability whereas PU meets the requirements perfectly.

When its electrostrictive nature is combined with the high piezoelectric properties of piezoceramics, flexible energy harvesters can be designed. Also, noise reduction at high frequencies and energy damping behavior is attractive to the electronics industry where these parameters are vital to handle [6]-[8].

2.3. Lead Based Ferroelectric Ceramic Materials

2.3.1. Lead Zirconate Titanate (PZT)

The effect of piezoelectricity is being extensively studied since it was first discovered in 1880. Among many, PZT is the major piezoelectric ceramic material that will be chosen due to the ability to the formation of solid solutions over a large range of Zr: Ti ratios. A wide range of dopants can be chosen to modify the crystal structure.

PZT is a combination of a ferroelectric lead titanate ($PbTiO_3$) and anti-ferroelectric lead zirconate ($PbZrO_3$) which is basically a solid solution. For “Zr” rich compositions (Zr: Ti > 54:46), the structure is rhombohedral while it is tetragonal for “Ti” rich compositions (Zr: Ti < 48:52). In the intermediate compositions by morphotropic phase boundary (MPB) both rhombohedral and tetragonal phases coexist. This boundary is at a point Zr: Ti ~ 53:47 at room temperature. Although it is commonly observed that the tetragonal and the rhombohedral phases coexist in a finite range of compositions around MPB, the MPB is represented by a line in the phase diagram. 14 possible polarization directions are the contributions of 6 tetragonal and 8 rhombohedral structures at MPB. Having a low energy barrier allows an efficient and optimal polarization during the poling process which leads to the generation of high piezoelectric and dielectric properties.

PZT is a polycrystalline material and belongs to the perovskite family with the general formula of ABO_3. Where “O” is the oxygen atoms at the face-centered positions of the cubic structure. “A” is a divalent cation that (Pb^{2+}) occupies at the corners of the cube, and “B” is a tetravalent cation (Zr^{4+} or Ti^{4+}) that occupies a body-centered position.

Lead and oxygen ions are close to each other in terms of ionic radii and they form a face-centered cubic array with a lattice parameter of approx. 4.0 °A. Zr and Ti ions move along the direction of the applied electric field and align up or down. Cations can be substituted in the perovskite structure according to the given formula:

$$t = (R_A + R_O) / \sqrt{2}(R_B + R_O) \qquad (2.6)$$

Where t is the Goldschmidt tolerance factor

- R_A is the radius of large cation A (Pb^{2+})
- R_B is the radius of small cation B (Zr^{4+} or Ti^{4+})
- R_O is the radius of anion (O^{2-})

The structures depending on the t factor are as follows:

- $t = 0.95\text{-}1.00$ for cubic perovskite structure
- $t < 0.95$ for non ferroelectric
- $t > 1.00$ for ferroelectric

If the dopants' ionic radius exceeds 15% of the radius of replaced ion, substitution is not possible.

Larger alkali metal ions, rare-earth ions, etc. will substitute on the A-site while smaller ions like transition metals will be replaced on the B-site. Amphoteric dopants are replaced either on the A or B-site, whose ionic radii are intermediate. Isovalent, donor, and acceptor dopants are employed in the modification of PZT's properties. For example, Ba^{2+} or Sr^{2+} replaces Pb^{2+} and Sn^{4+} replaces Zr^{4+} and these ions are whose valance and ionic radii are similar to that of the replaced ions. While donor dopants substitute on the A-site, acceptor dopants with lower valance substitute on the B-site.

Donor dopants for substitution in A site are Nd^{3+}, and La^{3+} in A site, and for substitution in B site Nb^{5+}, Ta^{5+}. Acceptor dopants are of lower valence cations such as Na^{+}, K^{+} for A site and Mg^{2+}, Fe^{3+} and Sc^{3+} for B site substitution.

Table 2.3: Types of dopants in PZT and their major effect(ionic radii in A° are mentioned in parantheses).

Dopants	Major effects
Isovalent type	
Ba^{2+} (1.34), Sr^{2+} for Pb^{2+} (1.32) site.	(i) Lower Curie point
Sn^{4+} (0.71) for Zr^{4+} (0.79) and Ti^{4+} (0.68) site.	(ii) Higher permittivity
Donor type	
La^{3+} (1.22), Nd^{3+} (1.15), Sb^{3+} (1.14), Th^{4+} (1.10) for Pb^{2+} (1.32) site.	(i) Cerate cation vacancy
	(ii) Higher permittivity
	(iii) Higher mechanical coupling factor (k_p)
Nb^{5+} (0.69), Ta^{5+} (0.68), Sb^{5+} (0.63), W^{6+} (0.65) for Zr^{4+} (0.79) and Ti^{4+} (0.68) site.	(iv) Very high piezo properties (d_{33})
	(v) Decrease in mechanical quality factor (Q_m)
Acceptor type	
K^{+} (1.33), Na^{+} (0.94) for Pb^{2+} (1.32) site.	(i) Create anion (oxygen) vacancy
Fe^{3+} (0.67), Al^{3+} (0.57), Sc^{3+} (0.83), In^{3+} (0.92), Cr^{3+} (0.64) for Zr^{4+} (0.79) and Ti^{4+} (0.68) site.	(ii) Lower permittivity
	(iii) Lower dielectric loss
	(iv) Lower k_p
	(v) Increase in mechanical quality factor

By co-precipitation, sol-gel, spray pyrolysis, mixed oxide, hydrothermal synthesis, and molten salt synthesis routes PZT is processed. The mixed oxide route is favorable among other methods but it has some drawbacks as expected.

- Difficult to maintain the stoichiometry because the powders are inhomogeneous at the micro-level.
- Relatively high reaction temperature leads to Pb loss.
- Low diffusion process, therefore, a slow reaction rate.

The degradation of ferroelectric and piezoelectric properties caused by these problems can be prevented by the wet-chemical route. In this process, by adding diluted NH_4OH solution an aqueous solution of precursors convert to hydroxides then similar steps were followed as in the mixed oxide route [9].

2.3.2. Lead Magnesium Niobate - Lead Titanate (PMN-PT)

$(1-x)Pb(Mg_{1/3}Nb_{2/3})O_3$-$xPbTiO_3$ is a solid solution of lead magnesium niobate and lead titanate. Its dielectric and piezoelectric properties are high enough, but not a match for the PZT. Although, its relaxor nature and electrocaloric performance are invaluable and experimental studies are currently focused on the investigation of enhancement of these properties. Nowadays, research efforts are to design a new solid-state cooling technology without any need for a refrigeration system like vapor cooling just by using the electrocaloric cooling effect (ECE) in which the cooling is achieved by applying an electric field to ferroelectric material. Additionally, in normal ferroelectrics, the ECE is observed in the narrow range which is close to the Curie temperature. Still, when it comes to the relaxor ferroelectrics this drawback is maintainable since relaxors are good at showing high performance at a broad range of temperatures. Also, a wide range of compositions such as 67.5PMN-32.5PT, 70PMN-30PT, and 90PMN-10PT are studied which is seen in Figure 2.14 [11].

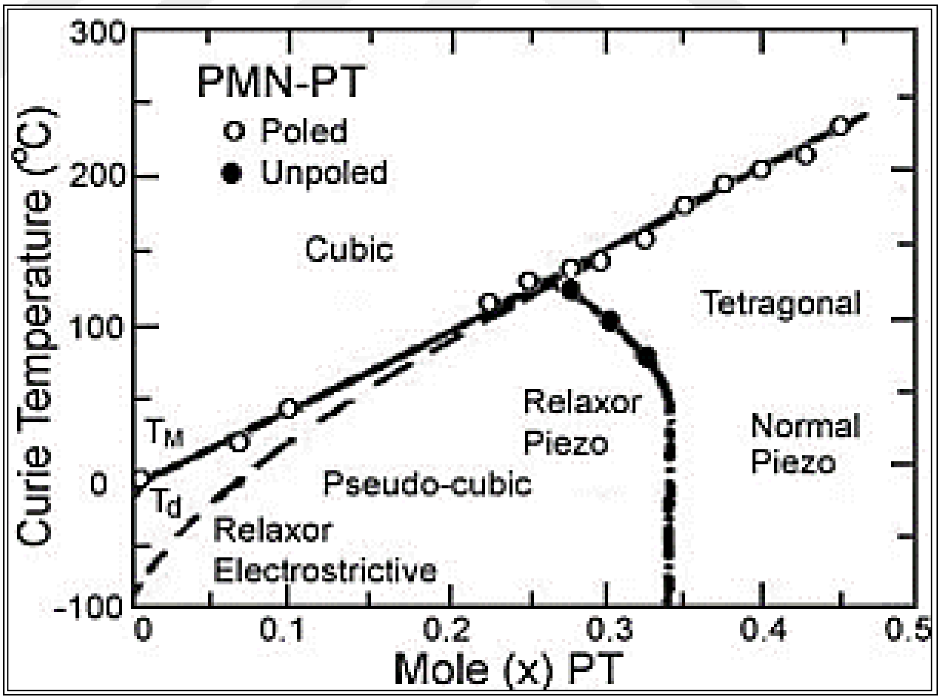

Figure 2.14: The phase diagram of PMN-PT.

Basically electrocaloric cooling or ECC in short is an adiabatic temperature change and entropy change of the polar material. The idea of the ECC is desirable from the perspective of the electronics industry where it can have adjustable shape and size, is low cost, is reliable, has no mechanical moving parts, and most importantly, is environmentally pollution-free. The beauty of the PMN-PT lies in the core of the fabrication process since it contains a normal ferroelectric $PbTiO_3$ (PT) phase to stabilize the perovskite structure. Preferably, compositions that are close to the MPB are chosen to get the most of the performance of PMN-PT.

Various shapes and types of these ceramics have been investigated and bulk ceramics with larger ECE coefficients ($\Delta T_{ECE}/ \Delta E$), was found to be the best option to be selected. Thin films with large areas and small capacities are unfavorable to be used in the cooling technology. The theory behind this technology is related to the indirect calculation of Maxwell's equation which is shown below.

$$\Delta T = -\frac{1}{C\rho}\int_{E_1}^{E_2} T\left(\frac{\partial P}{\partial T}\right)_E dE \tag{2.7}$$

where C is heat capacity, ρ is density, E is applied electric field, P is the polarization and T is temperature. The lack of instruments limits the work on the direct measurement but it was reported that there is a huge discrepancy between the magnitude and temperature dependence of ECE measured by direct and indirect methods. There are many ways to improve the performance by using a single crystal form of PMN-PT, doping, and texturing. Previous works stated the elemental doping, transforms phase transition, microstructure, and electrical properties of PMN PT-based relaxor ferroelectric ceramics. Since the single crystal form of PMN-PT exhibits a high piezoelectric coefficient and electromechanical coupling coefficient, promising studies of energy harvesting are emerging. A combination of a single-crystal form of PMN-PT and polymers is preferred to design this sort of energy harvester by researchers, lately.

Microstructural engineering and modification of composition by texturing using barium titanate ($BaTiO_3$, BT) and strontium titanate ($SrTiO_3$, ST) and adding a 'hard' dopant like multivalent Mn, which prevents the domain wall motion are beneficial where texturing and doping is both considered.

Mn introduces oxygen vacancies to pin domain wall motion. previous works stated the elemental doping, transforms phase transition, microstructure, and electrical properties of PMN PT-based relaxor ferroelectric ceramics [10],[12]-[14].

2.4. Piezoactive Composites

2.4.1. Composites with 0-3 Connectivities

Piezo-active composites are a group of heterogeneous dielectrics whose physical properties and related parameters depend on the domain structure, microstructure, connectivity, and arrangement of components. The considerable piezoelectric activity, sensitivity, and electromechanical coupling are key factors that are of great importance among modern applications. Ferroelectric components that are highly effective as poled ferroelectric ceramics or domain engineered relaxor single crystal ferroelectrics.

In the near future, potential transducer, hydroacoustic, and energy harvesting technologies with piezo-active materials are to be taken into account. Heterogenous systems as composites consist of two or more components and the chemical composition of these components differ along with composition-related properties and are separated by interfaces. Composite materials are characterized by the following features:

- In comparison to the entire composite sample, the typical sizes of the individual structural parts that make up the component are modest.
- The typical sizes of structural elements are greater than the individual atoms or molecules, hence each component is treated as a continuous medium in this scenario.

Elements that make up the composite are distributed irregularly or regularly and can be in different shapes and sizes. The composite can be distinguished by using a set of micro geometric characteristics like connectivity, components spatial distribution, and their volume fractions.

Due to the ability to change the microgeometry, effective physical characteristics, and anisotropy of ferroelectric-based composites across a large range, they are very useful. When the components of two-component composites are combined, these variances arise such as

- Polymer and FC (that can be either piezoelectric or piezo-passive),
- FC and ferroelectric single crystal, and
- Polymer and ferroelectric single crystal.

The link of hierarchy is formed in ferroelectrics-based piezo-active composites as follows:

single-domain single-crystal→polydomain single-crystal→FC→composite' and 'single-domain single-crystal → polydomain single-crystal → heterophase single crystal → composite.

We can create a micro geometric picture of the piezo-active composite to be examined thanks to the connectedness of the structural parts. We may classify the composites into three main categories based on connection characteristics. The first group is generated by matrix composites wherein at small volume fractions, the other structural elements do not touch each other and are isolated within the structural elements of the first component. The second group is called interpenetrated wherein each component is regarded as a monolithic or interconnected framework. The third group is comprised of isolated or not interpenetrated structural elements of each component. We examine composites as materials having a regular (determined) or irregular (stochastic) structure, taking into account the arrangement of structural parts. Rectangular (parallelepiped or ellipsoid) and a regular (equidistant and uniform) arrangement in the sample is a characteristic of a regular structure. The shape of structural elements can be either arbitrary or appointed at the irregular structure and the distribution of structural elements are random. Additionally, spacial distribution affects the arrangement characteristics.

A new categorization system for two-component composites with planar interfaces has been proposed. This categorization is based on the notion of the connectedness of each component in the composite and takes into consideration micro geometric properties. Defines connectivity as the number of dimensions (or co-ordinate axes) in which each component is continuously distributed amongst the composite sample's limiting surfaces. A component's self-connected state can be distributed along with zero, one, two, or three coordinate axes, with connectivity α = 0, 1, 2, or 3 for component 1 and connectivity β = 0, 1, 2, or 3 for component 2. A two-component composite's connection is stated with the piezoelectric or most piezo-active component's connectivity taking the first place (α).

Table 2.4: α–β connectivity patterns with planar microgeometry composites.

	First component				
Second component		$\alpha = 0$	$\alpha = 1$	$\alpha = 2$	$\alpha = 3$
	$\beta = 0$	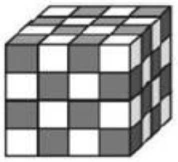	Like a pattern at $\alpha = 0$ and $\beta = 1$	Like a pattern at $\alpha = 0$ and $\beta = 2$	Like a pattern at $\alpha = 0$ and $\beta = 3$
	$\beta = 1$	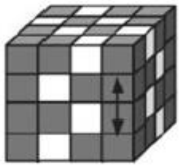	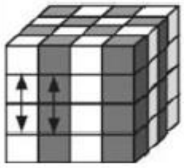	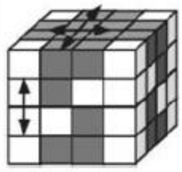	Like a pattern at $\alpha = 1$ and $\beta = 3$
	$\beta = 2$	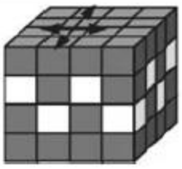	Like a pattern at $\alpha = 2$ and $\beta = 1$	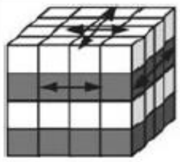	Like a pattern at $\alpha = 2$ and $\beta = 3$
	$\beta = 3$	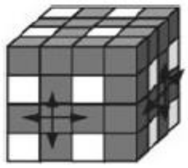	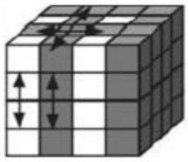	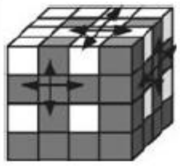	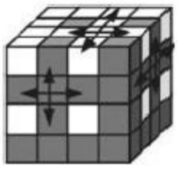

Arrows show co-ordinate directions along which the first and second components are distributed continuously

Generally, a two-component composite is described in terms of 16 connectivities: 0–0, 0–1, 0–2, 0–3, …, 3–2, and 3–3. Among these connectivities some of the patterns are similar. For instance, 3-2 and 2-3 or 3-1 and 1-3, etc. Since the connectivity is crucial in terms of electromechanical coupling, and piezoelectric properties 0–3, 1–3, 2–2, 2–3, 3–1, 3–2 and 3–3 patterns have been studied. For example, 0-3 connected composites consist of a system of isolated FC inclusions surrounded by a polymeric matrix. Whereas, FC rod chains or fibers form a continuous distribution along the coordinate axis in 1-3 connectivity.

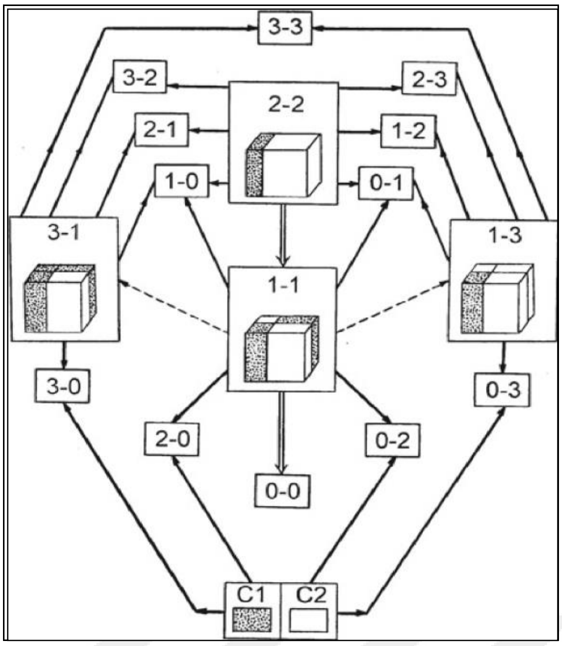

Figure 2.15: The α–β links. C1 and C2 represent components 1 and 2, respectively. At transformations, 2–2→1–1 and 1–1→0–0, double lines connecting the 2–2 and 1–1 connectivity patterns as well as the 1–1 and 0–0 connectivity patterns denote structural elements multiplication. At transformations, 1–1→3–1 and 1–1→1–3 dashed lines connecting the 1–1 and 1–3 connectivity patterns with the 1–1 and 3–1 connectivity patterns show a simplification of the 1–1 structure.

To forecast the electromechanical properties related to ferroelectrics, theoretical approaches can be divided into three major groups. The composite system is modeled by dielectric spheres spread in a continuous matrix in group 1, and no interactions between components are considered. Interactions between a filler and neighboring particles are taken into account in group 2 when an electric field is applied to the composite sample. The form and direction of the inclusions in the composite are considered in group 3. Effective piezoelectric properties of the 0-3 and 1-3 FC/Polymer composites are concerned with the longitudinal piezoelectric effect where external stress or electric field is along the poling direction of the sample. At large volume fractions of the FC, values of the piezoelectric coefficient d^*_{33} of the 0–3 composite are achieved. On the contrary, the piezoelectric coefficient d^*_{33} of the 1–3 composite converges $d^{(1)}_{33}$ of the FC component at the volume fractions over 0.3.

As compared to g^*_{33} of the 1–3 composite, the piezoelectric coefficient g^*_{33} of the 0–3 composite remains relatively small in the whole volume-fraction range. There are reasons for different volume fraction dependencies that are accounted for by the specifics of the composite microgeometry.

In the 1–3 composite, the FC component is distributed continuously along the poling axis. Conversely, in the 0–3 composite, the FC component is distributed in the form of isolated inclusions. Furthermore, because of the larger permittivity, and lower resistivity of the FC component, the electric flux concentrates more effectively on the polymer component and does not affect the FC particles efficiently. The thickness of the polymer layer separating the FC particles in the composite sample decreases as the volume fraction of FC increases. Such a smaller polymer layer thickness causes the poling of the composite, as a smaller fraction of the applied external electric field is imposed on the polymer matrix rather than on the poling of the FC particles. The 1–3 composite exhibit a higher piezoelectric performance due to the continuous distribution of the FC component along the poling direction.

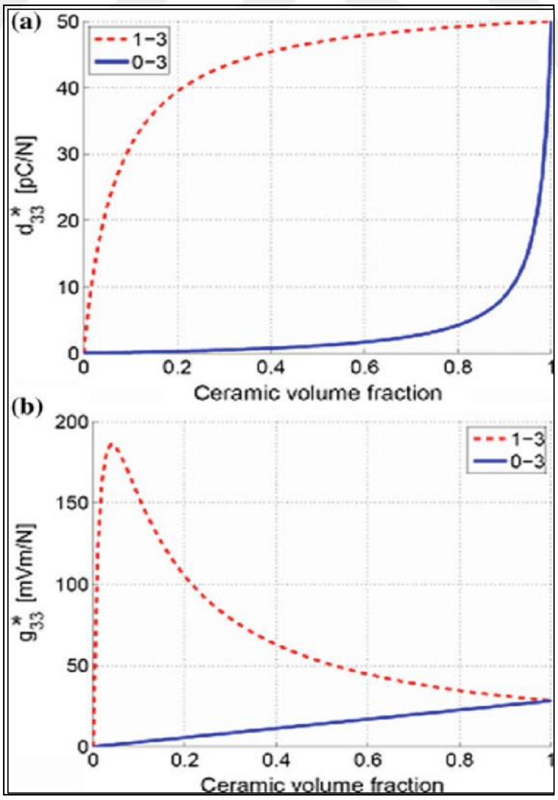

Figure 2.16: At various volume fractions of FC, longitudinal piezoelectric coefficients d^*_{33} and g^*_{33} of 0–3 and 1–3 $PbTiO_3$-type FC/epoxy composites.

In addition to the knowledge above, in electromechanical systems, piezoelectric energy harvesting performance is critical and three major stages are concerned and characterized in the following:

- Mechanical–mechanical energy transmission, including piezoelectric transducer mechanical stability under high mechanical stress and mechanical impedance matching
- Mechanical–electric energy transfer in a piezoelectric element owing to electromechanical coupling
- Electric–electric energy transfer, including electric impedance matching in the presence of a DC/DC converter to store energy in an electric rechargeable battery.

Modern piezo active composite manufacturing requires a combination of knowledge of physics, chemistry, material science, and technology. Specific characteristics of composites have been demonstrated to differ significantly from those of the composite components and can be obtained, for example, in the presence of specific connection patterns.

This is due to a combination of component characteristics, the introduction of an extra component, the impact of electric-field structure, and so on.

The methods can be separated into the groups as follows:

- Methods for manufacturing the FC/polymer composites,
- Methods for manufacturing ferroelectric single-crystal/polymer composites,
- Methods for manufacturing ferroelectric single-crystal/FC composites, and
- Methods for manufacturing three-component FC-based composites.

As an extra, CAD programs are useful in terms of designing composites with intricate geometries also robocasting and rapid prototyping are stimulated thanks to the CAD programs. The main advantage of the CAD programs is the support for a wide range of geometry patterns while constructing composites. Below is a list of manufacturing methods that are specific to different types of piezo active composites.

Table 2.5: Two-component piezo active composites production by various methods.

Connectivity α–β	Methods for manufacturing
2–2	Dice and fill, injection moulding, tape lamination, jet machining, co-extrusion, rapid prototyping
1–3	Rod placement (pick and place), dice and fill, injection moulding, co-extrusion, tape lamination, lost mould, DEP, robocasting, rapid prototyping
0–3	DEP, pressing mixture of ceramic and polymer, colloid processing method, mixing and hot rolling, rapid prototyping
3–3	Lost-wax method and replamine process, burned-out plastic spheres technique, relic procession, distorted reticulated ceramics, robocasting, rapid prototyping
1–1	Laminating the layers, dice and fill, rapid prototyping

The improvement of the properties of composites is strongly related to the connectivity index of the component, features of the microgeometry on the local composite level, etc. Additionally, knowing the electromechanical properties of FCs and polymers is the best way to reach up to more predictable and reproducible composites. There are two major effects that are to be considered when forming a composite and are listed below:

- The effect of the addition of the properties (forming the *sum* properties)
- The effect of the combination of the properties (forming the *combination* properties).

Also, role of electric poling is a key factor that determines the performance of the piezo active composites. As an example, The electric flux concentrates more effectively on the polymer component (that is, the matrix in the 0–3 composite) and does not affect the FC inclusions (isolated particles in the polymer medium) due to the lower electric resistivity and large dielectric permittivity of the FC component in the FC/polymer composite. The thickness of a polymer layer that separates the FC inclusions in a matrix composite shrinks as the volume percentage of FC increases. The electric poling of the composite sample as a whole is made easier as a result of this.

The applied external electric field is imposed on the polymer matrix rather than the FC inclusions in smaller volume fractions of FC (often less than 50 %). When attempting to improve the electromechanical characteristics of FC/polymer composites, this scenario must be considered. Comparing the 0-3 and 1-3 patterns it is obvious that when the composite consists of a continuous rod-like structure, the applied electric field is very effective and it is easy to maintain remnant polarization vectors (P_r) oriented parallel to the electric field which leads to the more sensitive and high piezo activity. Many technical factors and methods for improving the piezoelectric characteristics of such composites are strongly bound to poling conditions. To minimize significant heating of the sample and softening of its polymer component, as well as dielectric breakdown processes in the sample, the electric field E and temperature T at poling must be adjusted within specific limits. A depolarising field created by an FC inclusion in an FC/polymer medium that surrounds this inclusion must also be considered when choosing the poling electric field E [15].

2.4.1.1. 0-3 PZT/ PDMS

Due to their technological potential, composites comprising piezoceramics and polymers have gotten a lot of attention and have been the focus of a lot of primary studies. These composites, often known as "smart materials," are designed for specific purposes and may be used as sensors and actuators in a variety of technological systems. The conversion of mechanical energy into electrical energy is the operating principle. In comparison to ceramics with smaller diameters and lower working voltages, combining a piezoelectric ceramic with a polymer provides more flexibility and formability. Lead zirconate titanate ($Pb(Zr_xTi_{1-x})O_3$ or PZT) is the most extensively utilized ceramic for such composite materials. It has a perovskite structure and is a good candidate material owing to its outstanding electromechanical capabilities. Linear actuators, underwater acoustic signals, naval sonar equipment, medical diagnostic systems, and tactile sensors all use piezoelectricity created by polar materials like PZT. Due to their simplicity of manufacture, good structural performance, and flexibility control, composites with so-called 0-3 connectivity are gaining popularity.

Isolated (ceramic) particles (PZT) in a three-dimensionally linked (polymer) matrix are represented by the label 0-3 for connectivity. According to previous research, the addition of dopants such as CNT or CB gives a significant rise to properties. Experimental data on the electromechanical properties can be seen clearly from the graphical data along with the contribution of the doping of CNT and CB.

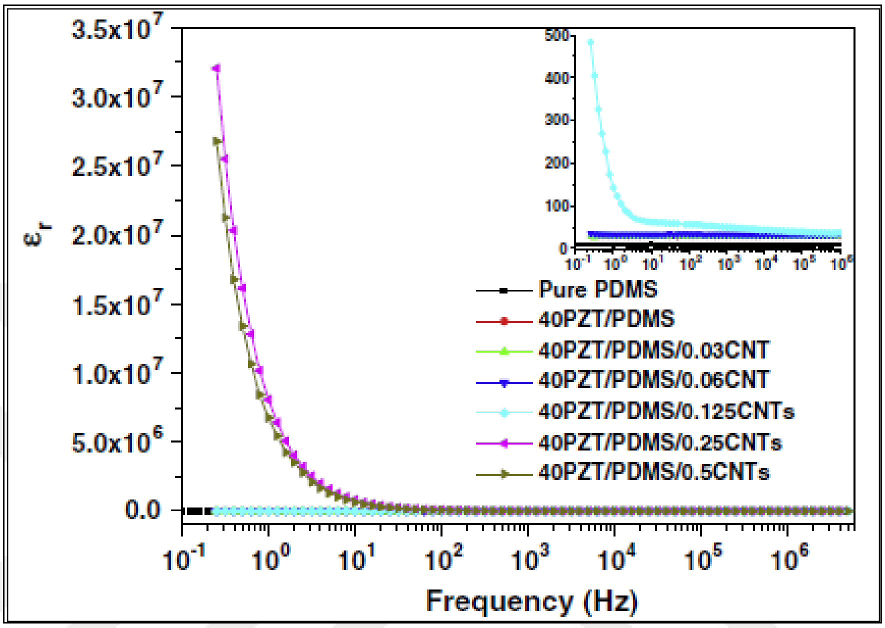

Figure 2.17: As a function of frequency, the permittivity ε_r of PZT/PDMS/CNT composites, 40PZT/PDMS composites, and pure PDMS enlarged picture of ε_r is displayed in the inset.

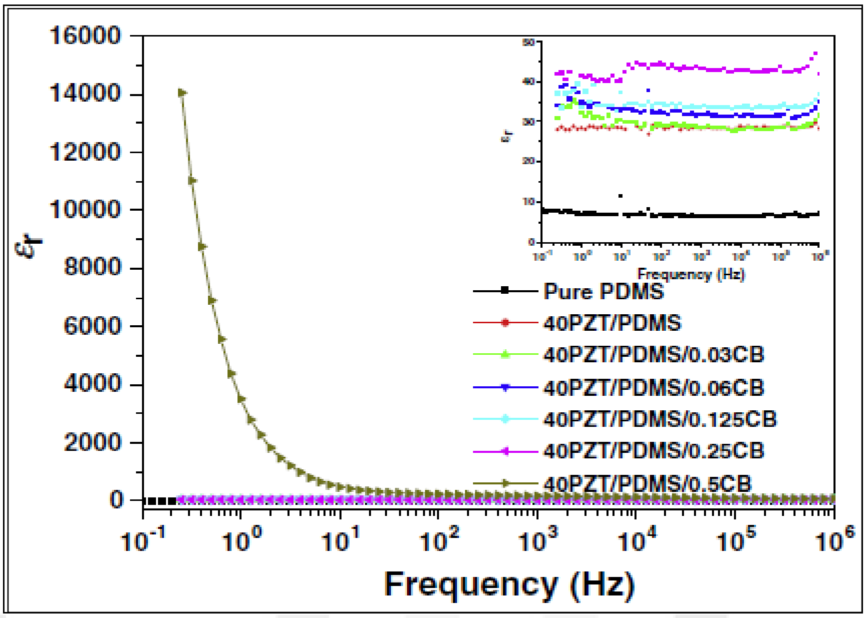

Figure 2.18: As a function of frequency, the permittivity ε_r of PZT/PDMS/CB composites, 40PZT/PDMS composites, and pure PDMS enlarged picture of ε_r is displayed in the inset.

Table 2.6: At 1000 Hz, the measured values of σ, ε_r, and tanδ are compared. For comparison, the static elastic modulus (T_g) and piezoelectric charge constant d_{33} of CNTs and CB integrated composites are also included.

	σ (S/m)	ε_r	tan δ	E (MPa)	d_{33} (pC/N)
Pure PDMS	2.83×10^{-7}	7	0.009	0.78 (−47 °C)	–
40PZT/PDMS	1.57×10^{-6}	28	0.010	7.32 (−45 °C)	11.4
40PZT/PDMS/0.03CNT	1.88×10^{-6}	29	0.011	7.42	12
40PZT/PDMS/0.06CNT	1.86×10^{-6}	32	0.014	2.51	16
40PZT/PDMS/0.125CNT	2.75×10^{-6}	50	0.083	3.42 (−41 °C)	24.6
40PZT/PDMS/0.25CNT	4.43×10^{-4}	7991	32	2.51	–
40PZT/PDMS/0.5CNT	3.58×10^{-4}	6500	123	3.12 (−42 °C)	–
40PZT/PDMS/0.03CB	1.59×10^{-6}	28	0.014	7.59	13
40PZT/PDMS/0.06CB	1.75×10^{-6}	31	0.014	7.9	14
40PZT/PDMS/0.125CB	1.87×10^{-6}	35	0.016	5.05 (−41.5 °C)	18
40PZT/PDMS/0.25CB	2.33×10^{-6}	43	0.021	3.03	–
40PZT/PDMS/0.5CB	9.38×10^{-4}	168	0.213	3.10 (−42 °C)	–

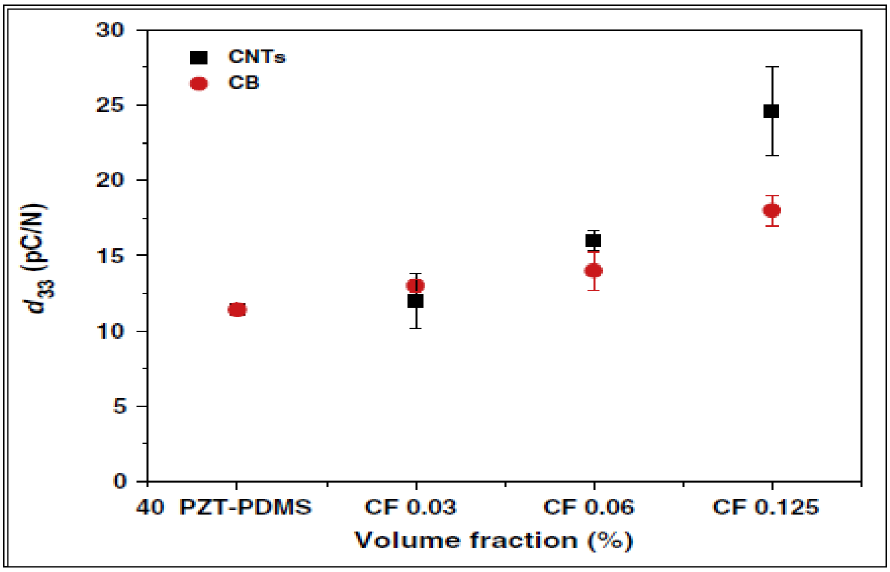

Figure 2.19: The effect of conductive fillers on the d_{33} of PZT/PDMS composites (CF).

Along with the doping [16], there are other ways to improve the performance such as changing the filler content ratio and particle size. The larger the particle size the greater the effect of piezoelectricity where particle agglomeration and polymer/particle interface area is of great importance [17].

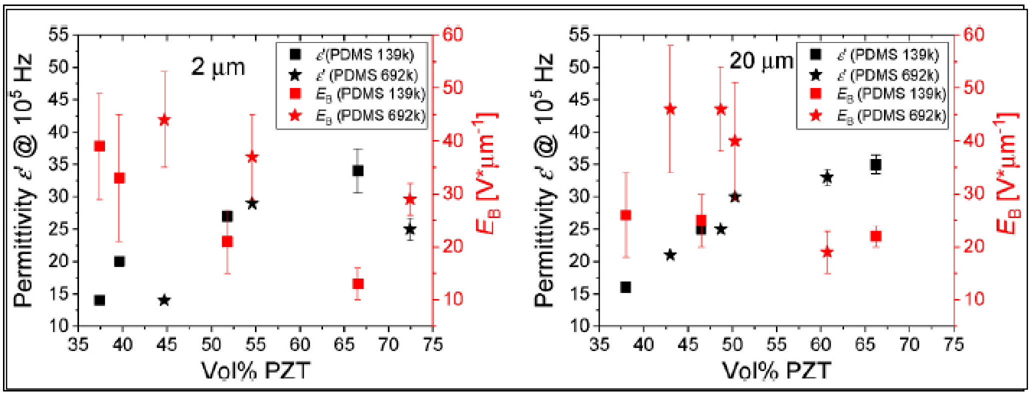

Figure 2.20: Permittivity Ɛ′ and breakdown field E_B of PZT/PDMS nanocomposites in PDMS 139 k and 692 k matrices with an average particle size of 2 and 20 μm.

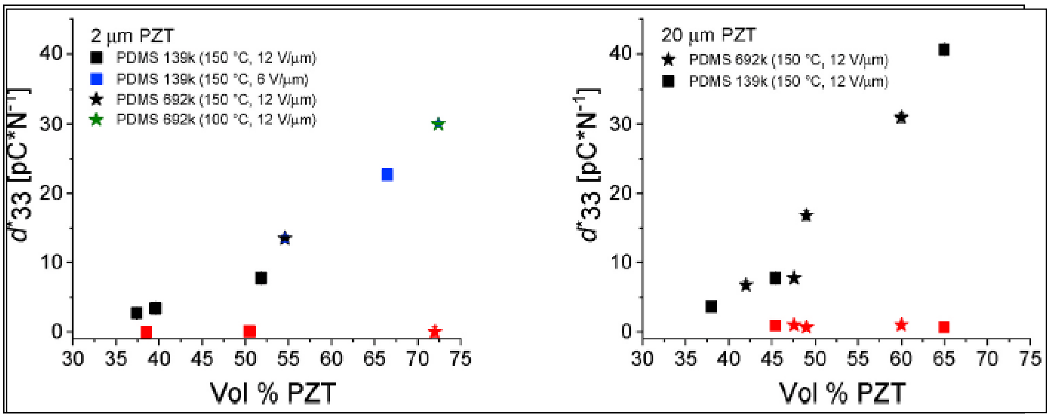

Figure 2.21: Longitudinal piezoelectric coefficient d^*_{33} of various composites containing PZT with particle sizes of 2µm (left) and 20 µm (right), poled under varied circumstances. In red, non-poled reference samples made with PDMS 139 k (square) and 692 k (star) are shown.

2.4.1.2. 0-3 PZT/ PU

PZT/PU composites are very similar to that of PZT/PDMS ceramic particulate composites. The percentage of filler content, particle size, doping, poling conditions, fabrication process, etc. affect the electromechanical properties. The only difference is PU polymer with its specific properties as compared to the PDMS. Any change in the properties will be certainly in the polymer basis if other related parameters are not changed. The graphical representation of the dielectric permittivity and electrical conductivity are below [18],[19].

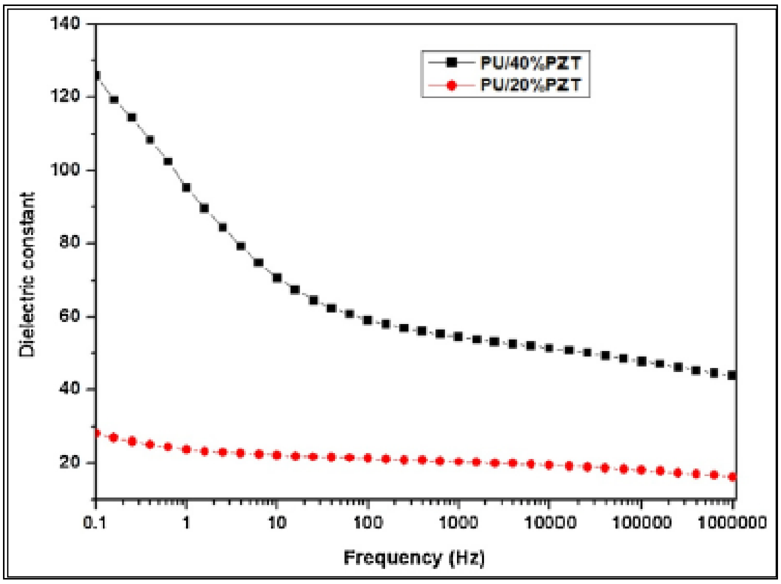

Figure 2.22: Two samples of PU/20% PZT and PU/40% PZT were compared in terms of relative permittivity.

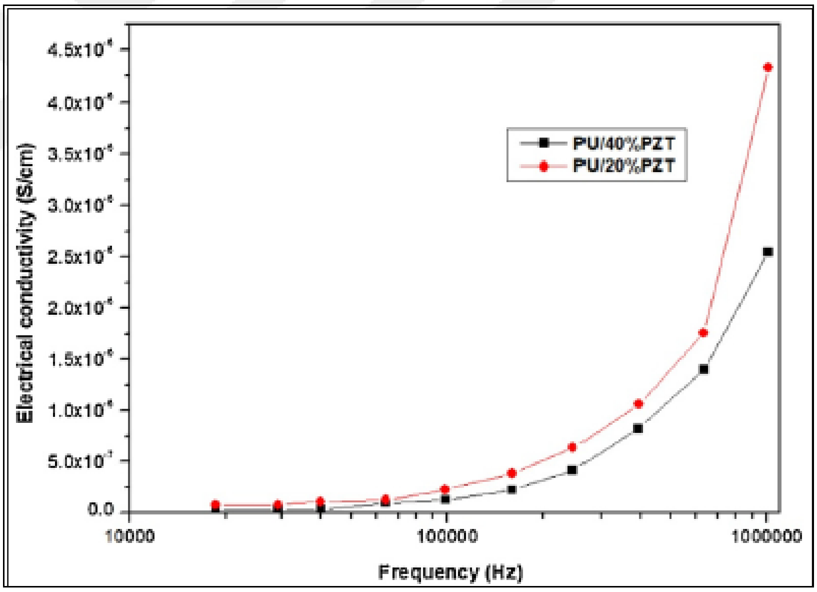

Figure 2.23: PU/20% PZT and PU/40% PZT having similar electrical conductivities were shown.

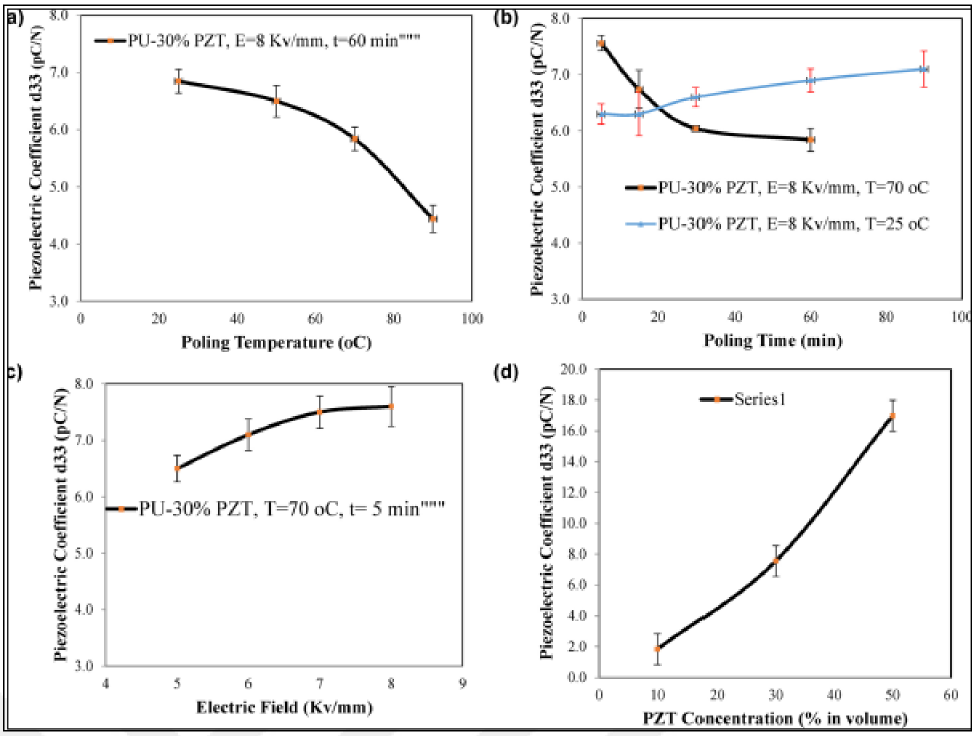

Figure 2.24: The representation of the effect of poling conditions on the 30 vol% PZT/PU composite was given together with the change of d_{33} with respect to different volume percentages.

2.4.1.3. 0-3 PMN-PT/ PU

PMN-PT is a solid solution of PMN and PT where the best quality in terms of electromechanical properties is achieved. As known, there are two forms of PMN-PT where the single crystal form is mainly preferred and utilized in energy harvesting, electrocaloric applications, etc. For example, texturing is the way that many researchers find useful by using templates such as STO and BTO considering the drawbacks and trying to get the best. Recently, there have been investigations on the PMN-PT particulate composites and this added another combination of electroactive composites. This ceramic can be combined with any polymer but mainly with PU and PDMS.

The piezoelectric properties of this electroactive composite are strongly related to the above-mentioned parameters. The pure or doped form of this ceramic is not a match for PZT in some aspects but it is considered to be better than many, among the lead-based piezoceramics. An example of an energy harvester that has PMN-PT as an electroactive component with a PDMS polymer matrix is shown in Fig 2.25. with energy harvesting abilities [20]-[22].

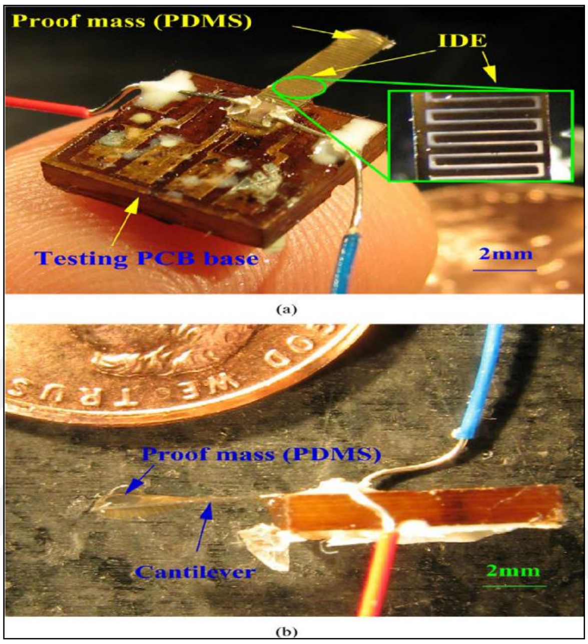

Figure 2.25: An energy harvester made of PMN-PT/PDMS. (a) Aerial view. (b) A view from the side.

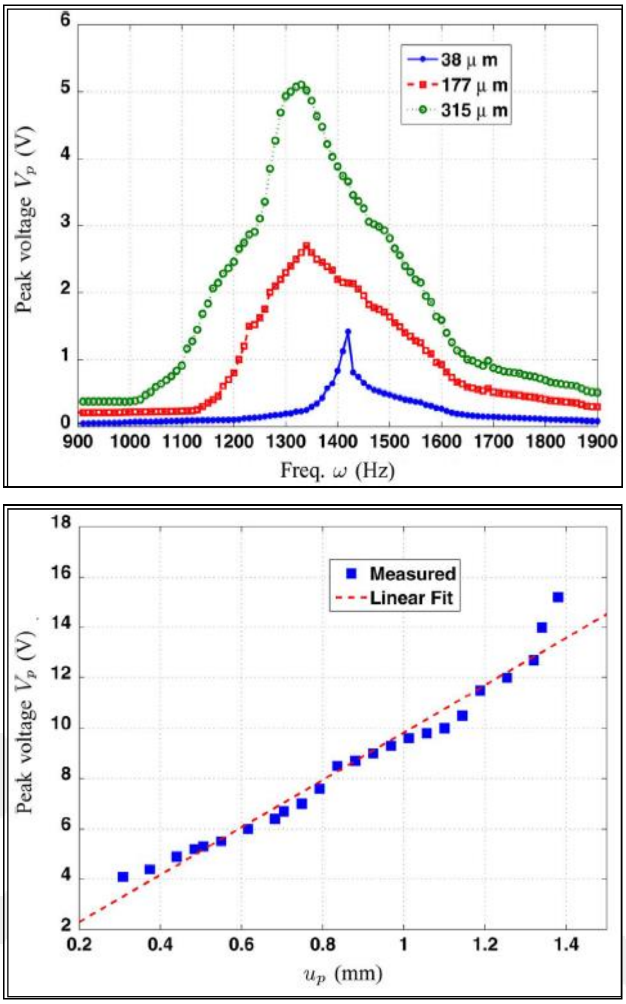

Figure 2.26: Harvester output voltage vs. excitation frequency for three distinct base peak amplitudes (a). (b) Base peak amplitudes around the first natural frequency against output voltage.

2.5. The Electrocaloric Effect

The cooling technology that involves ferroelectrics, antiferroelectrics, and relaxor ferroelectrics is the electrocaloric effect. When an electric field is applied in dielectrics, the reversible thermal changes can be driven either adiabatically or isothermally. Electrocaloric cooling is the replacement of vapor-cycle cooling technology. Theoretically, near the phase transition region, ferroelectrics exhibit higher electrocaloric performance. Throughout the years, studies including this phenomenon have led to significant reports.

$Pb_{0.99}Nb_{0.02}(Zr_{0.75}Sn_{0.20}Ti_{0.05})O_3$ and $PbSc_{0.5}Ta_{0.5}O_3$ ceramics exhibited nearly 2.5K temperature change under the adiabatic conditions. Later on, in antiferroelectric $PbZr_{0.95}Ti_{0.05}O_3$ thin film, the temperature change was 12K under adiabatic conditions and a high electric field of 780kV/cm. Another study proved that high electric fields could be achieved at low voltages in thin films where organic P(VDF-TrFE) was used. Conversely, the negative electrocaloric effect exists when an electric field is applied adiabatically. In this, if the electric field is withdrawn adiabatically material gets warm. In antiferroelectric $Pb_{0.8}Ba_{0.2}ZrO_3$ thin films, a giant positive electrocaloric effect of 45.3 K at 17 ^oC was predicted whereas, $PbZrO_3$ and $Pb_{0.94}Ba_{0.06}ZrO_3$ ceramics near room temperature revealed a moderate negative electrocaloric effect. Furthermore, a large negative electrocaloric effect (about 5K) was demonstrated in La-doped $Pb(Zr_{0.95}Ti_{0.05})O_3$ thin films (0.65 μm) near room temperature, whereas only a positive electrocaloric effect was reported in La-doped $Pb(Zr_{0.85}Ti_{0.15})O_3$ thin films (1 μm) over the entire temperature range of interest, including both room temperature and higher temperatures.

2.5.1. Electrocaloric Phenomena and Basic Explanation with Maxwell Equation

Thermodynamically, Carnot, Brayton, and Ericsson cycles are typical refrigeration cycles. In the Ericsson-like cycle, the external stimulus is either isothermally applied or removed. On the other hand, Carnot-like cycles consist of two isothermal steps and two adiabatic steps.

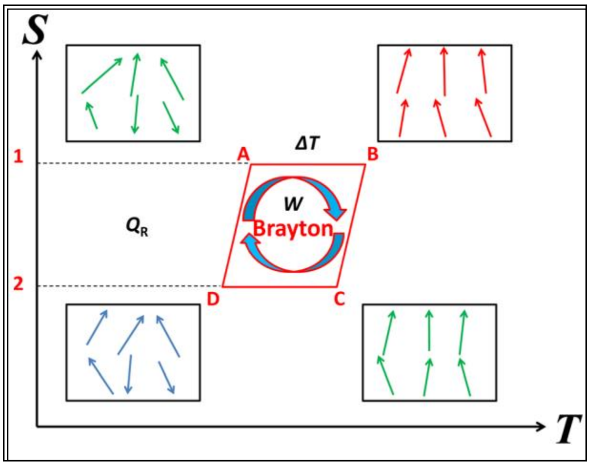

Figure 2.27: In the space of total entropy temperature, a schematic of an ideal electrocaloric Brayton refrigeration cycle is shown.

Details of steps of Brayton refrigeration are given below:

- (A-B) Adiabatic application of external electric field (with no contact with any sink);
- (B-C) Electrocaloric material isofield cooling (with contact with the cold sink);
- (C-D) Adiabatic removal of the external field (with no contact with any sink); and
- (D-A) Isofield heating of the electrocaloric material (with contact with the hot sink).

The region defined by the surface A–B–C–D corresponds to the particular electrical work, but the maximum extracted heat of the electrical Brayton refrigeration cycle is designated as Q_r, i.e., inside the surface 1-A-D-2.

Based on the Maxwell equation (Indirect Method), under adiabatic circumstances, the reversible electrocaloric change in temperature ΔT of an electrically sensitive material caused by a change in external electric field $\Delta E = E_2 - E_1$ may be calculated.

$$\Delta T = -\int_{E_1}^{E_2} \frac{T}{C(E,T)\rho} \left(\frac{\partial P}{\partial T}\right)_E dE, \qquad (2.8)$$

Where P is the polarization, T is the temperature, q is the mass density, and C(E, T) is the heat capacity and all of these variables are affected by both the electric field and the temperature. The isothermal entropy change is of importance since it helps to describe the electrocaloric effect. ΔT or ΔS is frequently maximum around the phase transition, where thermally induced variations in observed polarization P coming from changes in the magnitude $\left(\frac{\partial P}{\partial T}\right)_E$ are biggest.

2.5.2. Characterization Methods of Electrocaloric Materials

The the most of the measurement and characterization of the electrocaloric effect, the indirect method is preferred althought there are discrepancies between direct and indirect method. In addition to that, Clasius- Clapeyron equation has not found large area in the literature but including the latent heat from the first order phase transition distinguishes this calculation from indirect method that is based on the Maxwell equation. The subscript 0 denotes in which order parameter changes across first-order phase transitions.

$$\Delta S = \Delta D_0 (dT_0/dE)^{-1}. \tag{2.9}$$

The pie chart represents the ratio of the indirect and direct method that was utilized in 2016 across the electrocaloric measurements.

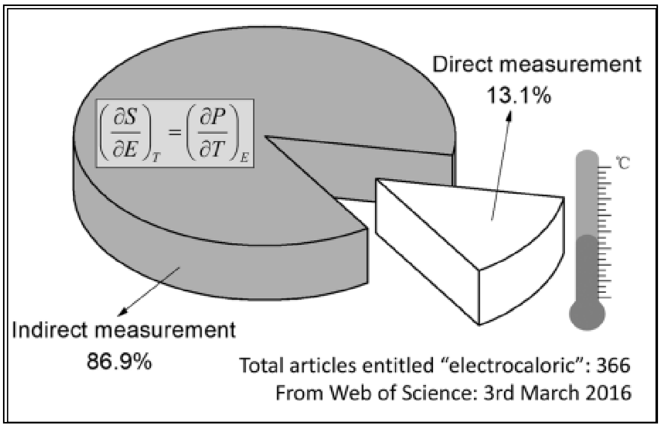

Figure 2.28: According to Web of Science, statistical results on electrocaloric articles include direct and indirect measures.

Mainly the most of the work was carried out to seek for new materials and to improve their properties while the least was done to design heat pump or refrigeration system etc. The effort to design electrocaloric systems and pursuing the direct method has a long way to go considering the fact that Fig 2.28. implies.

There are several ways in measuring and characterizing the direct method as follows:

- Thermocouple and Thermometer
- Differential Scanning Calorimetry (DSC)
- Specifically designed calorimeters
- Infra-red camera
- Scanning thermal microscopy

A comparison of thin/thick film electrocaloric performance can be seen in the table below where different methods are included.

Table 2.7: Comparison of typical electrocaloric effect values measured directly in thin and thick films.

Material	h (μm)	T (°C)	ΔE (kV/cm)	ΔT (K)	$\lvert\Delta T/\Delta E\rvert$ (K cm/kV)	Method
$(Pb_{0.86}La_{0.08})(Zr_{0.65}Ti_{0.35})O_3$	0.45	45	1200	40	0.033	SC
$PbZr_{0.8}Ti_{0.2}O_3$	0.15	25	67	0.1	0.0015	SC
$BaZr_{0.2}Ti_{0.8}O_3$	12	40	97	4.9	0.051	SC
0.9PMN-0.1PT	13	25	105	0.23	0.0022	SThM
$(Cd_{0.83}Pb_{0.17})_2Nb_2O_7$ MLCs	45	−179	100	0.8	0.008	SC
$Pb(Sc_{0.5}Ta_{0.5})O_3$ MLCs[a]	64–72	18	125	3.5	0.028	SC
Doped $BaTiO_3$ MLCs	6.5	47	300	0.5	0.0017	TC
$BaTiO_3$ MLCs	1.4	80	176	1.8	0.010	DSC
$BaTiO_3$ MLCs	1.4	80	800	7.1	0.0089	DSC
P(VDF-TrFE) 68/32 mol. %	10–15	33	1600	20	0.0125	SC
P(VDF-TrFE-CFE)[b]	4–6	30	1500	16	0.011	SC
P(VDF-TrFE-CFE)[c]	50	27	1000	4	0.004	DSC/IR
P(VDF-TrFE-CFE)[d]	11–12	25	900	5.2	0.0058	IR
Terpolymer/BNNSs/BST67[e]	6	30	2500	50.5	0.0202	SC
P(VDF-TrFE)/BST75[f]	80	79	600	2.5	0.0042	DSC
Terpolymer[g]/PMN-PT	7–15	30	1800	31	0.017	SC
Polymer[h]/graphene	11	25	400	5.2	0.013	SC

In a conclusion, indirect measurement based on Maxwell relations might offer broad patterns for analyzing the behavior of electrocaloric responses and could be useful for comparing various results from the same class of materials. At this point of the study, it may still be useful as an approximation tool for estimating the electrocaloric effect. Direct measurements of heat and temperature change are needed at this point for conclusive verification of the electrocaloric action [23].

3. EXPERIMENTAL STUDY

This chapter includes the fabrication of ceramic pellets and piezo-active composites with their structural, mechanical and electrical characterizations. The fabrication of bulk 67.5PMN-PT ceramic pellets was achieved through the solid-state calcination method. Following the fabrication of ceramic powder, 0-3 PMN-PT-PU piezoactive composite was produced. Additionally, PZT5A-PU was fabricated to find out the effect of the powders. Also, PDMS polymer was used to obtain PZT5A-PDMS composites to understand the difference between the structural and electronic behavior of 0-3 piezo-composites with different polymer matrices.

Core materials that were utilized and purchased in the fabrication of pellets and composites are given below:

- PZT5A powder w/o Binder from Sunnytec Co., Ltd., Taiwan with particle size: 4-5µm
- 0.675PMN-0325PT powder Solid State Method (fabricated) with particle size: 4-5µm
- SLYGARD 186 (Two Part Silicone Elastomer) from Dow Chemicals
- Sika Polyurethane (Two Part Polymer) & Sikamoll as Elastisizer from TEKNO Chemicals
- Silver Electrode G3692 ACHESON Silver DAG 1415 mit Pinsel 25g

3.1. Fabrication of 0.675PMN-0325PT and Ceramic Pellets

Before the fabrication, the stoichiometric calculation was performed according to the given chemical reaction formula to determine the amount of ceramic powders required.

$$0.225\ MgNb_2O_6 + PbO + TiO_2 \longrightarrow 0.675[Pb(Mg_{1/3}Nb_{2/3})]O_3 + 0.325\ [PbTiO_3].$$

Necessary materials and the amount of powders are as follows:

- 6.887 g $MgNb_2O_6$ which was fabricated from Niobium (V) Oxide (Nb_2O_5) 99.5% (metals basis) 100 Mesh powder (Alfa Aesar), and Magnesium carbonate hydroxide penta-hydrate ($4MgCO_3.Mg(OH_2).5H_2O$), light, 98% (Alfa Aesar)
- 22.319 g PbO Lead(II) oxide, 99.9% 325 mesh powder from Alfa Aesar
- 2.596 g TiO_2 Titanium (IV) oxide, rutile, 99.5% min (metals basis) 1.0-2.0 micron APS powder
- Binder: Polivinil Butrial (PVB) Polietilen Glikol (PEG) Benzil Butil Phatalat
- After the calcination: Calcined PMN-PT + 2wt% excess PbO ball-milled to press the pellets

***Columbite method was chosen to produce $MgNb_2O_6$ and calcination at 1000°C for 6h was necessary for the pure phase formation.

At first, PbO, TiO_2, and $MgNb_2O_6$ were tared and mixed thoroughly in ethanol media and ball-milled for a day. Following the ball-mill process, the powder was dried and calcined at 850^{O}C for 4h. After the calcination the powder was taken and weighed to add 2wt% excess PbO, ball-milled (*from MSE Engineering*) then dried. Considering the weight of the powder, a little amount of binder and desired amount of methyl-ethyl-ketone were added, ball-milled, and dried again. The powder was crushed in the mortar to get a finer-sized grain structure and sieved by a 425µm mesh-sized sieve. Eventually, 1g of powder was weighed and put in the mold and pressed under 2.04-tonne pressure for 2 minutes to reach the 16mm in diameter circular shape. Shaped green body placed in a furnace (*MSE Furnace*) for sintering. Before placing pellets into the furnace, atmosphere powder (PbO) was added in the ratio of 1/3 weight of the pressed pellets, to compensate for the loss of the PbO in the furnace atmosphere. The sintering process was slow-paced and made of 9 steps:

- 275 min 250°C (Heating)
- 30 min 250°C (Heating)
- 50 min 275°C (Heating)
- 30 min 275°C (Waiting)
- 435 min 600°C (Heating)
- 60 min 600°C (Waiting)
- 110 min 1150°C (Heating)
- 120 min 1150°C (Waiting)
- End

When the pellets were ready for characterization, Ag electrode was applied for conductivity. The furnace regime is shown below:

- 140 min 700°C (Waiting)
- 30 min 700°C (Heating)
- End

3.1.1. Structural Characterization of Ceramic Powders

X-Ray diffraction (XRD) patterns, particle size analyses, and scanning electron microscopy (SEM) images are necessary to gather data about structural properties and electrical performance since both of them are strongly related. XRD patterns help to detect any secondary phase because it plays a crucial role in the electrical properties. On the other hand, particle size analyses are required to see if the fabrication process ended up having particle sizes in the range of the desired scale. The characterization involves both PZT5 and 67.5PMN-32.5PT. Rigaku Dmax 2200, Tokyo, Japan X-Ray diffraction device, Philips XL30, FEI Co., USA SEM microscope, and Malvern Mastersizer 2000 particle size analyzer, UK were utilized in this work.

3.1.2. Structural and Electrical Characterization of Ceramic Pellets

PMN-PT ceramic powders were fabricated by the solid-state calcination method and then pressed (*MSE Single Axis Press*) with 2.04Mpa for 2 minutes and sintered to a final shape of pellets. After these steps, structural and electrical characterizations were carried out to obtain results and discuss the differences in pellets with respect to the PMN-PT-PU piezo composites. In doing so, characterization methods were utilized as follows:

- XRD and SEM (*names of the devices were stated in the previous chapter*.)
- Dielectric constant and admittance (*HIOKI 3532-150 LCR HiTESTER, HIOKI 9261 Test Fixture*.)
- Electrocaloric and hysteresis-strain (*RADIANT Tecnologies Inc. Precision HV Interface, RADIANT Tecnologies Inc. Precision LC, TREK Model 610D Amplifier Controller, MTI Fotonic Sensor, VWR Advanced VMS-C10 Hot Plate, Labo Stirrer and Labo 5M 2 Heat Exchanger*.)
- Piezoelectric coefficient measurements (*G^{W}INSTEK GPD-3303S DC Power Supply,Trek High Voltage Amplifier, SINOCERA YE2730A d_{33} Meter*.)

3.2. The Fabrication of Composites

This section includes composite manufacturing steps in details. It starts with PZT5A/PDMS and ends with PMN-PT/PU composites.

3.2.1. Fabrication of Composites: PDMS - PZT5A

PDMS is a two-component silicone elastomer and to cure the polymer, part A and part B have to be mixed. Part A is the base polymer and part B is the curing agent where the ratio of these components should 10:1 to get the best result. When the polymer is ready after stirring for 5 minutes, desired volume percentage of PZT5A (*weighed on Precisa XB 220A*) was crushed in the mortar and divided into three groups to reach optimum mixing.

Then the powder was added to the PDMS part by part and each time stirred for 5 minutes. Then, the polymer-ceramic composite was desiccated in for 3 minutes. Finally, the composite was poured onto the glass surface (*Tape Casting device*) and put into the stove (*BINDER brand*) and waited for 20 minutes at 120°C for curing at a high temperature.

3.2.2. Fabrication of Composite PU - PZT5A

PU is a another polymer that involves the base polymer and the curing agent to be cured at room temperature but elastisizer can be added to get a more flexible PU. First, part A and elastisizer were mixed and stirred for 3 minutes together. Then, part B was added to cure the polymer. Following the same preparation steps as PDMS-PZT5A fabrication, the desired volume percentage of PZT5A was crushed in the mortar and divided into three groups. Then the powder was added to the PU part by part, and each time stirred for 5 minutes then desiccated for 3 minutes. Lastly, the composite was poured onto the glass surface and let rest for 4 to 5 hours or sometimes waited until the next day.

3.2.3. Fabrication of Composite PU – 67.5PMN-PT

PU was fabricated as mentioned earlier and following the same steps as PU-PZT5A fabrication, the desired volume percentage of 67.5PMN-PT was crushed in the mortar and divided into three groups. Then the powder was added to the PU mixed and stirred as same as the previous fabrications. Lastly, the composite was poured onto the glass surface and let rest for 4 to 5 hours.

3.3. Characterization of the Composites

The following two sections consider structural, mechanical and electrical characterization steps of the composites. The same manner was followed here to be convenient as in the previous sections.

3.3.1. Structural and Mechanical Characterization

Composites are versatile and their electrical and mechanical properties are not high but in the middle of their parent material classes. The mechanical properties are strongly related to the microstructure of composites. SEM analysis is necessary since surface and cross-sectional areas are visible with higher resolutions and magnifications and to obtain data about the microstructure. Imperfections, cracks, voids, and loosely-bound ceramic particles caused by insufficient sintering time or temperature may cause an electrical and mechanical performance dropdown. Thus, an inspection of composites microstructure via SEM analyses is highly recommended and required. In tensile tests, polymer to ceramic powder ratio is important thus, samples were carefully chosen, considering the fact that, if the samples were high in powder ratio that would affect the results and end up early rupture of the specimen.

3.3.2. Electrical Characterization

The electrical characterization is the core element of the study thus, characterizations has to be carefully studied. The applied methods were listed below as follows:

- Capacitance
- Hysteresis
- Energy harvesting, and (*RIGOL DG1022 Function Arbitrary Waveform Generator, Agilent Technologies InfiiVision DSO-X 2024A Digital Storage Oscilloscope, LDS PA500L Power Amplifier with LDS Sample Shaker.)*
- d_{33} measurements via Berlin court

Other than energy harvesting, all measurements were recorded by the same devices which were highlighted in section 3.1.2.

4. RESULTS AND DISCUSSION

4.1. Structural Characterization of Ceramic Powders

This section provides data about PZT5A powder, and PMN-PT. Structural inspection is necessary since electrical properties are closely bound to the microstructure. Hence, XRD, particle size analyses and SEM images must be taken as vital results.

4.1.1. Results for PZT5A Powder

The XRD pattern of the pure PZT5A ceramic powder is shown in Figure 4.1. The pattern represents the perovskite (pseudocubic) structure without any secondary phase. The secondary phase must not be in the crystal structure since it deteriorates the electrical performance.

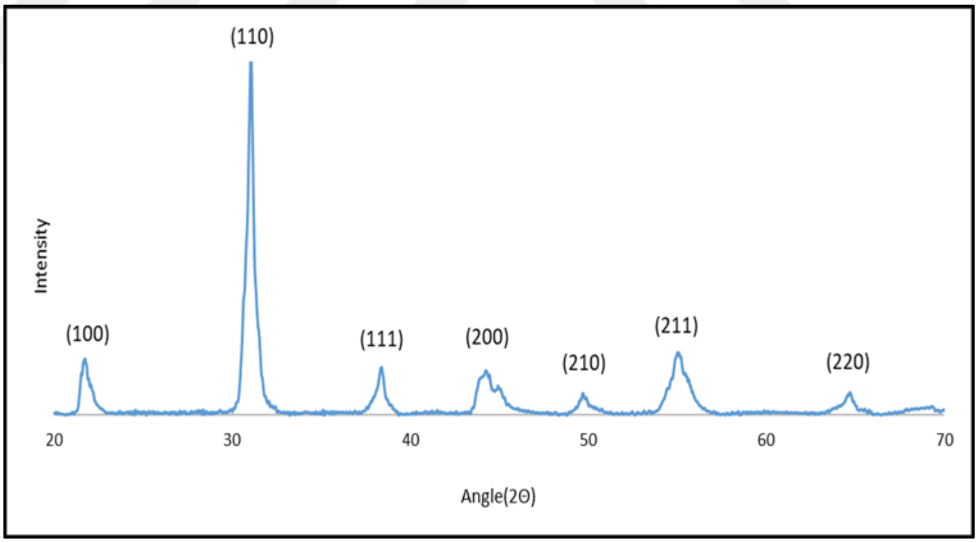

Figure 4.1: The XRD pattern of PZT5A.

This analysis indicates that the size distribution of particles is in the range of 1-10µm with an average particle size of 4.42µm.

Normally, the particles would be in the range of less than or equal to the 1µm but the ceramic powder that was used in this work was commercial purchased and no post-processing was applied. The SEM image was taken at 1000x magnification and the scale is 20µm. It is not possible to observe each particle alone since they tend to stick together as clusters because of particle interactions caused by electrical forces.

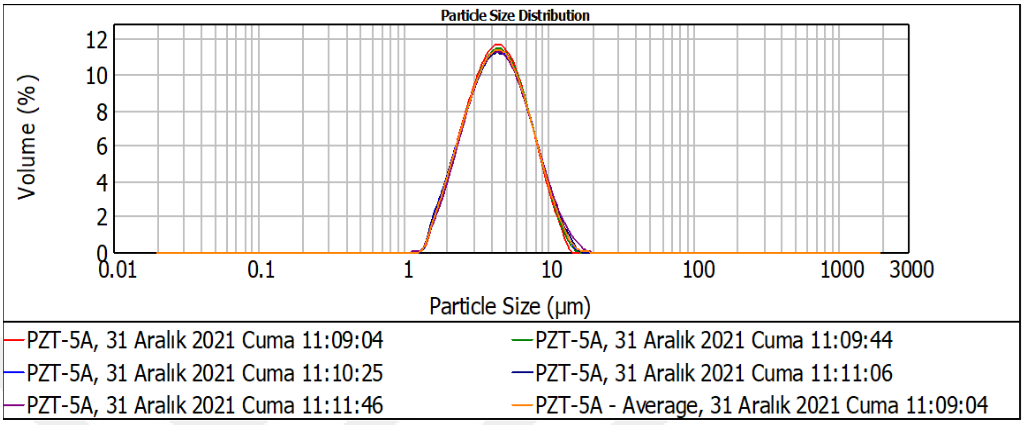

Figure 4.2: The particle size distribution of PZT5A.

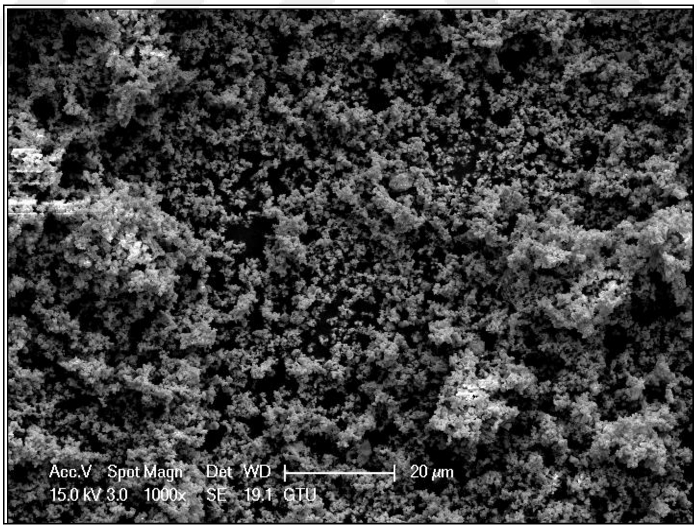

Figure 4.3: The SEM image of PZT5A-1000x magnification.

4.1.2. Results for 67.5PMN-32.5PT Powder

The 67.5PMN-32.5PT powder was fabricated by the solid-state calcination method. After the main procedure, the powders were calcined at 850˚C for 4 hours to obtain purity. The XRD pattern proves that the fabrication process was successful without generating any secondary phase existence. Later on, the fabricated ceramic pellets showed superior performance due to their structural purity.

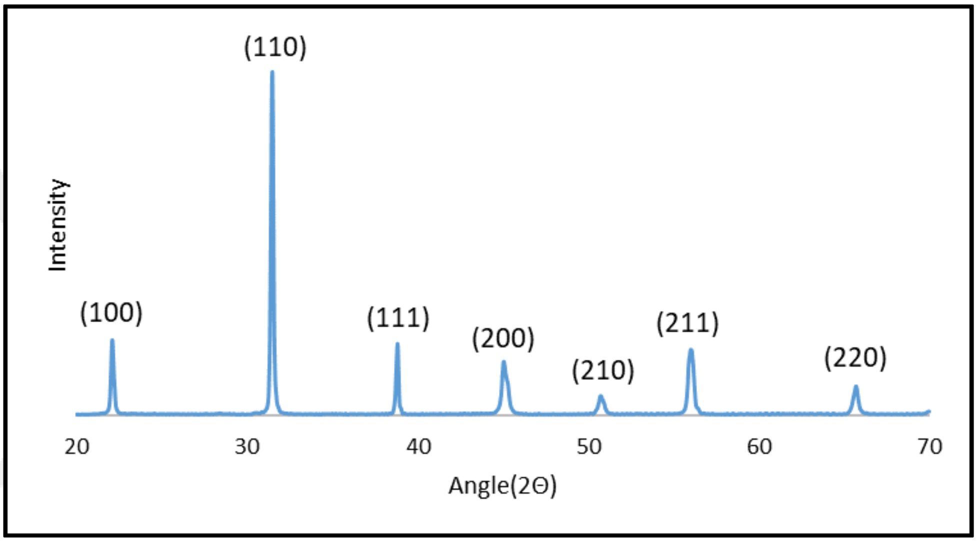

Figure 4.4: The XRD pattern of 67.5PMN-32.5PT.

Figure 4.5. represents that the size of the particles is in the range of 0.1-100µm but most of the particles are populated in the 1-10µm range with an average particle size of 4.48µm. In order to decrease the size of the particles and to avoid clustering, sieving, and crushing in the mortar before the analysis is necessary and has to be applied for several times.

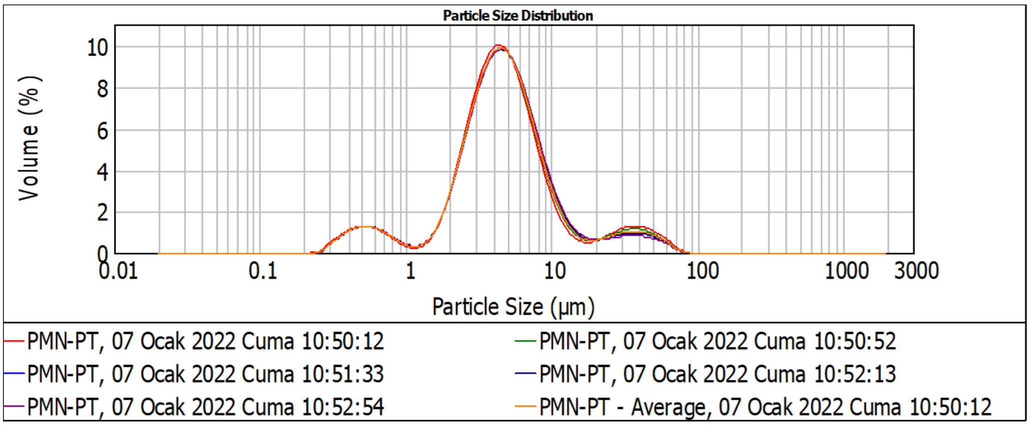

Figure 4.5: The particle size distribution of 67.5PMN-32.5PT.

The SEM image of the 67.5PMN-32.5PT powder at 2000x with a scale of 10µm is shown. Again, the morphology of the ceramic particles is not distinctive. They are seen as clusters in the image.

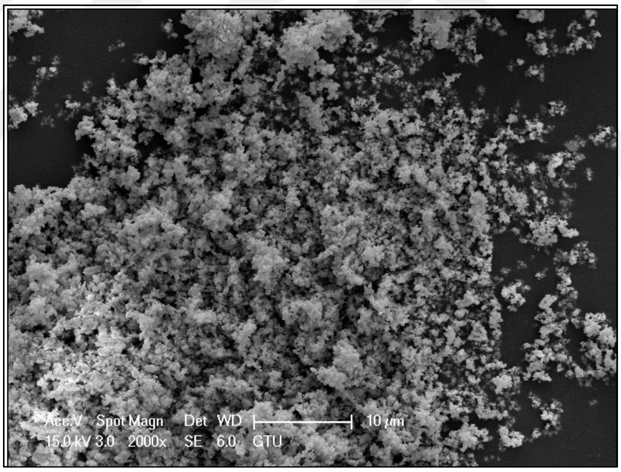

Figure 4.6: The SEM image of 67.5PMN-32.5PT–2000x magnification.

4.2. Characterization of 67.5PMN-32.5PT Pellets

Both the structural and electrical characterizations are explained in detail below.

4.2.1. Structural Characterization

Microstructural imperfections cause a deterioration of the electrical performance thus, SEM images are needed to have a vision of whether the sintering was sufficient or if any structural impurities are present. Figure 4.7 indicate that at 250x and 1000x magnifications sintered grains are equiaxed without any porosity in the microstructure. Mechanical integrity can be seen as a whole with small voids which does not affect properties in a larger perspective.

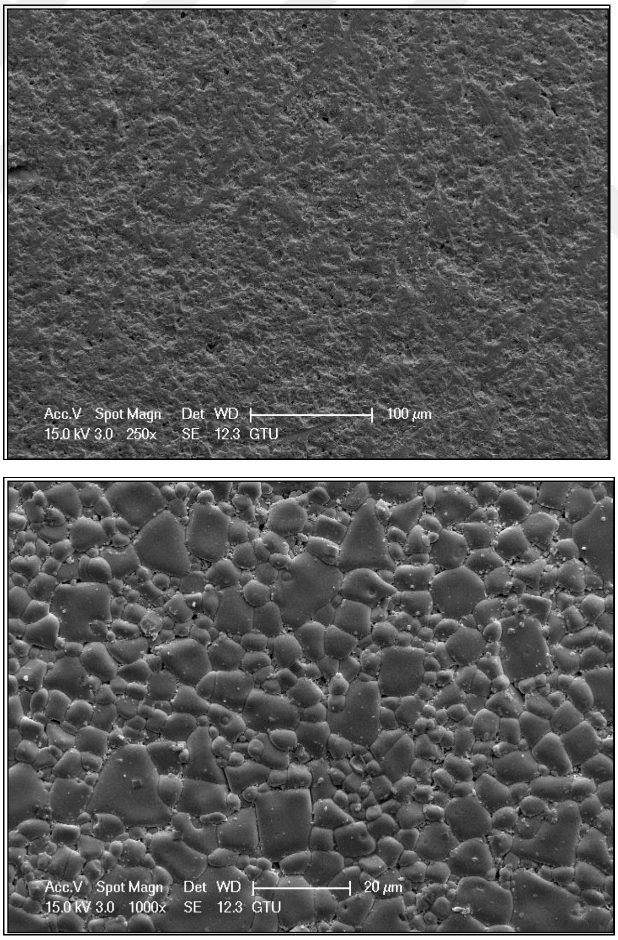

Figure 4.7: The SEM image of sintered 67.5PMN-32.5PT pellet at 250x and 1000x magnification.

The support from the XRD data is also required which informs that the pure perovskite phase exists and therefore secondary phases shall not affect the properties. The XRD pattern showing the pure phase can be seen below.

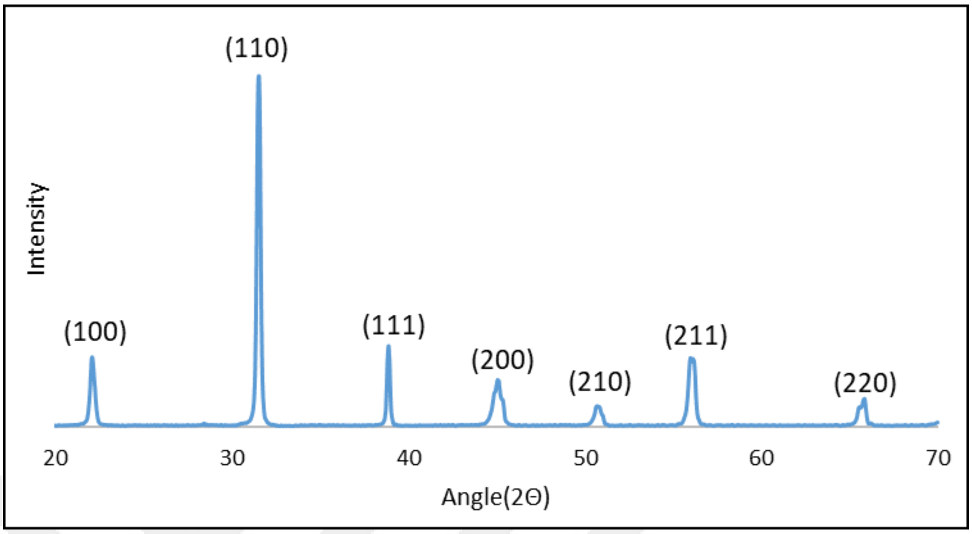

Figure 4.8: The XRD pattern of 67.5PMN-32.5PT pellet.

Inspection of piezoelectric properties along with the dielectric constant (ε_r) and admittance to get familiarized with the ceramic product is vital. Therefore, a dielectric constant at room temperature and temperature dependency of the dielectric constant is required to modify the pellets thus achieving better properties for device applications.

4.2.2. Electrical Characterization

Three pellets were prepared for electrical characterization. The silver electrode was applied to the surfaces of ceramic pellets and d33 values were recorded after poling. The first pellet was poled at 60 kV for 50ms under AC electric field and as a result, 404pC/N was achieved . The second and the third was poled at 25 kV/cm for 15 minutes under DC field. The obtained results for these pellets were 569 and 557pC/N, respectively. The first pellet was insufficiently poled. Although it would be enough to pole a pellet for 50ms by 60kV under an AC field, this pellet was not the best candidate to obtain results with high precision.

Microstructural imperfections or electrodes might be problematic while taking care of these experiments. Nevertheless, hysteresis and electrocaloric measurements were better than expected.The hysteresis curve was slightly formed under 30ms-10kV/cm, and 30ms-20kV/cm poling conditions. The electric field and frequency were not enough to generate domain wall motions and align the domains. It appears that polarization is not sufficient and either electric field or frequency has to be increased. Apparently, 50 ms was better than 30ms and the sample was tested all the way up from 20 kV/cm to 60kV/cm. By applying the electric field for 50ms and increasing the field voltage by 3 times 20kV/cm, the improvement of the hysteresis behavior was achieved. The remnant polarization was 3 times higher than that of the 30 ms test values but the coercive field was at the same position on the axis. After rising the frequency, the well-known typical hysteresis curve was seen but electric fields higher than 40kV/cm was not performable. Due to the long exposure to the electric field, the risk of an electrical breakdown is highly likely possible. The final test was performed under 1000ms which is a long time under the AC field, and it forces ceramic pellets more. Each time the remnant polarization was raised but the coercive field remained the same. It can be seen that the upper limit to pole the pellet is close. Because there are no big differences between 100ms and 1000ms where each time the applied electric field has to be decreased to prevent the electric breakdown. The hysteresis curve reached its final form as in Figure 4.9.

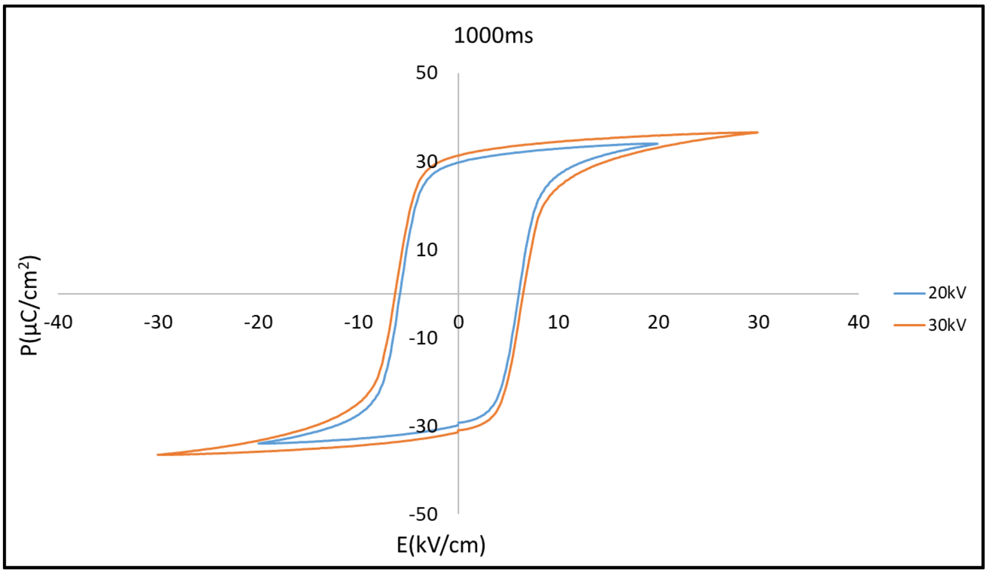

Figure 4.9: The hysteresis behavior at room temperature, under 20 kV/cm and 30 kV/cm for 1000 ms.

This test is proof of the piezoelectricity and the characteristics of PMN-PT pellets produced by the solid-state calcination method. Poling efficiency under an AC field with a variety of frequencies and applied voltages can be clearly seen. The decision of the optimum poling conditions and the duration of the field is determined by the hysteresis curve but the temperature dependency of these pellets has to be considered. Hysteresis behavior at different temperatures are necessary if these pellets are to be used in solid-state cooling. Polarization vs electric field graph with respect to temperature changes are shown under 40kV/cm for 300ms. As temperature rises remnant polarization along with the coercive field gets wider and increased. High temperature behaves as an obstacle that causes harder domain rotation and prevents the domain wall motion but as it gets cooler this happens inversely. The area inside the hysteresis curve shows the dielectric loss and a narrow field is preferred if the ceramic is chosen to use for capacitive applications.

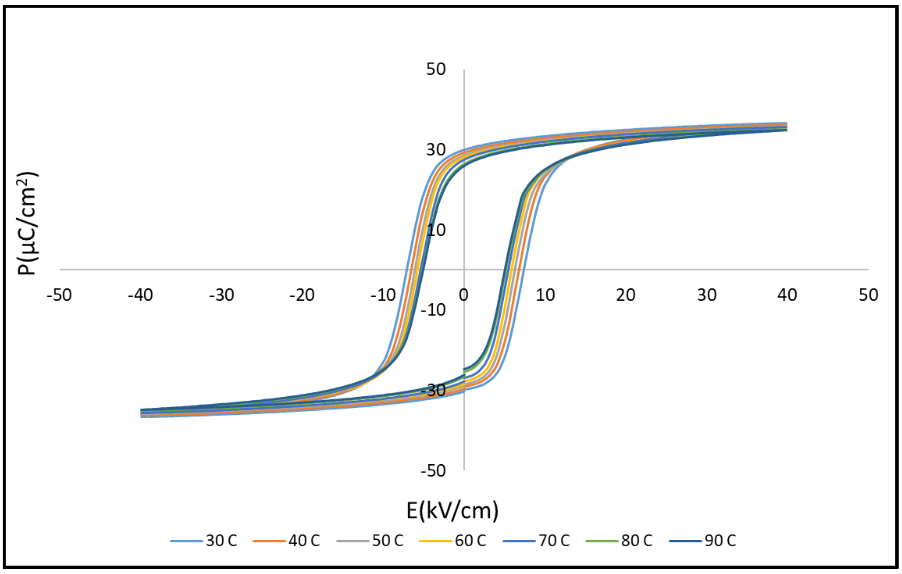

Figure 4.10: The hysteresis behavior at different temperatures under 40kV/cm for 300 ms.

Investigation of piezoelectricity requires the ability to transform electrical energy into mechanical energy, and strain is the property that has to be considered. When the electric field is applied mechanical energy is generated that allows ceramic to oscillate in the direction of the electric field. Two pellets were used during the experiment and the strain values were gathered by applying a 10, 20, and 30kV/cm electric field for 1000ms. Each time when the electric field was increased, the strain values became stronger and larger. It proves that under 1000ms and 30kV/cm this ceramic shows better performance.

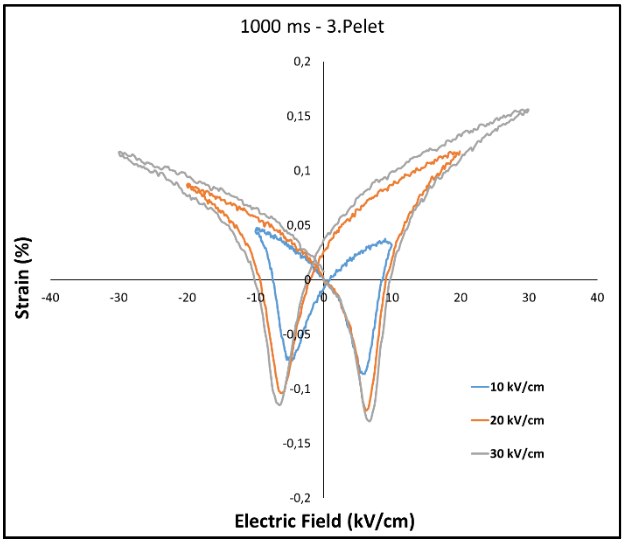

Figure 4.11: The strain behavior of pellet from 10-30kV/cm for 1000 ms.

Inspection of piezoelectric properties along with the dielectric constant and admittance to get familiarized with the ceramic product is vital. Therefore, a dielectric constant at room temperature and temperature dependency of the dielectric constant is required. The results were satisfying because the larger the value, the greater the performance of the capacitance. Thus, capacitive applications need higher dielectric values. The frequency range is between 1000 to 100000Hz and the scale is logarithmic. Broad range scanning is necessary to detect the change in the behavior of ceramics.

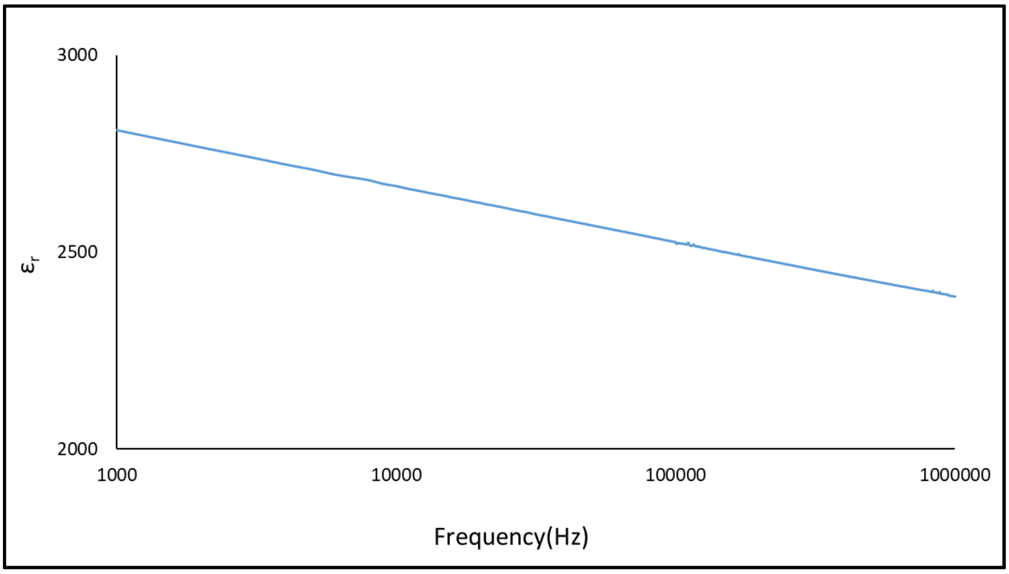

Figure 4.12: 67.5PMN-32.5PT dielectric constant vs frequency graph showing the dependency of the dielectric constant to the frequency.

The dielectric constant at different frequencies with respect to the temperature is shown and this data represents the Curie temperature of the ceramic. At approximately 175°C, the Curie temperature is visible along with the highest dielectric constant value at different frequencies. At 1kHz, the dielectric constant and dielectric loss are relatively high, but the dielectric loss is so small that it can be negligible. After the Curie temperature, the perovskite phase shifts to the cubic phase, and the dielectric constant goes downwards.

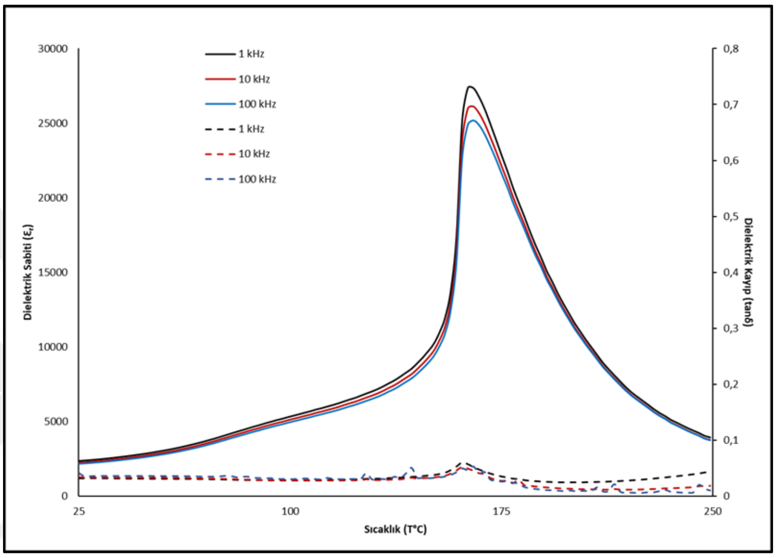

Figure 4.13: 67.5PMN-32.5PT dielectric constant vs temperature graph showing the dependency of the dielectric constant to the temperature.

In the Figure 4.14, the blue line shows the admittance data. The admittance graph basically shows resonance and anti-resonance peaks which are the specific frequencies that trigger the ceramic body and cause-specific electrical pulses to detect environmental changes. The signals are vital in ultrasound devices, and underground, and marine applications. The orange line represents the poling efficiency of the ceramic. If the ceramic is poled, the phase angle shifts from lower to higher values. It has to be noted that the phase angle increases at the point where resonance frequency is increasing and vice versa is also happening at the anti-resonance frequency.

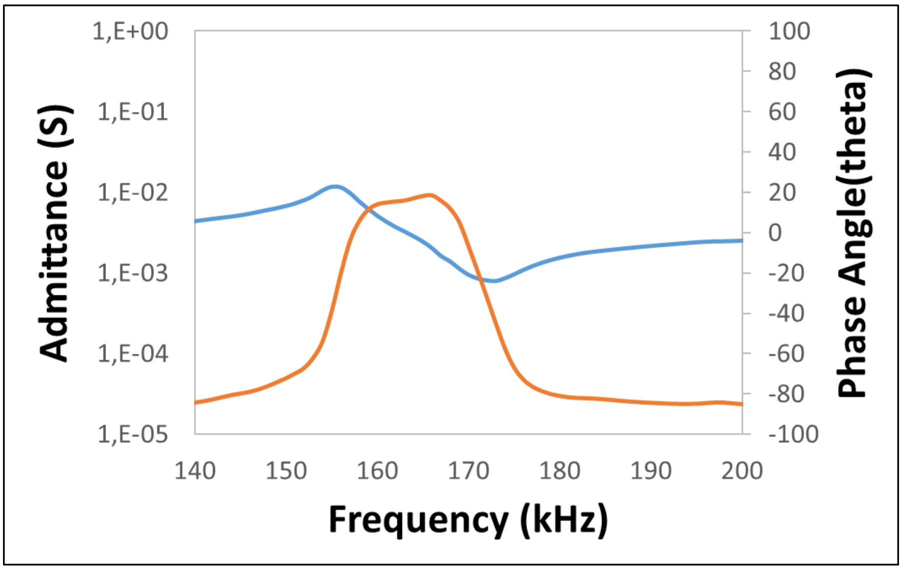

Figure 4.14: 67.5PMN-32.5PT admittance and phase angle graph.

4.3. Characterization of Composites

4.3.1. Structural and Mechanical Characterization of Composites

In the first section, SEM images and tensile test results will be inspected and following this, electrical test results of the composites will be discussed in detail. The comparison of each characterization is given as a whole for every composite type. For example, if the dielectric constant is going to be discussed then PZT5A-PU, PMN-PT-PU and PZT5A-PDMS will be examined together.

4.3.1.1. Tensile Test of Specimens

Composites are versatile and their electrical and mechanical properties are not high but in the middle of their parent material classes. The mechanical properties are strongly related to the microstructure of composites. In our tests, polymer to ceramic powder ratio is important thus, samples were carefully chosen, considering the fact that, if the samples were high in powder ratio that would affect the results and end up early rupture of the specimen.

PZT5A-PDMS, PZT5A-PU, and PMN-PT-PU composites with altering powder contents from 0 to 45 vol% were fabricated and cut in the size of 90 mm initial length and 20 to 22mm width. The first test belongs to pure PDMS. Due to the early break of the pure PDMS-2, it is not included. In the table 4.1, all PDMS composite samples are shown. Tests start from pure PDMS and go up to 15 vol% PZT5A-PDMS. The initial length of the samples is equal because of the device standards but width and thickness are free to change to some extent.

Table 4.1: The PDMS samples with their initial dimensions.

Test Number	Sample Name	Sample Type	Thickness(mm)	Width(mm)	Initial Length(mm)
1	Pure PDMS	Polymer	0.853	20	90
2	Pure PDMS-3	Polymer	0.923	20	90
3	PDMS-5VOL-1	Polymer	0.841	20	90
4	PDMS-5VOL-2	Polymer	0.811	20	90
5	PDMS-5VOL-3	Polymer	0.883	20	90
6	PDMS-10VOL-1	Polymer	0.912	21.5	90
7	PDMS-10VOL-1-Repeat	Polymer	0.912	21.5	90
8	PDMS-10VOL-1-Repeat	Polymer	0.912	21.5	90
9	PDMS-10VOL-2	Polymer	0.881	19	90
10	PDMS-10VOL-3	Polymer	0.838	20	90
11	PDMS-15VOL-1	Polymer	0.889	20	90
12	PDMS-15VOL-2	Polymer	0.905	20	90
13	PDMS-15VOL-3	Polymer	0.809	20	90

Table 4.2: The summary of the tests of PZT5A-PDMS specimens.

Test Number	Color	Fmax N	Max force elongation %	Stress Mpa	Breaking Strength N	Elongation at break mm
Pure PDMS		16.519	191.21	0.968	16.519	172.09
Pure PDMS-3		42.7	363.17	2.313	42.7	326.85
PDMS-5VOL-1		23.972	226.88	1.425	22.518	204.33
PDMS-5VOL-2		32.018	299.17	1.974	32.018	269.25
PDMS-5VOL-3		37.209	320.87	2.107	37.167	288.97
PDMS-10VOL-1		11.402	129.74	0.581	0.144	0.1
PDMS-10VOL-1-Repeat		16.475	178.43	0.84	16.186	161.46
PDMS-10VOL-1-Repeat		30.219	309.34	1.541	30,05	279.06
PDMS-10VOL-2		30.756	380.46	1.837	30.739	343.34
PDMS-10VOL-3		26.196	288.23	1.563	0.242	0.12
PDMS-15VOL-1		21.569	181.54	1.213	21.562	165.29
PDMS-15VOL-2		21.896	207.58	1.21	21.744	187.19
PDMS-15VOL-3		15.315	151.33	0.947	14.531	142.62

At first, pure PDMS samples were tested. The change in the test results was visible and there was an increment in the mechanical properties. Because of the sample holder jaws, the first measurement was not satisfying the expected values. But the true result belongs to pure PDMS-3. As the powder's volume percentage increases, mechanical properties become no longer high enough and it can be explained by the microstructure of specimens. Initially, there is only one component, and that is a polymer. Polymer chains are strong enough to compensate for high loads but if ceramic powders were introduced into the polymer that would no longer be possible. It separates polymer chains and makes the structure unstable in the terms of polymeric behavior. Also, in our table, there exist improper results that belong to PDMS-10 vol%-1, which had to be tested continuously due to the sample holder jaws. But, generally, considering the bigger picture, it can be said that, specimens' behavior change as a result of alternating powder volume. As the volume percentage increases, the maximum load that a sample can withstand reduces. It can be clearly seen in figure.

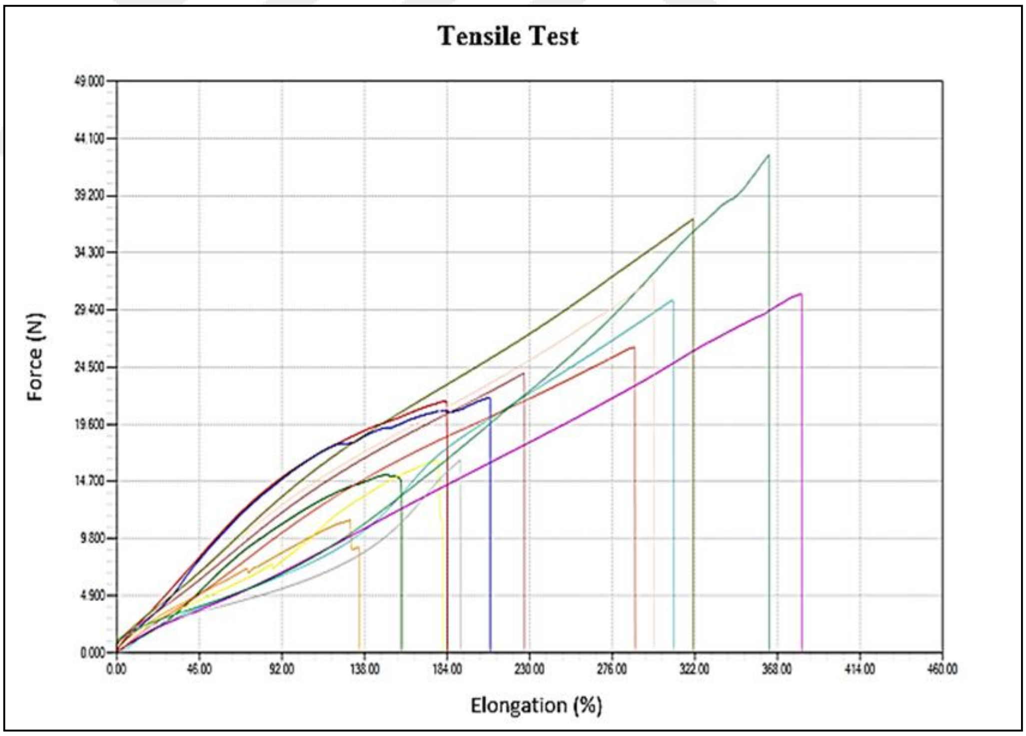

Figure 4.15: Graphical representation of the test results along with mean, standard deviation, maximum and minimum values.

The second part of the characterization includes PZT5A-PU and PMN-PT-PU samples. First, pure PU samples were tested then the powder ratio is continuously increased. By comparison, pure PU would not reach higher loads than PDMS can withstand. But, the powder volume ratio was higher than in PDMS samples. Because the limit was not achieved until samples reach 50 vol% vol percent. The limit for PDMS was 30 vol% so it was necessary to not get too close to that limit and stop the tests at a 15 vol% volume fraction of PZT5A. Alternatively, 25 vol% PMN-PT was also on the to-be-tested list. It was important to see if there would be any mechanical property change with the type of the powder.

Table 4.3: The PZT5A-PU and PMN-PT-PU samples with their initial dimensions.

Test Number	Sample Name	Sample Type	Thickness(mm)	Width(mm)	Initial Length(mm)
1	Pure PU-1	Polymer	0.896	20	90
2	Pure PU-2	Polymer	0.848	20	90
3	Pure PU-3	Polymer	0.88	20	90
4	PZ25-PU-1	Polymer	0.911	20	90
5	PZ25-PU-2	Polymer	0.869	20	90
6	PM25-PU-1	Polymer	0.877	20	90
7	PM25-PU-2	Polymer	0.877	20	90
8	PZ45-PU-1	Polymer	0.948	20	90
9	PZ45-PU-2	Polymer	0.9	20	90
10	PZ45-PU-3	Polymer	0.959	20	90

At first glance, PU and PDMS are far away from each other in terms of mechanical strength. The volume percentage of ceramic powders is the limiting factor that affects their performance mechanically. This is obvious if a comparison is made between 25 vol% PZT5A-PU and 45 vol% PZT5A-PU. Additionally, the type of ceramic powder may change mechanical properties but in our case, it is only a possibility and more tests have to be accomplished to record a trustworthy dataset. In the graphical representation, the overview of the current situation can be seen. The force that a sample can withstand decreases as the powder volume ratio is increased. 40 vol% PZT5A-PU, is showed mechanical performance between 25 and 45 vol%. Exceeding that volume percentage results in a drop in properties listed below.

Table 4.4: The summary of the tests of PZT5A-PU and PMN-PT-PU specimens.

Test Number	Color	Fmax N	Max force elongation %	Stress Mpa	Breaking Strength N	Elongation at break mm
1		19.817	39.71	1.106	0.144	0.14
2		18.723	41.83	1.104	18.686	37.77
3		21.442	46.78	1.218	0.144	0.13
4		22.888	17.84	1.256	22.626	16.18
5		26.735	23.44	1.538	25.926	21.24
6		18.843	12.13	1.074	16.845	11.5
7		17.502	6.87	0.998	0.068	0.1
8		27.373	9.03	1.444	0.111	0.36
9		12.319	7	0.684	0.037	0.01
10		11.76	3.16	0.613	0.135	0.29
Mean		19.74	20.78	1.104	8.472	8.77
St.Deviation		5.224	16.33	0.292	11.052	12.92
Max		27.373	46.78	1.538	25.926	37.77
Min		11.76	3.16	0.613	0.037	0.01

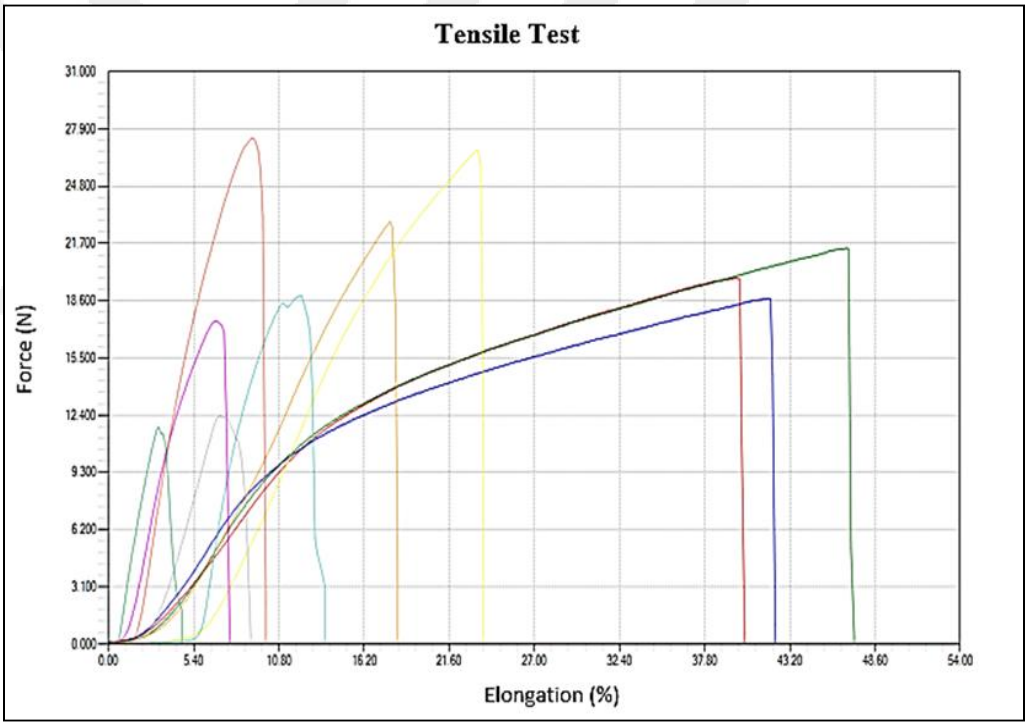

Figure 4.16: Graphical representation of the test results along with mean, standard deviation, maximum and minimum values.

Table 4.5: The 40 vol% PZT5A-PU samples with their initial dimensions.

Test Number	Sample Name	Sample Type	Thickness(mm)	Width(mm)	Initial Length(mm)
1	PZ40-PU-1	Plastic	0.85	20	90
2	PZ40-PU-2	Plastic	0.949	20	90
3	PZ40-PU-3	Plastic	0.893	20	90

Table 4.6: The summary of the tests of 40 vol% PZT5A-PU specimens.

Test Number	Color	Fmax N	Max force elongation %	Stress Mpa	Breaking Strength N	Elongation at break mm
1		14.778	9.37	0.869	0.02	0.16
2		18.488	11	0.974	0.054	0.16
3		16.284	10.07	0.912	14.685	9.66
Mean		16.517	10.15	0.918	4.92	3.33
St.Deviation		1.866	0.82	0.053	8.457	5.48
Max		18.488	11	0.974	14.685	9.66
Min		14.778	9.37	0.869	0.02	0.16

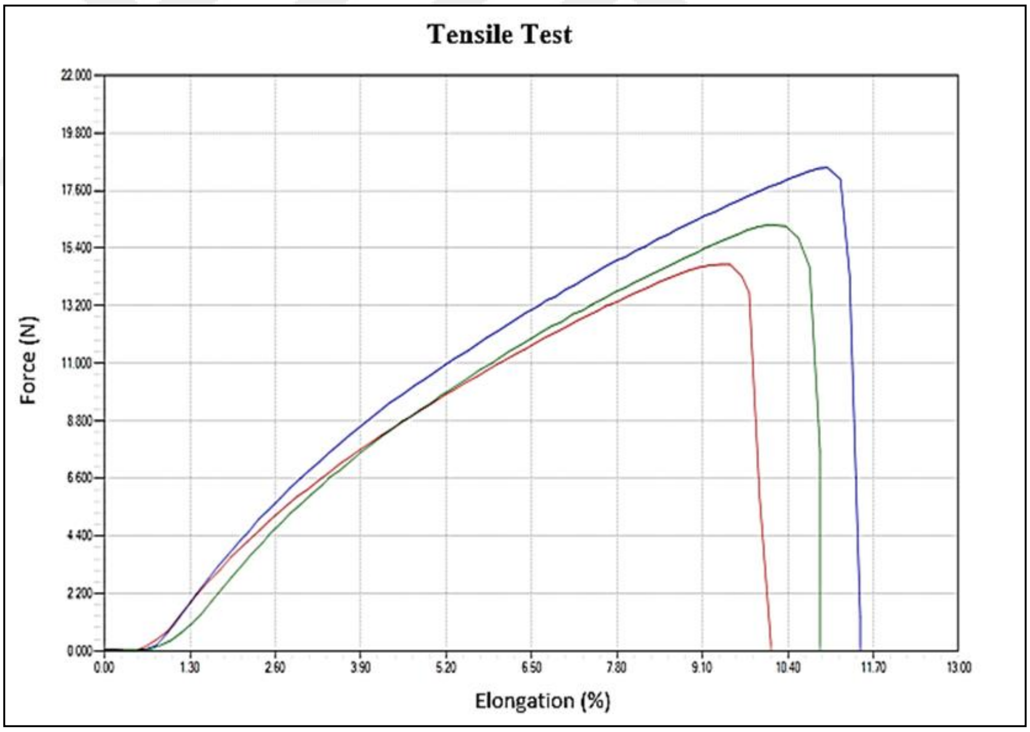

Figure 4.17: Graphical representation of the test results along with mean, standard deviation, maximum and minimum values.

4.3.1.2. SEM Analysis

SEM analysis is necessary since surface and cross-sectional areas are visible with higher resolutions and magnifications and to obtain data about the microstructure. Imperfections, cracks, voids, and loosely-bound ceramic particles caused by insufficient sintering time or temperature may cause an electrical and mechanical performance dropdown. Thus, an inspection of composites microstructure via SEM analyses is highly recommended and required. The PZT5A-PDMS composites were produced in different volume fractions of ceramic powder. 13, 16, 20, 25, and 30vol% PZT5A-PDMS samples SEM images were taken and analyzed. The surface was polymeric and shiny therefore, cross-sections of the composite samples were investigated.

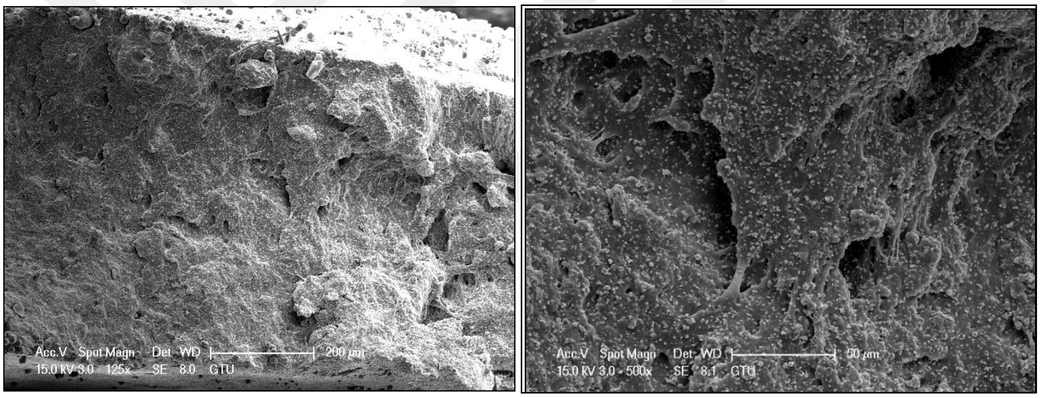

Figure 4.18: The SEM images of 13 vol% PZT5A-PDMS sample.

These images were taken at 500x and 1000x magnifications. The scale of the first image is 50 microns and the second is 20 microns. The small rounded shapes are ceramic particles. Some were aggregated and some were well dispersed in the polymeric matrix. The polymer separates each particle from the other. This is the main reason why ceramic-polymer 0-3 composites are not showing high performance as compared to other types of ceramic-polymer composites. The production process seems fine since most of the particles are homogeneously distributed in the polymer.

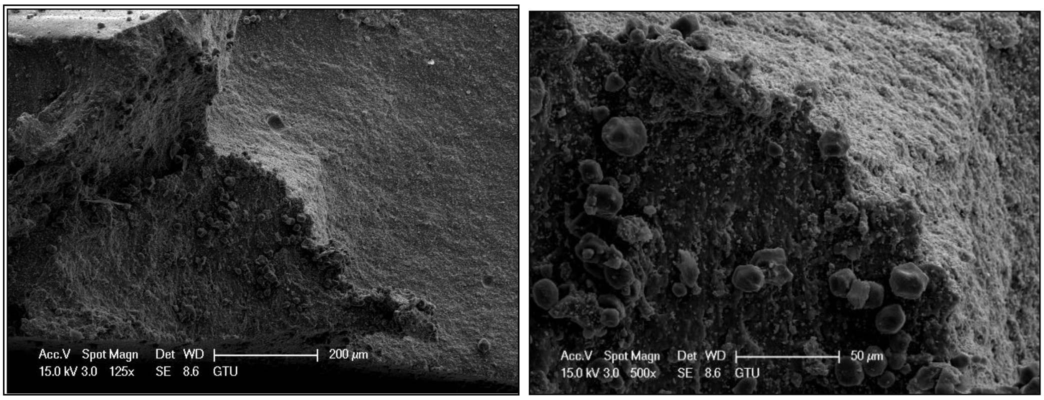

Figure 4.19: The SEM images of 16 vol% PZT5A-PDMS sample.

As the particle/polymer ratio increases, the microstructure gets almost fully occupied by ceramic particles. The particles tend to stick together because of the surface energy and the more aggregated particles dominate the sample.

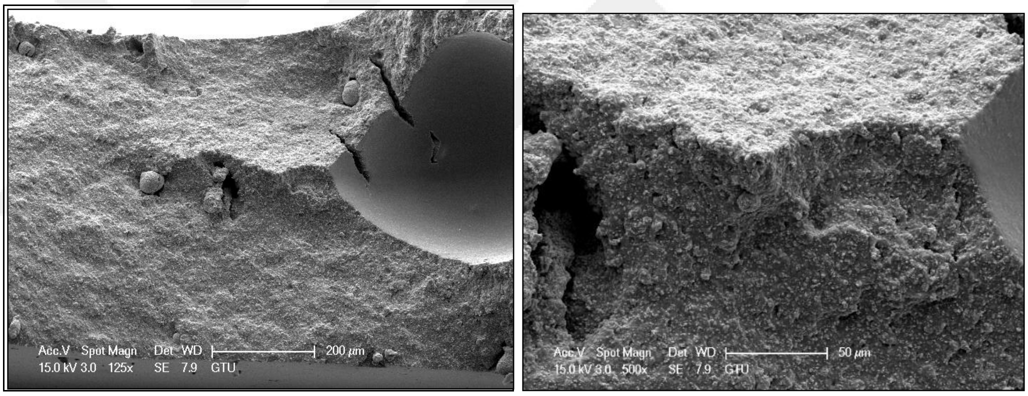

Figure 4.20: The SEM images of 20 vol% PZT5A-PDMS sample.

Images are very similar to the ones before. The ceramic particles dominate the structure. The more the ceramic particle the more fragile the sample but to enhance the properties particles are required to be higher in amount. When the sample was cut into pieces to take cross-sectional SEM images, some particles leave the structure and introduce voids or holes behind. On the right-hand side image, a surface without any ceramic particles can be seen because of the situation stated above.

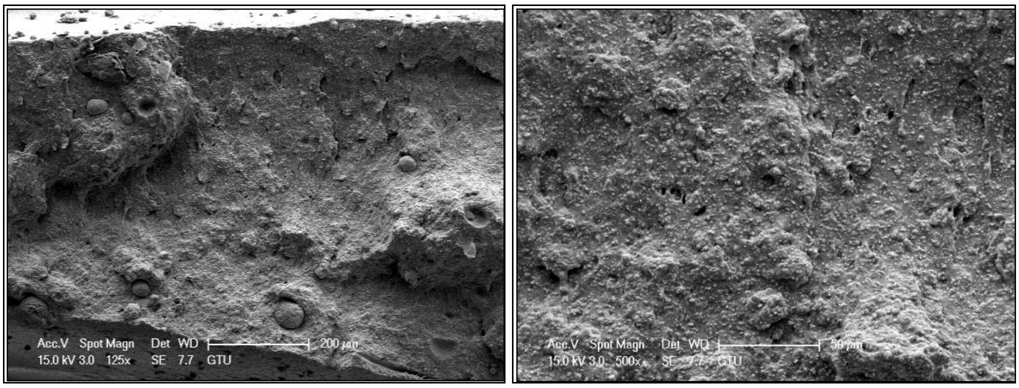

Figure 4.21: The SEM images of 25 vol% PZT5A-PDMS sample.

The SEM images that belong to 25 vol%PZT5A/PDMS are similar to that of 13, 16, and 20 vol% PZT5A/PDMS samples. The cross-sectional surfaces of the samples are not flat, because before the analyses samples were ripped off by hand.

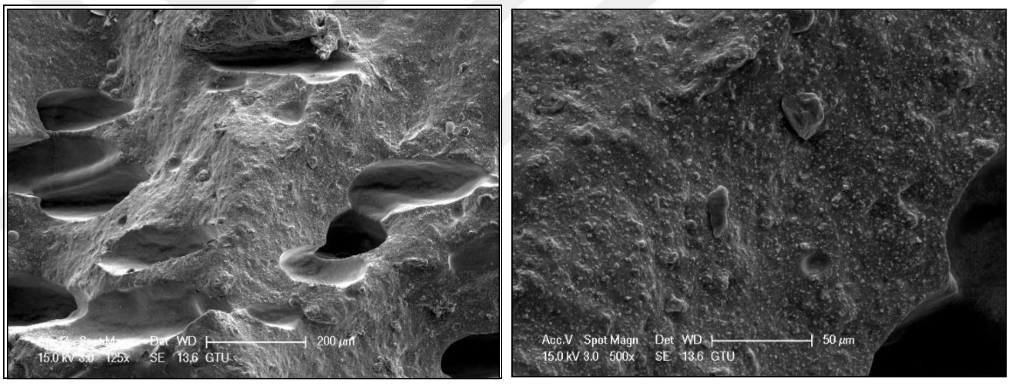

Figure 4.22: The SEM images of 30 vol% PZT5A-PDMS sample.

The 30 vol% PZT5A/PDMS was the last composite sample that was fabricated with the highest particle ratio. As a result of this, the microstructure is at the limit and can not accept higher ceramic powder additions. The holes are large and deep where the sample is almost at the edge of a rupture. But considering the whole structure, the ceramic particles are more or less gathered all together as aggregates. The PZT5A/PU samples were fabricated in different volume fractions. SEM images that were gathered from 25, 45, 50, and 55 vol% samples were very similar to that of the PZT5A/PDMS composites.

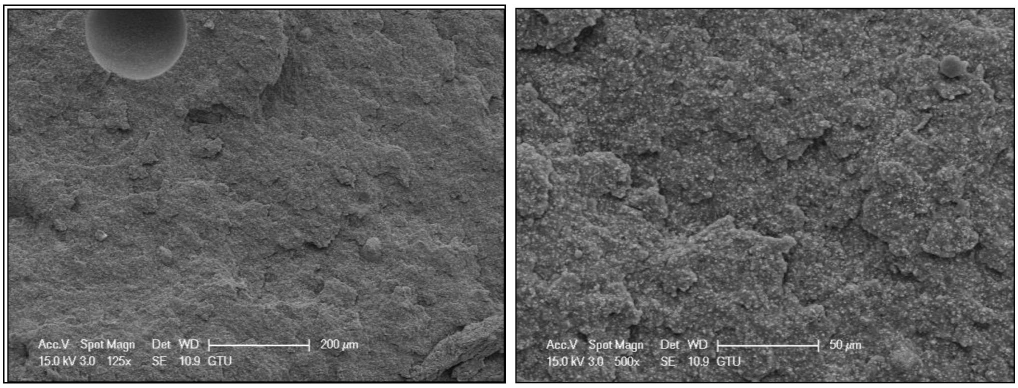

Figure 4.23: The SEM images of 25 vol% PZT5A-PU sample.

In the images, the sample's cross-section is very much plate-like. The polymer type hugely affects the microstructure since it forms the backbone of the composite structures.

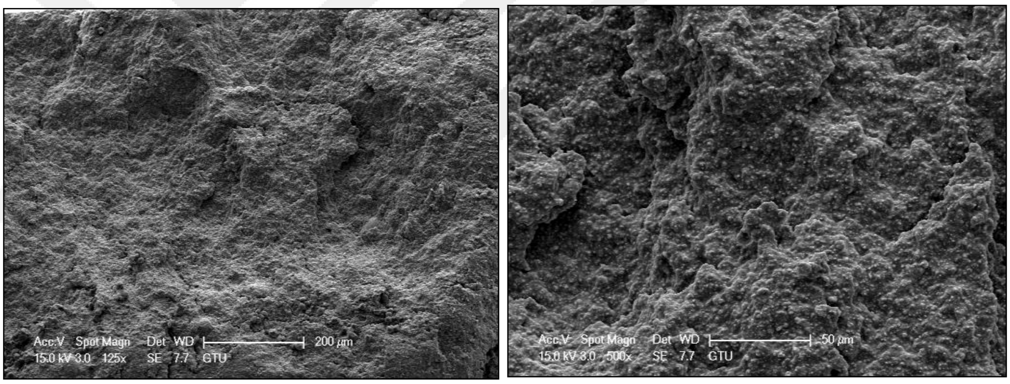

Figure 4.24: The SEM images of 45 vol% PZT5A-PU sample.

The microstructure is plate-like with ceramic particles as clusters. The surface of the cross-section is well formed.

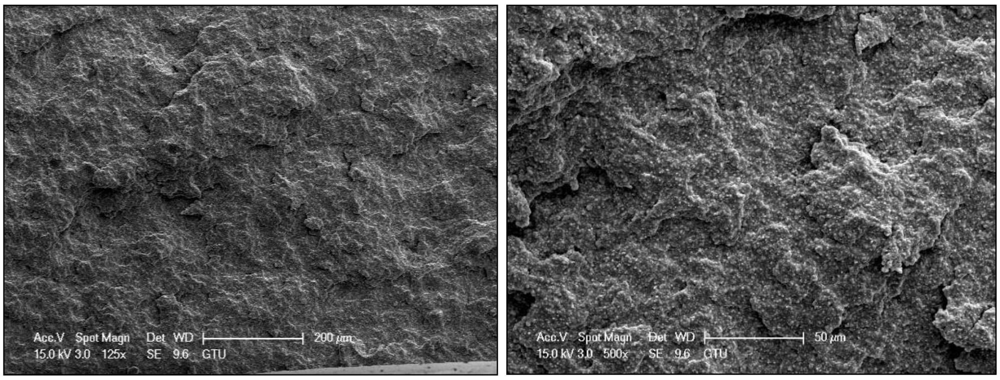

Figure 4.25: The SEM images of 50 vol% PZT5A-PU sample.

The 50 vol% is a high ratio but the polymer is still mechanically stable without any integration issue. The microstructure is as same as 25,45 vol% composites. The limit was 54 vol%, where holes were left behind by fallen down particle clusters. This is a sign where there is no further powder addition is possible. It was the same for PZT5A/PDMS composites. The holes can be seen in the figure below. The PZT5A/PU composites were more resistant as compared to the PZT5A/PDMS.

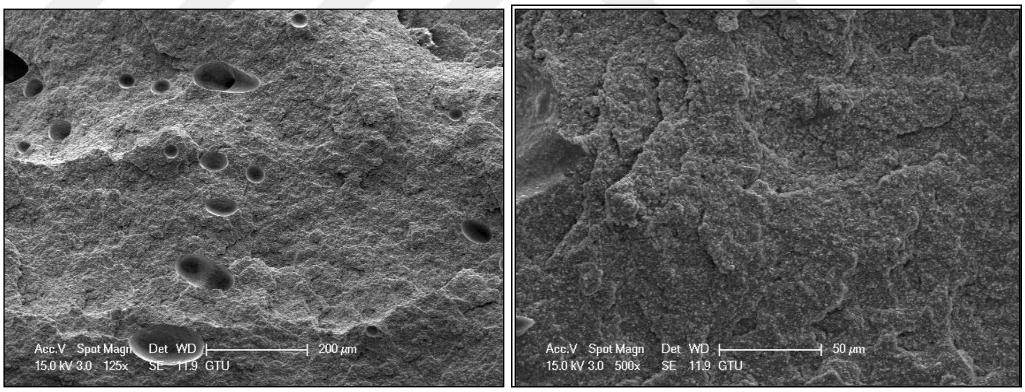

Figure 4.26: The SEM images of 54 vol% PZT5A-PU sample.

Lastly, PMN-PT-PU composite samples were prepared for SEM analyses according to the predefined powder contents which are 25, 40, and 45 vol%.

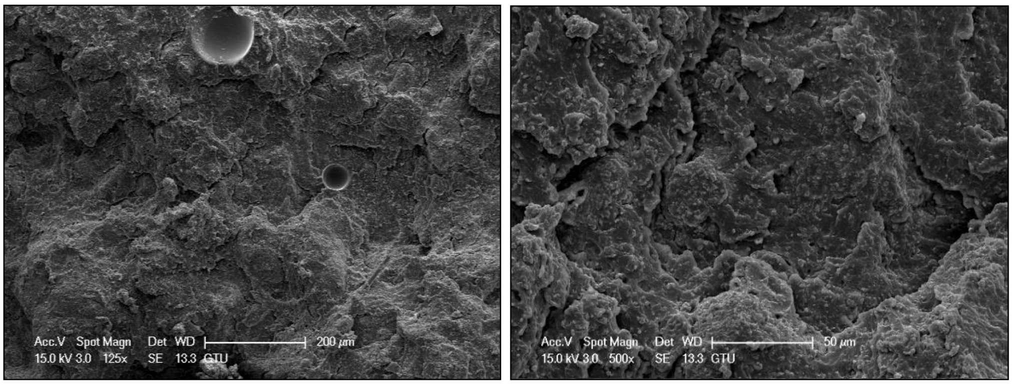

Figure 4.27: The SEM images of 25 vol% PMN-PT-PU sample.

The texture of the microstructure is very much like PZT5A-PU samples. Still, ceramic particles are trapped within polymer sections. The following SEM images are similar to that of the images above. Again, the surface of the composite was shinny, and the best way to inspect the microstructure was to cut the sample in half and take shots of the cross-section. The 40 vol% and 45 vol% samples were showing no difference from the 25 vol% samples. The only change in the structure was the amount of the powder and the more agglomerated ceramic particles within the polymeric matrix.

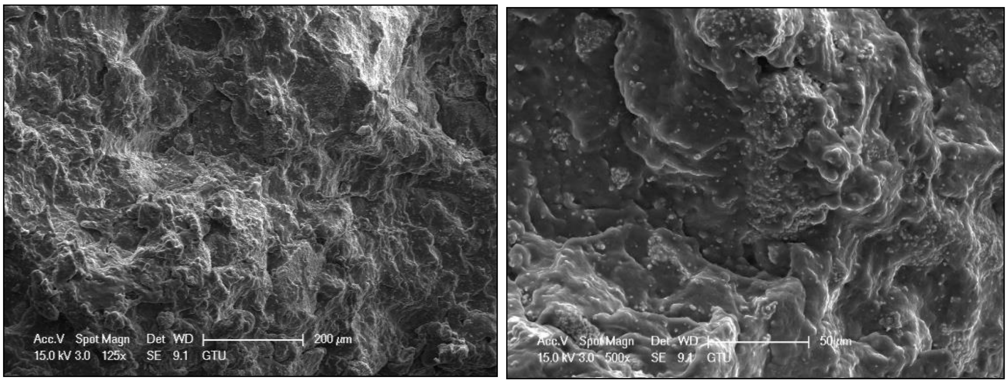

Figure 4.28: The SEM images of 40 vol% PMN-PT-PU sample.

As was said before, the agglomeration of ceramic particles became more striking as the ratio of the powder increased. It can be compared by investigating 40 and 45 vol% samples.

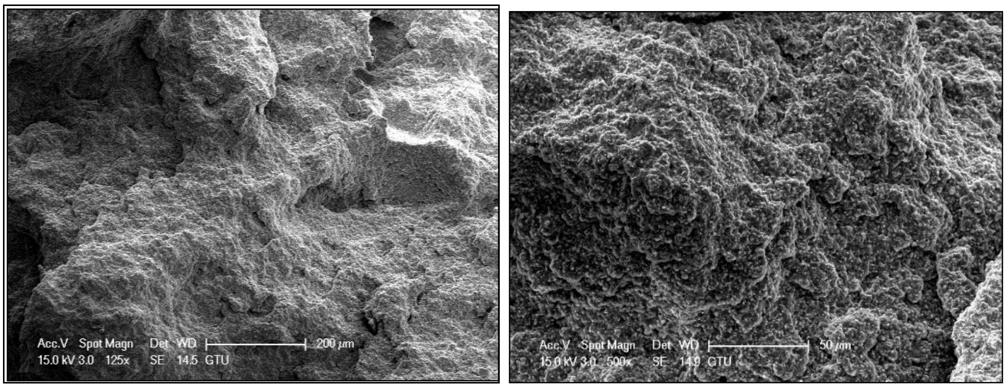

Figure 4.29: The SEM images of 45 vol% PMN-PT-PU sample.

4.3.2. Electrical Characterization

4.3.2.1. Dielectric Measurements

The dielectric constant is an important property since the composite materials can be chosen for specific capacitive applications. The higher the dielectric constant the better the capacitance. From the composites' point of view, the best way to improve the material is to add ceramic powder as much as possible. This thesis concept was to examine 0-3 composites which is why the amount of the powder had to be very well calculated. There is an amount of the powder that the polymer matrix can get interacted and mechanical integrity would not be compromised. This threshold value is vital since it is the maximum amount that can be added and mixed thoroughly within the polymeric matrix.

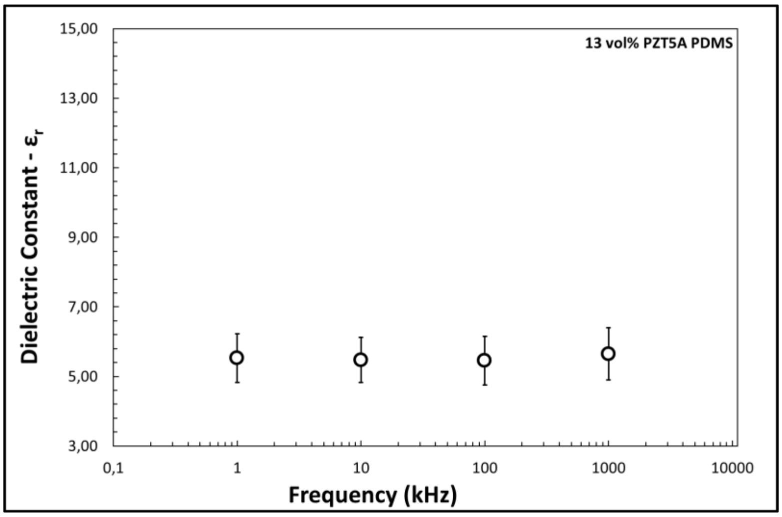

Figure 4.30: The dielectric constant vs frequency data of 13vol% PZT5A-PDMS composite.

The first attempt was to add small volume fractions of powder to the PDMS matrix. The amount of the powder was insufficient and the dielectric constant was relatively low. The range of the constant was between 5 and 7. If a comparison has to be made, these values are incomparable with the bulk ceramic pellets because the polymeric matrix prevents the interaction of ceramic particles and reduces the expected performance.

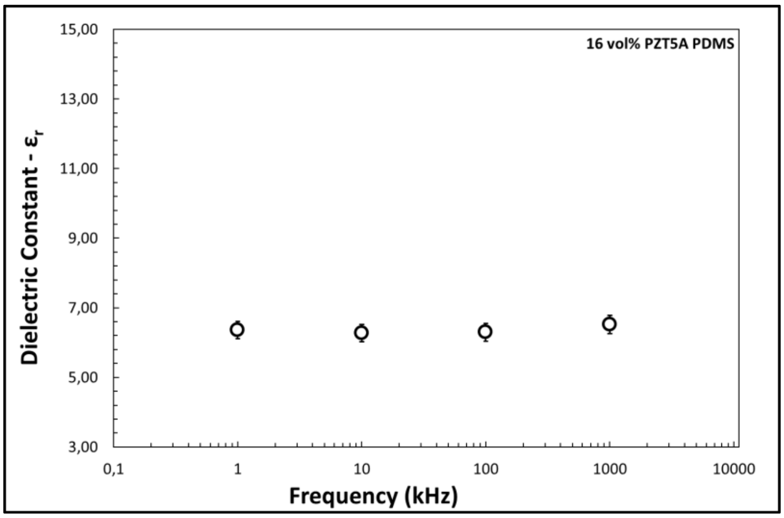

Figure 4.31: The dielectric constant vs frequency data of 16vol% PZT5A-PDMS composite.

To obtain a higher dielectric response from the composite, the volume fraction of the ceramic powder was increased to 16% and a slight increment was seen but not enough to be declared the best. Further addition of the powder was necessary to figure out the effect of the amount of powder.

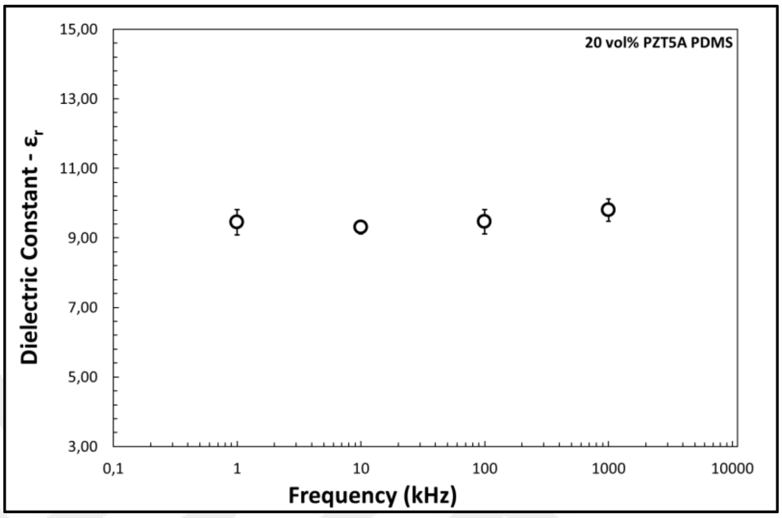

Figure 4.32: The dielectric constant vs frequency data of 20vol% PZT5A-PDMS composite.

Each time the dielectric constant was increased, the exact increment was just beginning, as seen from the graph. In these measurements, the values were in the range of 9-11. But according to further experiments, these values were not as high as the 30vol% powder-containing sample.

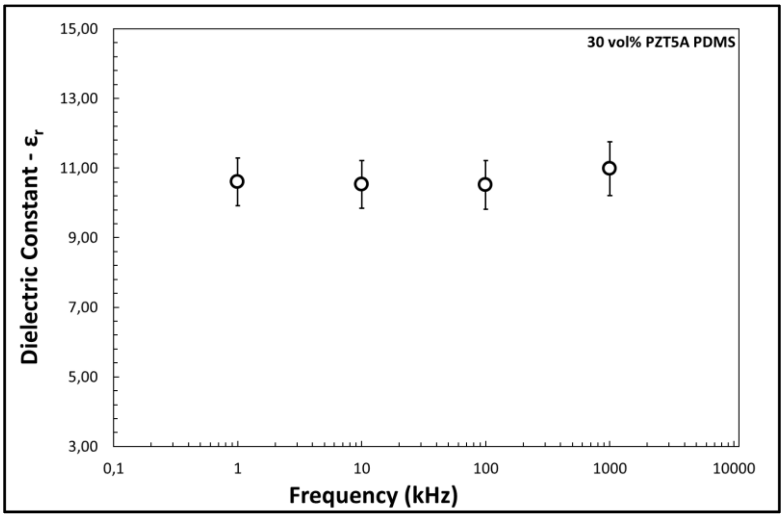

Figure 4.33: The dielectric constant vs frequency data of 30vol% PZT5A-PDMS composite.

The maximum volume fraction for the composite was 30vol%, extra additions made it harder to mix and polymeric matrices integrity was impossible. The nature of the polymer was sticky and the powder addition was limited to 30vol%. Nevertheless, the maximum dielectric constant was achieved and reached up to the 11-13 scale. The experience was gained after many trials with the PZT5A-PDMS. The next step was to change the polymer if there was a difference that might arise from the polymer. That was true because the nature of the polymer was different than PDMS. The PDMS was sticky and more viscous as compared to the PU itself. This allowed us to add an extra amount of ceramic powder and the maximum volume fraction was 54vol% which was far better than PDMS.

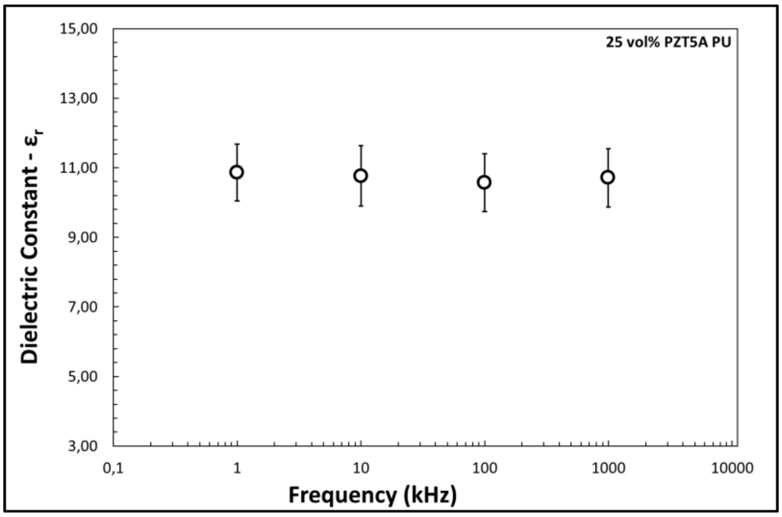

Figure 4.34: The dielectric constant vs frequency data of 25vol% PZT5A-PU composite.

The dielectric constant was the best result after the PDMS composite. The results were spectacular and these values were promising. The idea behind the 0-3 composites is to add the ceramic powder as much as it can take and mix thoroughly without mechanical integrity problems. After passing the limit dielectric constant values are expected to be reduced. Eventually, the mechanical failure and rupture were seen in the 54vol% PZT5A-PU as expected.

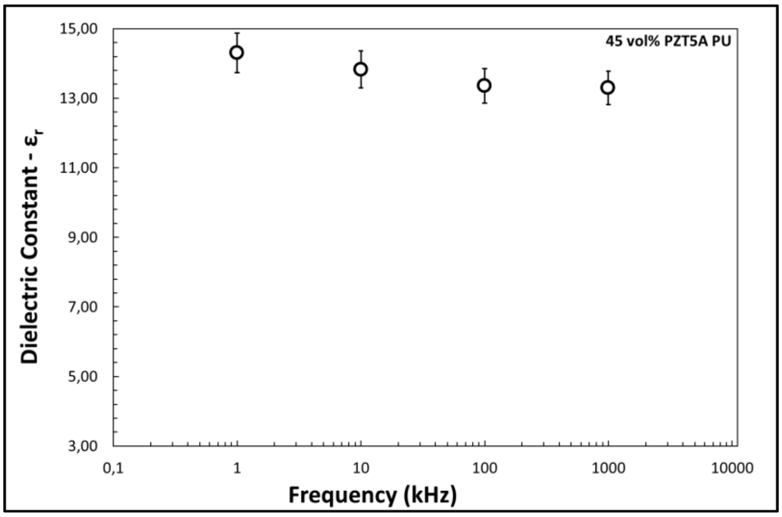

Figure 4.35: The dielectric constant vs frequency data of 45vol% PZT5A-PU composite.

The 45 vol% powder-containing composites had by far the best result that had been obtained from the previous experiments. For the first time, the dielectric constant values reached the scale of 13-15. This composite could be chosen as a device requiring higher dielectric constant values for capacitive technologies.

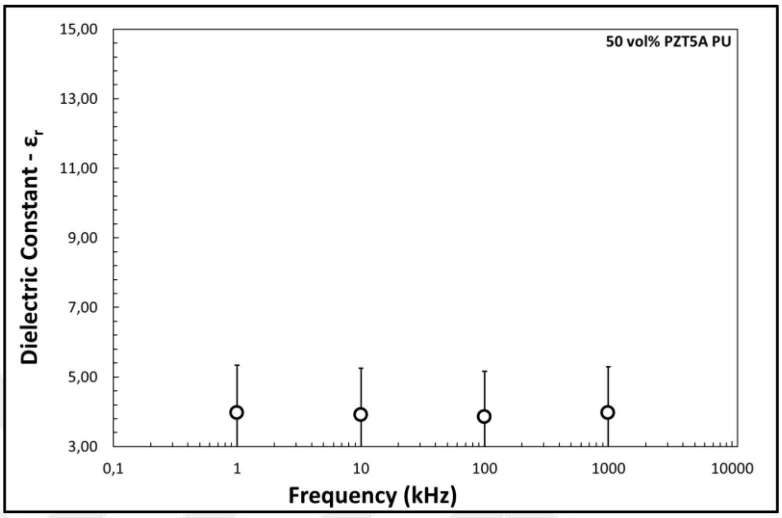

Figure 4.36: The dielectric constant vs frequency data of 50vol% PZT5A-PU composite.

50 vol% was the point where the constant of dielectric started to decrease dramatically. The results were inferior and far worse than the 13 vol% PZT5A-PDMS samples.

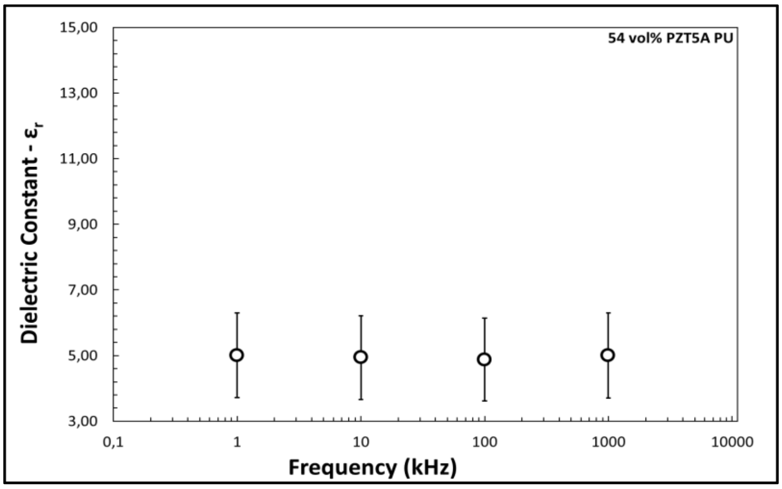

Figure 4.37: The dielectric constant vs frequency data of 54vol% PZT5A-PU composite.

The decrease in the value of the dielectric constant had reached the final stage where it can no longer reduce. The results after 50 vol% were not appropriate. The only explanation why the 50 vol% values were lower than the 54 vol% values is that the polymeric matrix was disrupted and the surface of the samples was no longer in contact properly. Finally, trying a new powder was necessary. In doing so, 67.5 PMN-PT and PU were preferred. PU was chosen because the maximum amount of the powder that can be mixed with the powder was only possible with PU.

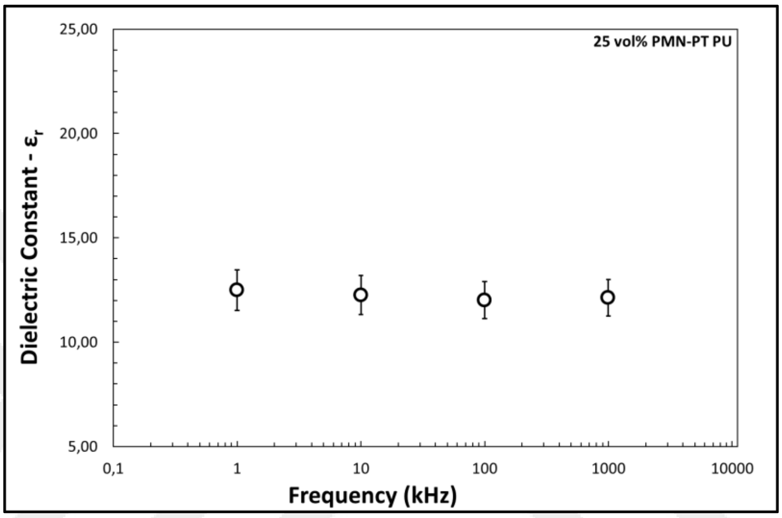

Figure 4.38: The dielectric constant vs frequency data of 25vol% PMN-PT-PU composite.

The characterization started with the 25vol% powder-containing sample. The dielectric constant was better than the 25 vol% counterparts.

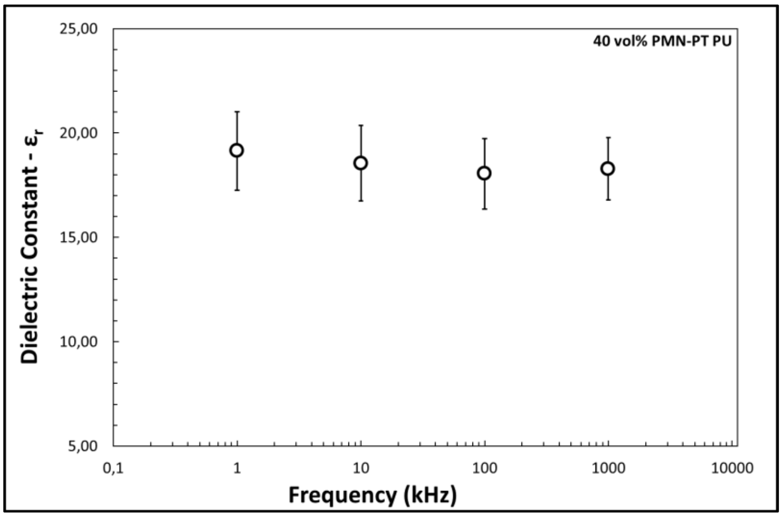

Figure 4.39: The dielectric constant vs frequency data of 40vol% PMN-PT-PU composite.

The change in the powder from PZT5A to PMN-PT was observable and the performance can be seen in the graph. By far, they were maximum dielectric constant values throughout the whole characterization.

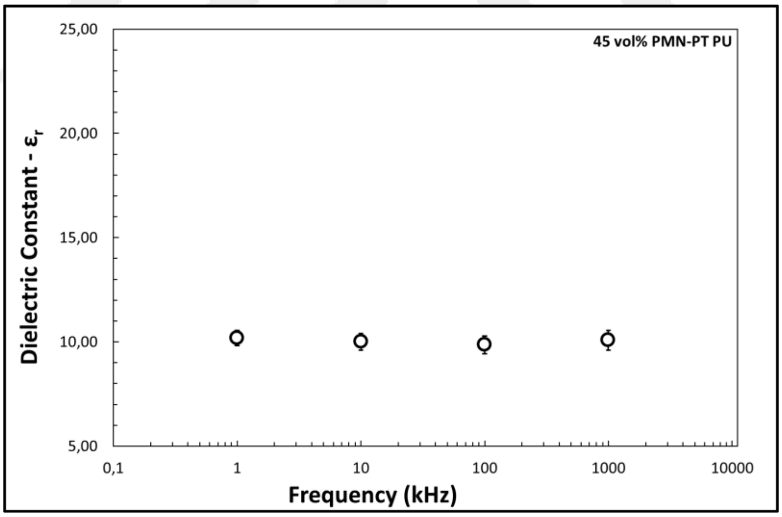

Figure 4.40: The dielectric constant vs frequency data of 45vol% PMN-PT-PU composite.

After the 40vol% volume fraction, the results decreased and 45 vol% powder-containing samples showed worse performance in comparison to 40 vol% samples.

4.3.2.2. Poling Efficiency of the Samples

As the name implies, 0-3 piezo active composites contain piezoelectric ceramic powders. Thus, poling efficiency of each sample is of utmost importance. The following study contains PZT5A-PU and PMN-PT-PU composites d_{33} measurements via the Berlin court method. PZT5A-PDMS could not be poled because the silver electrode had problems sticking onto the silicone surface. After many trials and literature studies, optimum poling conditions were set to 100kV/cm-60°C-40min for PZT5A-PU and PMN-PT-PU samples.

Table 4.7: PZT5A-PU samples with different volume fractions of powders under the same poling conditions.

Samples	d_{33}	Elektric Field(kV/cm)	Temperature (°C)	Time
25 vol%-1	8 pC/N	100	60	40 min
25 vol%-2	9 pC/N	100	60	40 min
25 vol%-3	10 pC/N	100	60	40 min
50 vol%-1	17pC/N	100	60	40 min
50 vol%-2	20pC/N	100	60	40 min
50 vol%-3	20pC/N	100	60	40 min
54 vol%-1	19pC/N	100	60	40 min
54 vol%-2	20pC/N	100	60	40 min
54 vol%-3	18pC/N	100	60	40 min

In this table, PZT5A-PU samples are shown. The effect of the amount of the powder can be seen, clearly. 25 vol% powder-containing samples had the lowest values of d_{33} because the composite was mostly made up of the polymer with a lesser amount of ceramic powder. Also, the polymeric matrix interferes with the interaction of ceramic particles and makes the domain wall movement harder. In the case of the 50 and 54 vol% ceramic powder containing samples, the amount was sufficient and the d_{33} values were close to each other. From these samples gained minimum d_{33} was 8pC/N and the maximum was 20pC/N. In a conclusion, if the composite is to be utilized in energy harvesting applications the d_{33} value of the sample has to be higher.

Table 4.8: PMN-PT-PU samples with different volume fractions of powders under the same poling conditions.

Samples	d_{33}	Electric Field(kV/cm)	Temperature (^{o}C)	Time
25 vol%-1	12 pC/N	100	60	40 min
25 vol%-2	11 pC/N	100	60	40 min
25 vol%-3	9 pC/N	100	60	40 min
40 vol%-1	14 pC/N	100	60	40 min
40 vol%-2	17 pC/N	100	60	40 min
40 vol%-3	15 pC/N	100	60	40 min

After the determination of the volume percentage of the PMN-PT composite samples, 25-40 vol% ceramic powder was sufficient to obtain the same performance as the PZT5A-PU composites. From these samples gained minimum d_{33} was 9pC/N and the maximum was 17pC/N. The type of ceramic powder has no observable effect on the poling because there is no significant result that points to that difference. The results are very close to each other and it concludes that the amount of the powder is no longer the first factor that affects the poling efficiency. Every material has a limit and in this case, the maximum volume percentage of the ceramic powder was 54 vol% and after the 40 vol%, there is no longer a great influence on the poling characteristics.

4.3.2.3. Hysteresis and Electrocaloric Characterization

The hysteresis measurements were conducted on PZT5A-PDMS, PMN-PT-PU, and PZT5A-PU samples to see how they behave under alternating electric fields concerning the frequency changes. The tests were performed under a 60kV/cm AC electric field for 5, 10, 15, and 20 ms. Samples did not show hysteretic behavior since they were made of the polymeric matrix. The response they gave was much like linear dielectric behavior. It is natural since polymers are dielectric materials. Even if, ferroelectric ceramic powders were introduced into the composite, it was not effective and did not cause any change other than slightly increasing the response to the electric field. But the response was not much only on the order of a maximum 0.2 of magnitude.

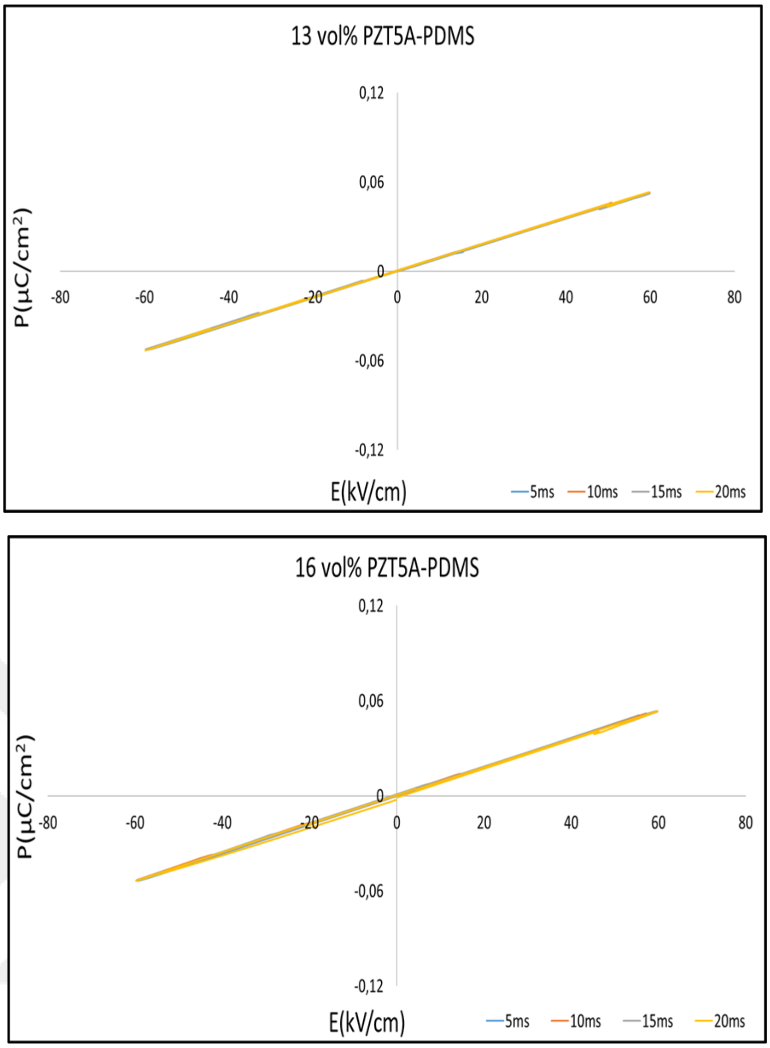

Figure 4.41: The hysteresis curves of both 13-16 vol% PZT5A-PDMS composites under 60kV/cm AC field and alternating frequencies.

The curves that belong to 13 and 16 vol% PZT5A-PDMS were similar to each other. The remnant polarization is approximately 0.06, which is very low as compared to ceramic pellets. It is hard to detect the coercive field which seems low since the graph does not show typical hysteresis behavior. The frequency dependency was almost the same without any distinctive changes because the frequencies are so close. The alternating electric field would be enough if these samples were bulk ceramic pellets but the polymer has a huge effect on the performance and restricts the pure potential of the ceramic powder.

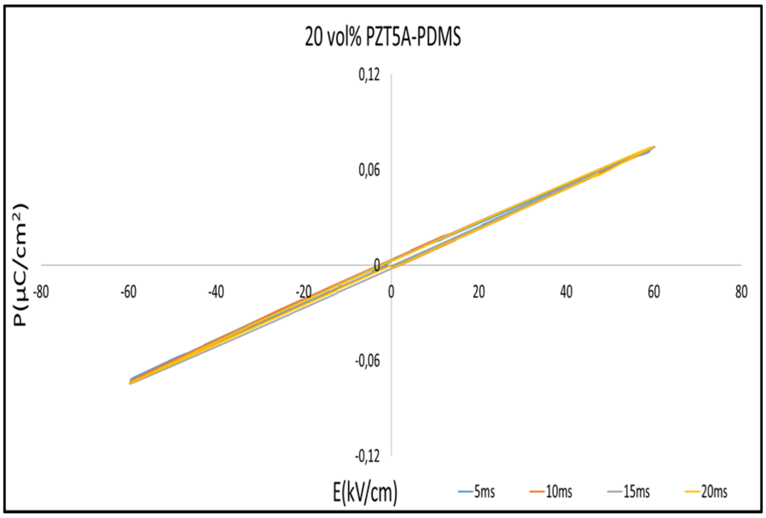

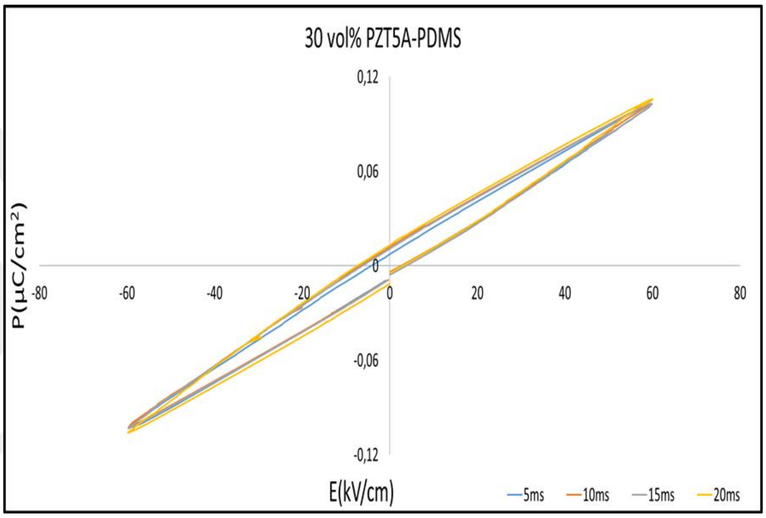

Figure 4.42: The hysteresis curves of both 20-30 vol% PZT5A-PDMS composites under 60kV/cm AC field and alternating frequencies.

As the particle content increases the remnant polarization increases. The 20 vol% sample is almost similar with a high remnant polarization value. There is a linear relationship between the particle content and remnant polarization. It has a positive effect on piezoelectric performance. The 30 vol% sample was the maximum limit where the remnant polarization had reached the approximate value of 0.12. Also, the leaky zone can be seen. Also, while the frequency dependency is negligible in 13, 16, and 20 vol% samples, this situation was changed for the 30 vol% composites. The leaky zone is caused by the frequency difference. When the frequency is higher, the area under the curve is bigger.

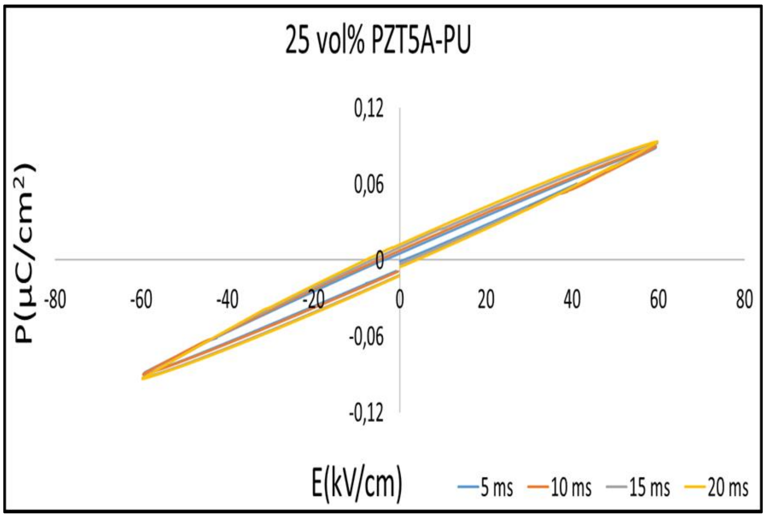

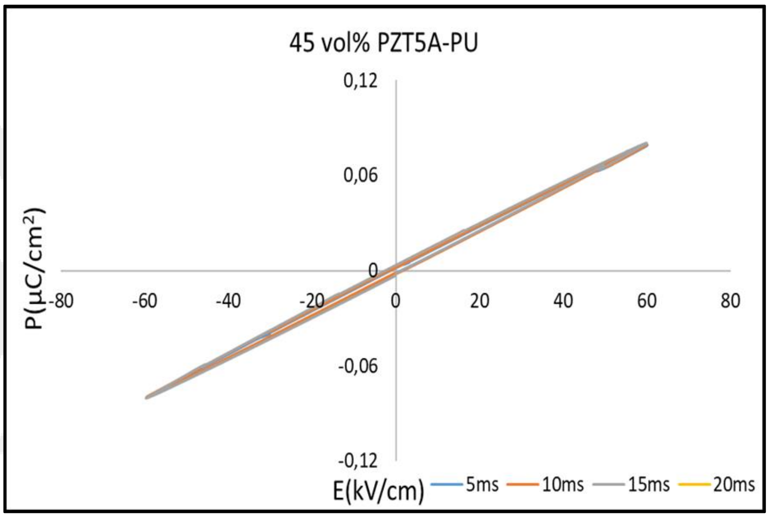

Figure 4.43: The hysteresis curves of both 25-45 vol% PZT5A-PU composites under 60kV/cm AC field and alternating frequencies.

Independent from the polymer matrix, the 25 vol% PZT5A-PU sample has a similar hysteresis graph as 30 vol% PZT5A-PDMS due to the amount of the ceramic powder being close to each other. Frequency dependency is as expected where the exposure to the AC field is higher the area under the curve gets broader. Strangely, 45 vol% PZT5A-PU does not show the same behavior the graph is tight and narrow almost hard to distinguish frequency from one another.

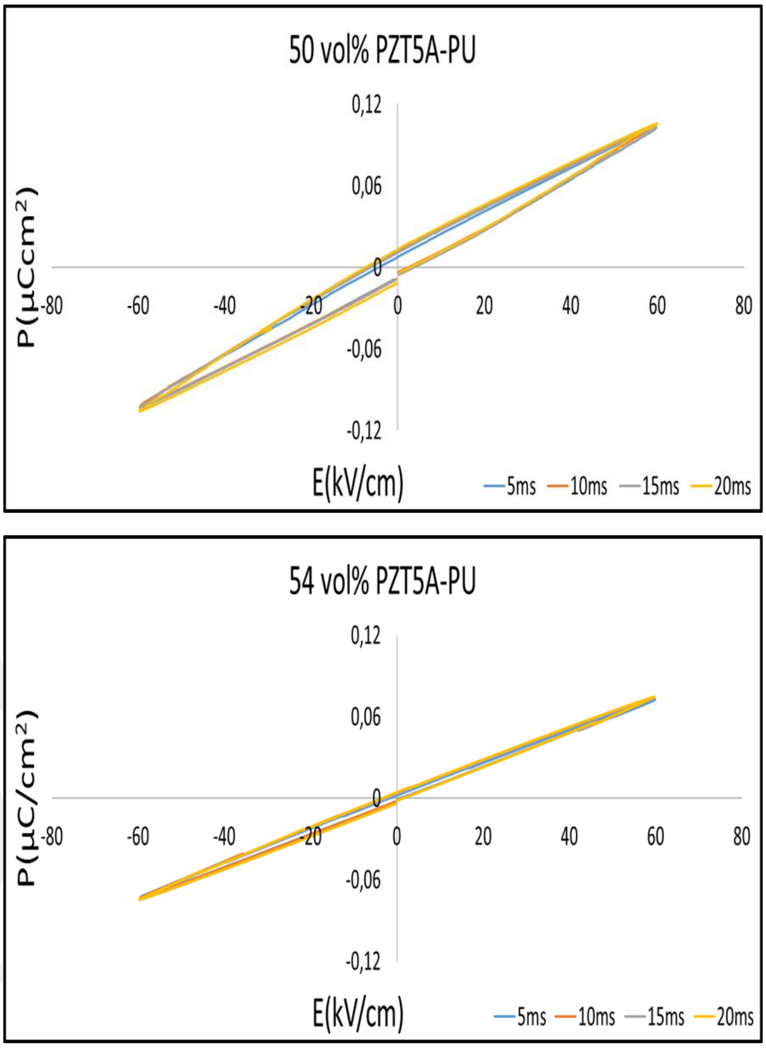

Figure 4.44: The hysteresis curves of both 50-54 vol% PZT5A-PU composites under 60kV/cm AC field and alternating frequencies.

As the powder content reaches its maximum limit the remnant polarization does not change much but the alignment of the curve changes from vertical to horizontal. But the horizontal alignment is because of the much higher powder ratio to the polymer. The mechanical integrity is no longer stable and the electrical properties get severely affected. In the case of the 54 vol% sample, the remnant polarization starts to decrease to the value of 0.06 which is quite small. In the last test case, the PMN-PT-PU composites were tried. There were no huge performance changes but the remnant polarization and the frequency dependencies were different other than PZT5A-PU and PZT5A-PDMS samples.

There was an improvement that was thought to be due to the ceramic powder characteristics. It was stated that the PMN-PT ceramic powder was better than PZT5A from an electrical point of view.

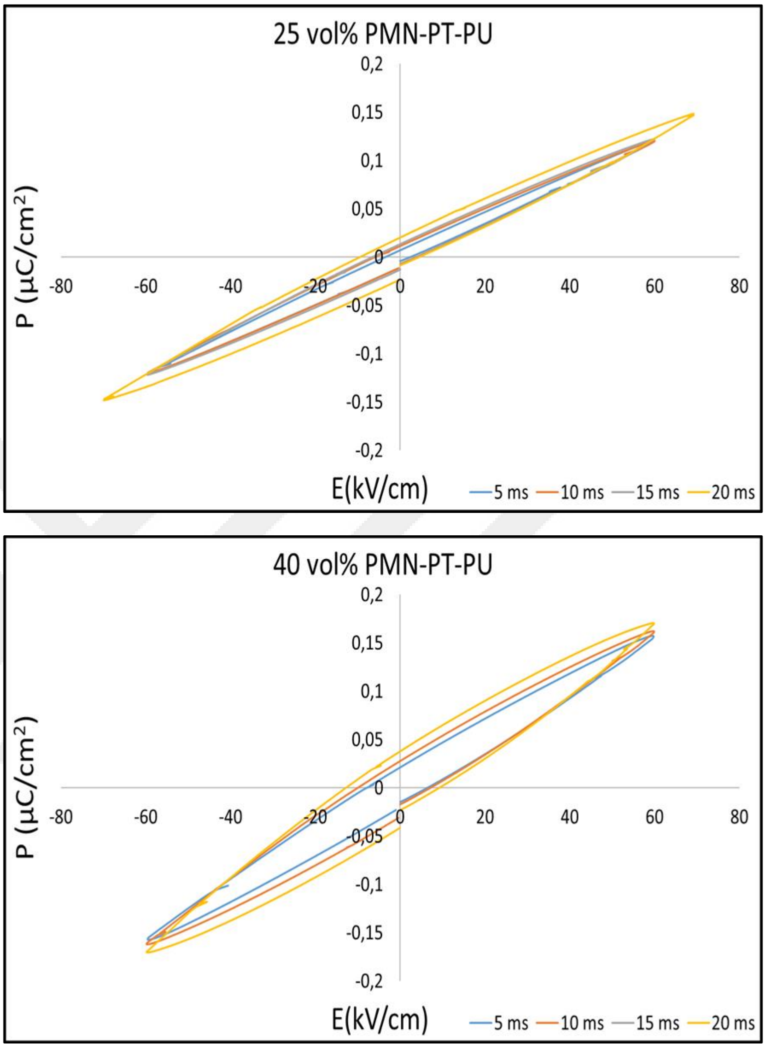

Figure 4.45: The hysteresis curves of both 25-40 vol% PMN-PT-PU composites under 60kV/cm AC field and alternating frequencies.

The graphs tell the difference quite perfectly. The frequency response of samples is unique and the remnant polarizations are higher than any other samples that were tested before. When the powder content is increased up to 40 vol% the area under the curve broadens and gets vertical.

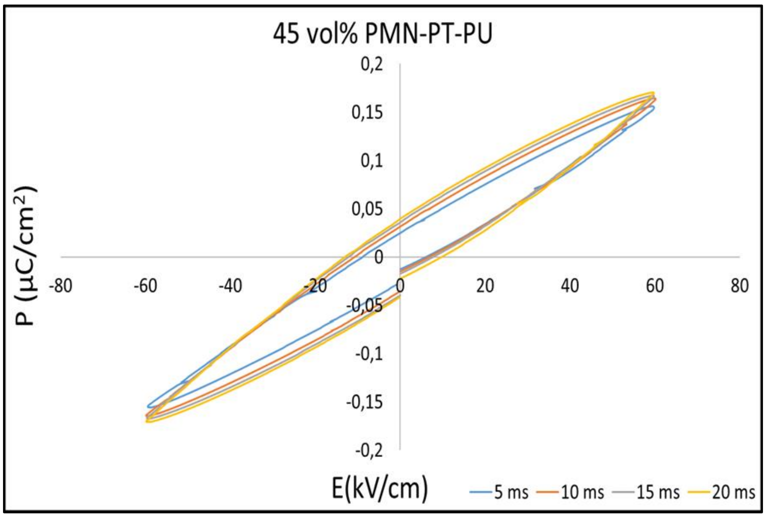

Figure 4.46: The hysteresis curve of 45 vol% PMN-PT-PU composite under 60kV/cm AC field and alternating frequencies.

40 and 45 vol% do not have much difference, tiny frequency behavior changes were recorded. It can be said that further addition of ceramic powder may affect the hysteresis curve in such a bad way or it may be useless to add any after that point. Also, there is another property of PMN-PT powder and it is called the electrocaloric response. PZT5A does not have this ability but PMN-PT is a famous candidate for certain applications. So, the test was highly required for PMN-PT-PU composites to record how they handle the situation or are there any differences as compared to the hysteresis behavior for given temperature changes. In doing so, the same volume percentages were used to tell the difference in hysteresis behavior. Tests were conducted for 10ms and under 60kV/cm AC field with changing temperatures from 30 to 60˚C.

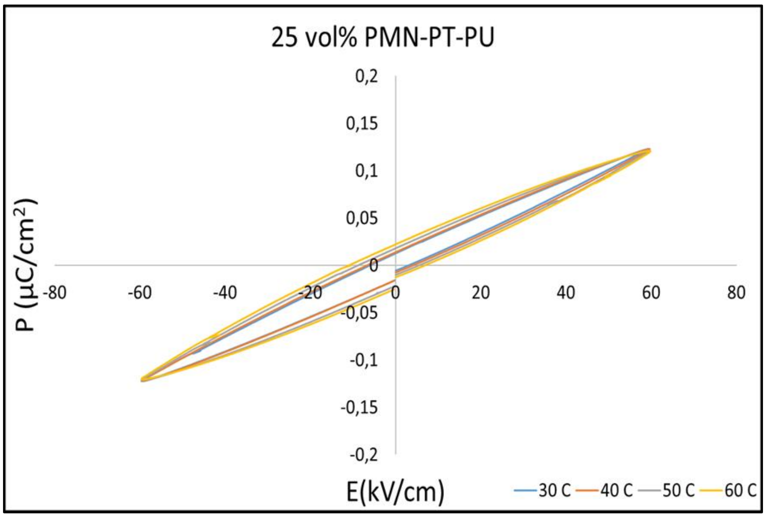

Figure 4.47: The electrocaloric hysteresis curves of 25vol% PMN-PT-PU composites under 60kV/cm AC field with different temperatures.

The remnant polarization increases concerning the powder to polymer ratio. Curves broaden as temperatures get higher and the curve's alignment is pretty similar to each other.

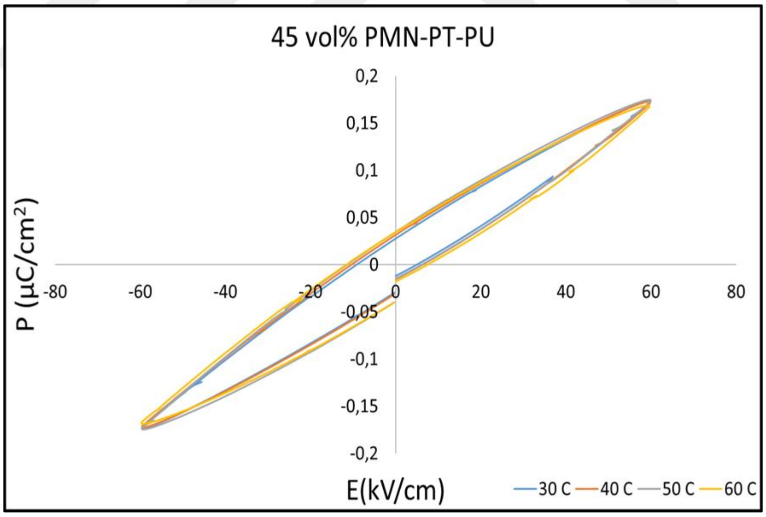

Figure 4.48: The electrocaloric hysteresis curve of 45 vol% PMN-PT-PU composite under 60kV/cm AC field with different temperatures.

The last graph belongs to the 45 vol% sample and the curve became a little bit vertical. The broadening rate was similar. The remnant polarization and temperature responses were similar to 25 vol% composite, as well.

4.3.2.4. An Application of Energy Harvesting via Composites

So far, many characterization methods have been applied to all types of composites, but there was no actual converse piezoelectricity. Energy harvesting was the last characterization method which was necessary to retrieve our composites' electrical performance fully. This technique basically allows us to record materials' activity under predefined loads, frequencies, and electric fields. If the composites are subjected to these three parameters we expect to see the voltage generation due to the converse piezoelectric effect. Before the tests specimens were carefully chosen according to their dielectric constant, tangent loss, mechanical integration, and d_{33} values. Below, tables are shown which point out the best candidates for energy harvesting procedure.

Table 4.9: d_{33} values of the chosen composites.

PZT5A-PU	d_{33} (pC/N)	PMN-PT-PU	d_{33} (pC/N)
PZ25-A	7	PM25-A	12
PZ25-B	8	PM25-B	11
PZ25-C	8	PM25-C	9
PZ45-A	19	PM40-A	14
PZ45-B	17	PM40-B	17
PZ45-C	17	PM40-C	15

The table belongs to PZT5A-PU and PMN-PT-PU composites. The volume percentages of powders were 25 and 45 vol% for PZT5A-PU along with 25 and 40 vol% for PMN-PT-PU, respectively. The powder fraction is the key element that is necessary if higher d_{33} values are to be reached. From the energy harvesting point of view, the purpose is similar. The higher the volume percentage of the ceramic powder in the composite the better. Additionally, d_{33} values are very close to each other for PZT5A-PU and PMN-PT-PU. After determining the piezoelectric coefficient of the composites, the next attempt was to find out which composites have higher dielectric constants. The final table contains information about mean values of the ε_r and $\tan\delta$ of samples at 1000Hz.

Table 4.10: ε_r and tanδ values of samples at 1000Hz.

PZT5A-PU	ε_r @ 1000Hz	tanδ @ 1000Hz	PMN-PT-PU	ε_r @ 1000Hz	tanδ @ 1000Hz
25 vol%	10,86	0,02773	25 vol%	12,48	0,01453
45 vol%	14,3	0,04347	40 vol%	19,14	0,03863

Dielectric constants of the samples were the highest as compared to other samples that were produced back at the beginning of the work. The increased volume percentage of the ceramic powder has an influence on the dielectric constant. While 45 vol% PMN-PT-PU has the largest among other samples, 25 vol% PZT5A-PU has the smallest dielectric constant. The tangent loss of each sample is very low, almost negligible.

Finally, the chosen composites are ready for energy harvesting. The tests were performed as follows:

- Three samples from each volume percentage were cut into specific dimensions.
- Electrode applications were performed by applying a silver epoxy layer onto sample-sized copper plates.
- Copper plates were stuck on both surfaces of each sample and by soldering a single filament of a cable on plates, the specimens were ready to be tested.

In these tests, 30Hz to 90Hz frequencies were chosen because samples exhibited their best under loads of 10 to 20g. A notation was made to name our samples professionally and to keep the names as simple as possible. For example, PZ25-A is the first sample of 25 vol% PZT5A-PU where PM40-C stands for the last sample of 40 vol% PMN-PT and, so on.

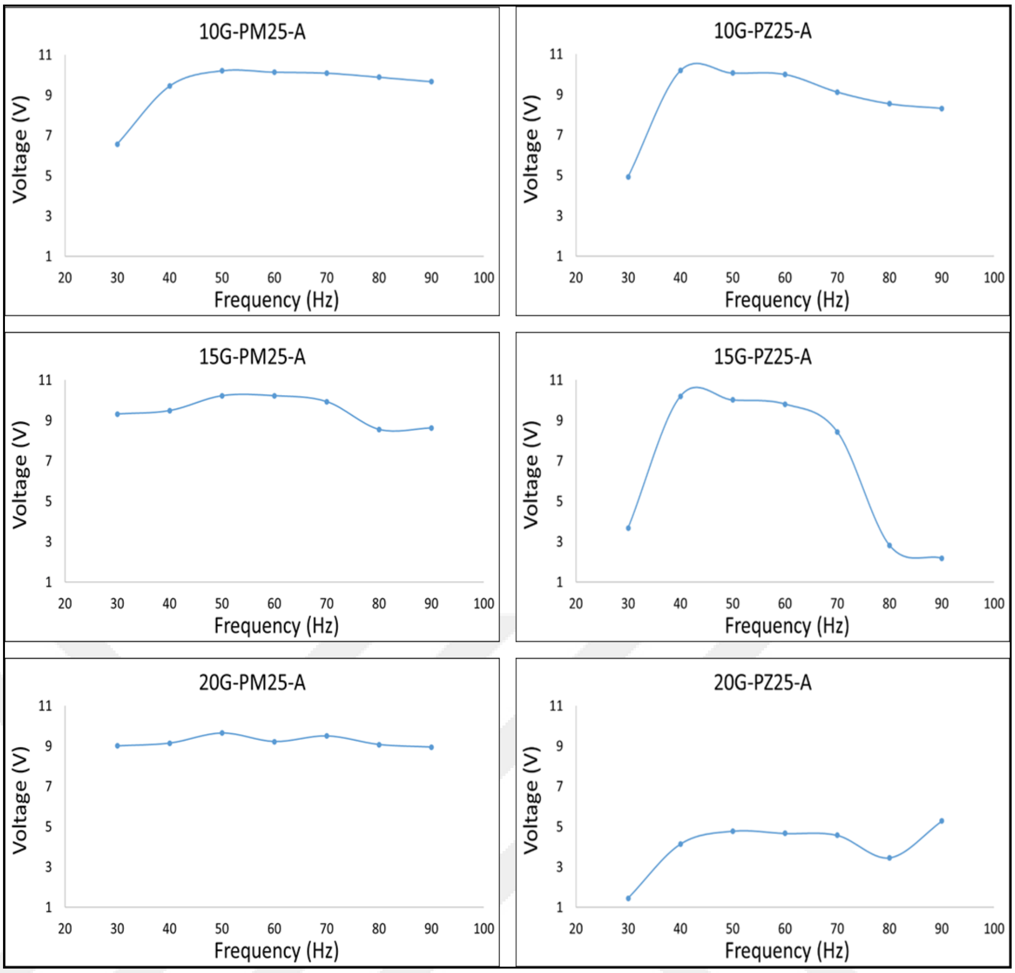

Figure 4.49: The comparison of the first samples of 25 vol% PZT5A-PU and PMN-PT-PU under different loads.

PMN-PT-PU composite generated higher voltage with respect to the PZT5A-PU. Each sample exhibited almost the same pattern of voltage. But PZT5A-PU showed the best performance between 40 and 70Hz frequencies. A fluctuation of voltage can be seen from PZT5A-PU which mght be due to the shaker and copper electrode. It appears that loads do not cause any specific voltage change for both composites, the pattern is very similar for each.

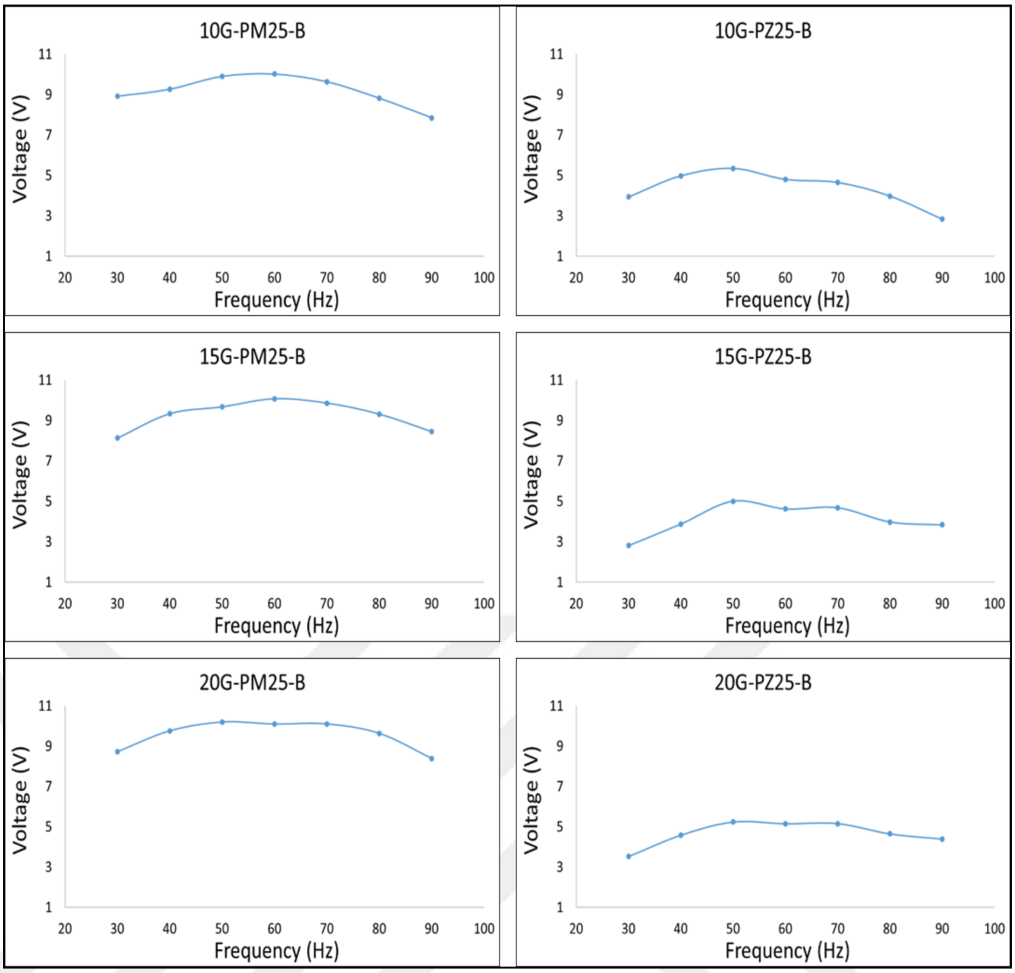

Figure 4.50: The comparison of the second samples of 25 vol% PZT5A-PU and PMN-PT-PU under different loads.

PM25-B generates the same voltage output as PM25-A. PZ25-B has more stable voltage values with respect to the first PZ25 sample. The change in the loads do not have any visible effect as in the previous case. The PMN-PT-PU is by far better at generating higher voltage outputs.

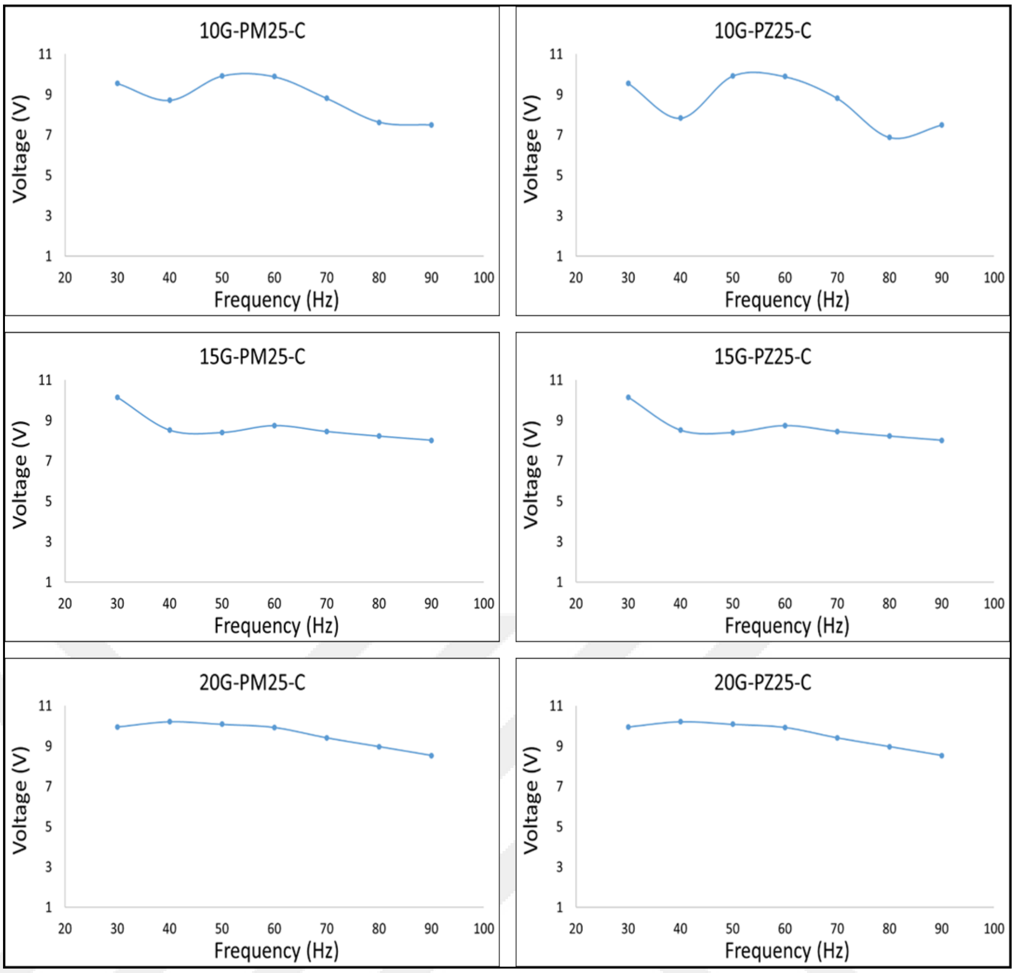

Figure 4.51: The comparison of the third samples of 25 vol% PZT5A-PU and PMN-PT-PU under different loads.

The comments that belong to the previous samples go for PM25-C. There is a huge difference in PZ25-C as compared to its counterparts. It shows a very similar and smooth performance which is closer to PM25. This difference may arise from the sample itself, electrode, or device.

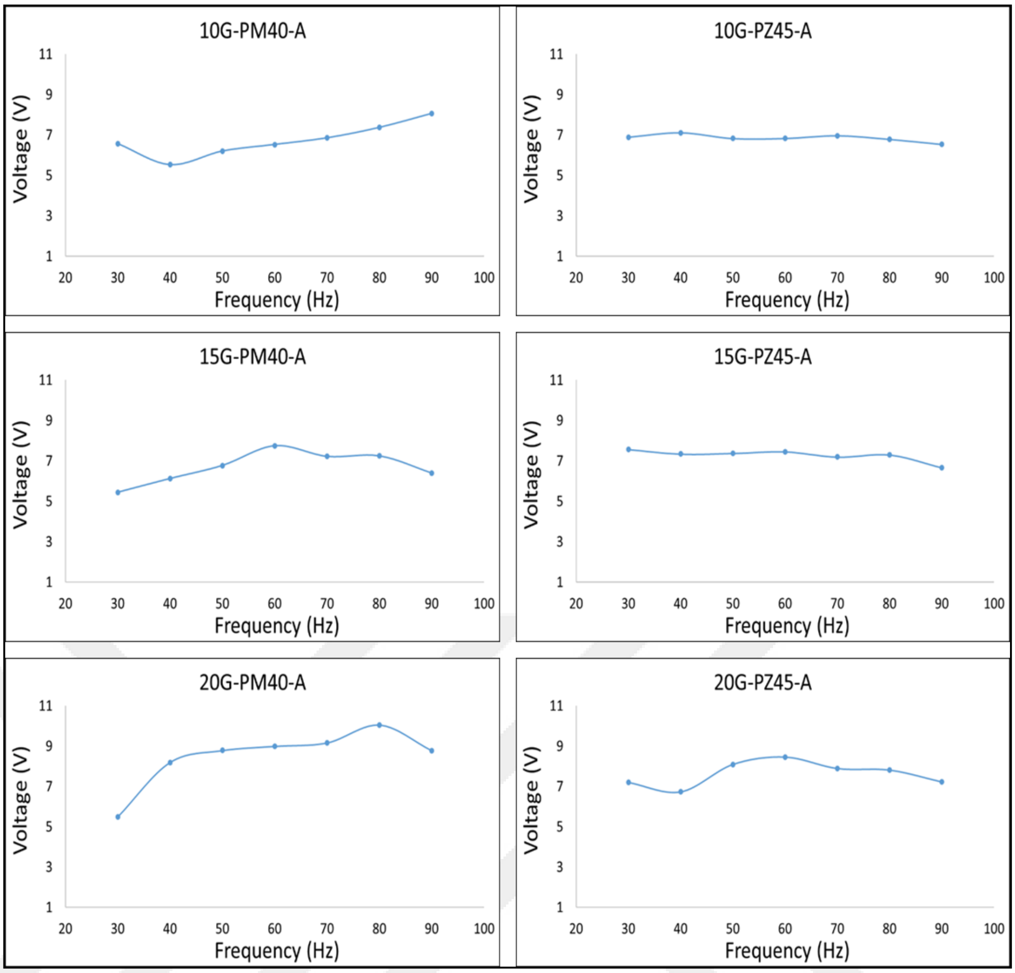

Figure 4.52: The comparison of the first samples of 45 vol% PZT5A-PU and 40 vol% PMN-PT-PU under different loads.

45 vol% PZT5A-PU and 40 vol% PMN-PT-PU exhibited similar performances. The voltage generated across the composites is in the range of 5-9V. There are smooth and stable curves under different loads. The generated voltages are relatively small in comparison to 25 vol% PMN-PT-PU and PZT5A-PU composites. These results might be caused by the microstructure of samples or related to the device.

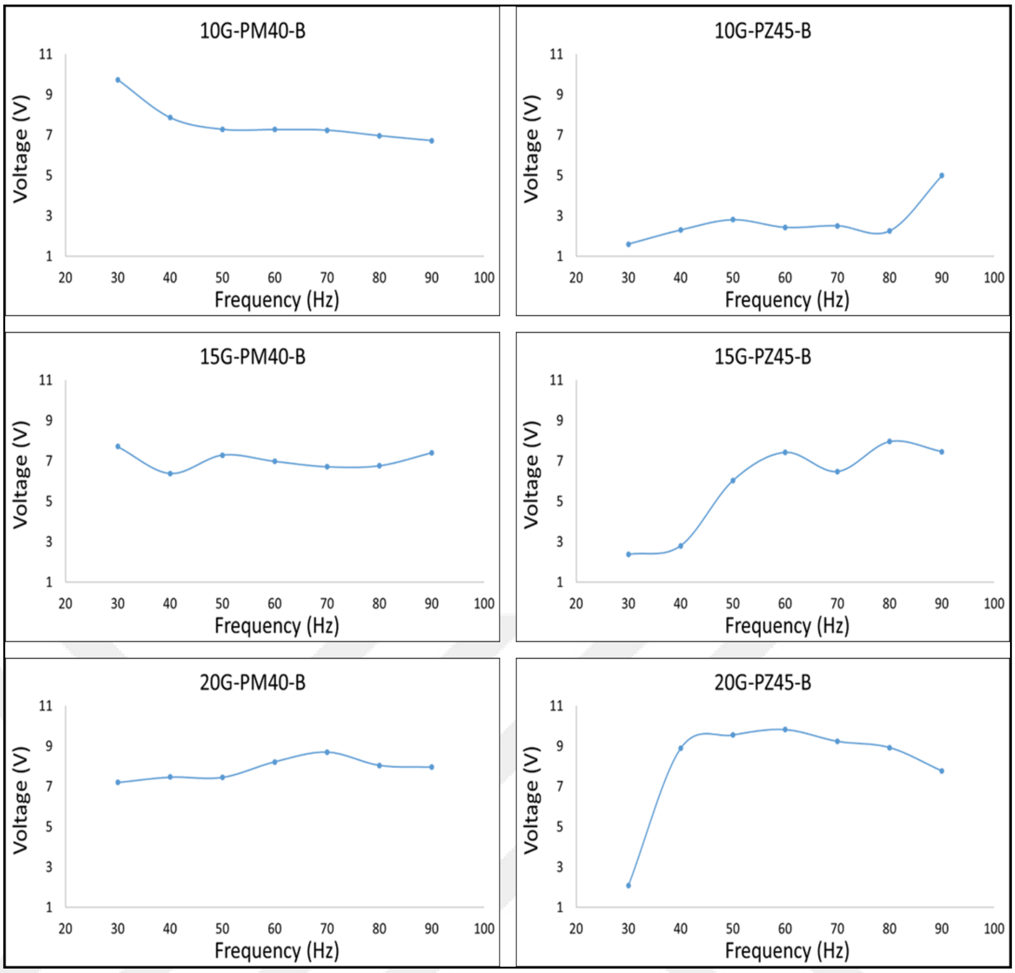

Figure 4.53: The comparison of the second samples of 45 vol% PZT5A-PU and 40 vol% PMN-PT-PU under different loads.

From the generated voltage point of view, there are similarities in PM40-B samples, but the results are complicated and it is not as easy to comment as in previous cases. (In our experiments, we used 3 different samples from each volume percentage because we expected mistakes as in the case of PZ45-B). With respect to these results, it can be said that PZT5A-PU samples showed incoherent results unlike any other. But, the results were not so bad and still as high as they could be.

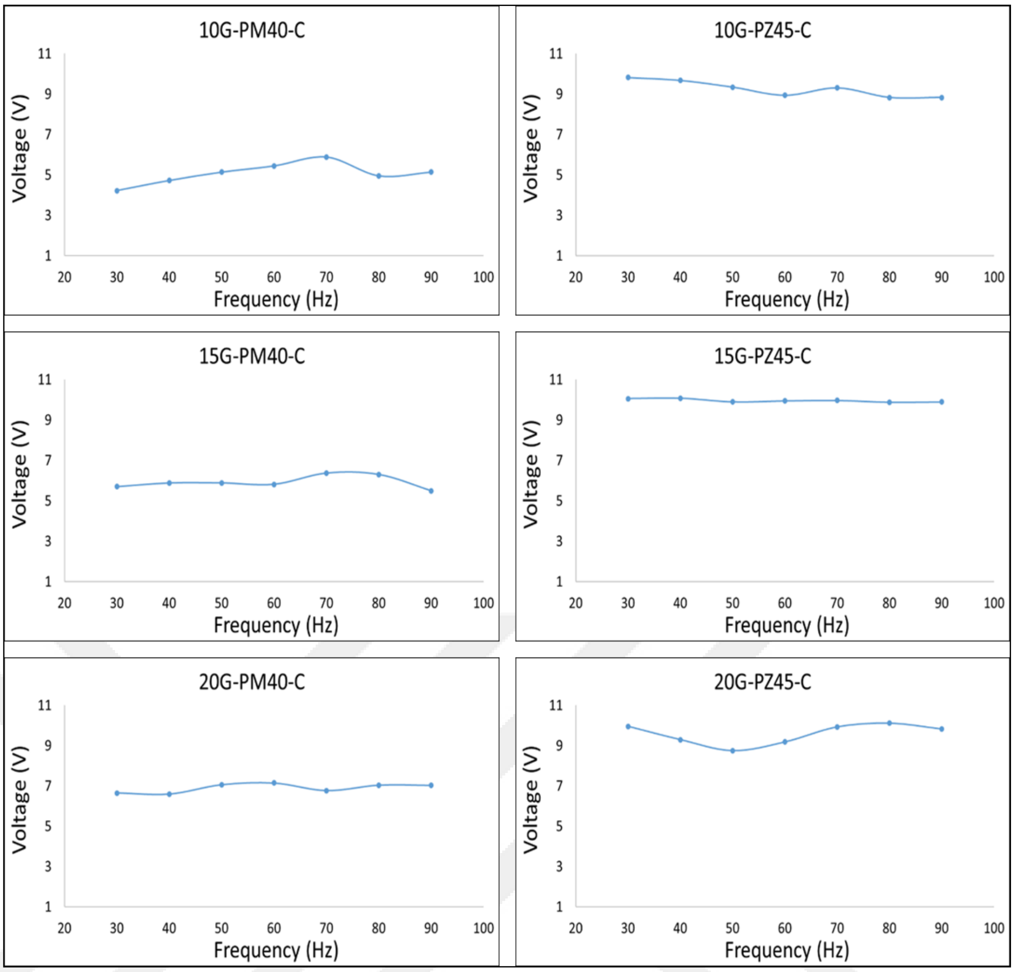

Figure 4.54: The comparison of the third samples of 45 vol% PZT5A-PU and 40 vol% PMN-PT-PU under different loads.

The results are coherent and proper which means that these samples are good at generating voltages without showing much difference between voltage values. Stability is important and sometimes maintaining it, could be hard. These data tell us that both composites have enough performance of converting mechanical energy into electrical energy. In a conclusion, the voltages were high enough to use these composites under different loads and frequencies as energy harvesters. Apart from device mistakes and microstructural effects, both the PZT5A-PU and PMN-PT-PU showed similar performance.

Finally, the next and last step of these experiments was to observe if any change would happen when pure PU was utilized instead of PZT5A and PMN-PT ceramic powders. In doing so 2 pure PU samples were prepared following the steps of the preparation of composites. The results are as follows:

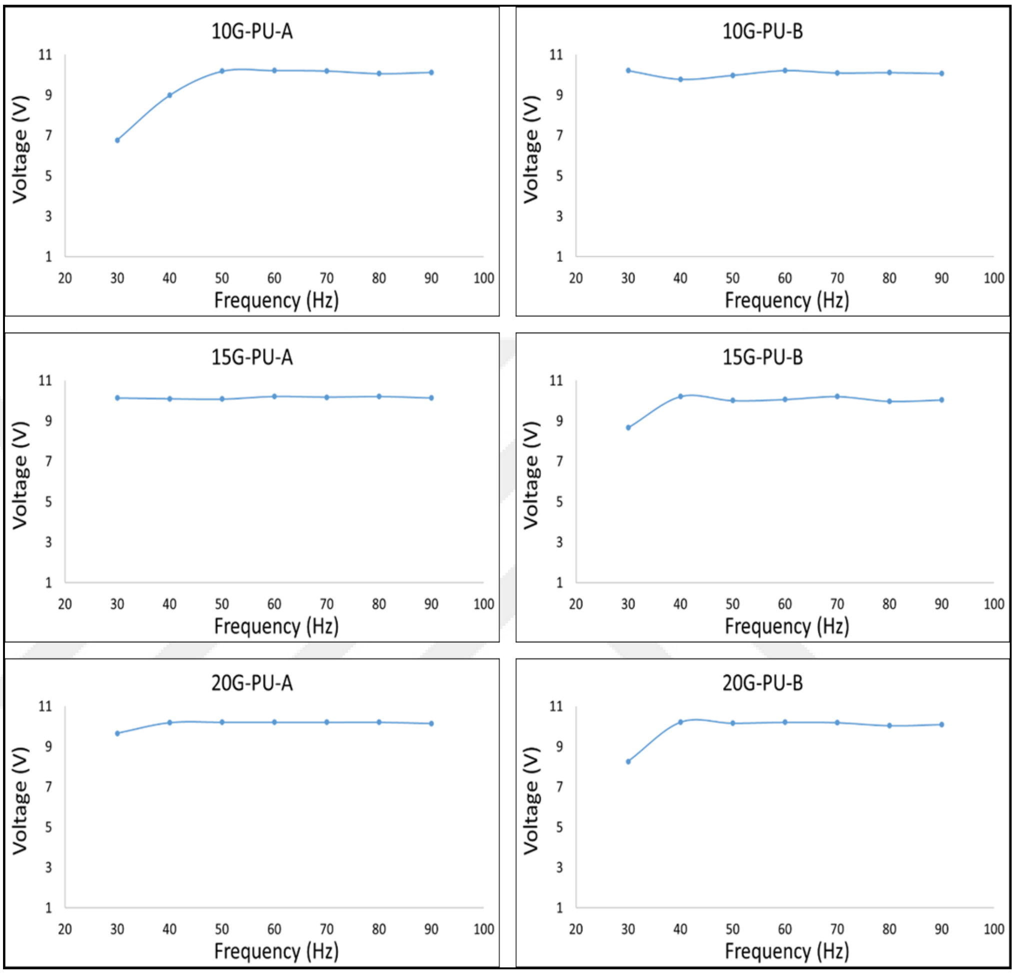

Figure 4.55: The comparison of the PU samples under different loads.

These charts may look weird since they have higher voltage values as much as the composites. At first glance, results are stable without fluctuations and voltages are between 8-11V. The results can be explained from the literature. Dielectric materials such as polymers are electrostrictive in nature. This phenomenon leads polymers to generate a voltage across their surfaces. PU is a polymer with the highest electrostrictive coefficient among others. The remarkable results of the study are thanks to that phenomenon.

5. CONCLUSION

At the end of the thesis, an overview of the steps of the thesis is necessary to see the full picture. To start with, the aim of our study was to discover 0-3 piezo composites and their electrical behavior. The study started with the inspection of PZT5A, 67.5PMN-PT piezoceramic powders characteristics by SEM and XRD. After that, various methods were applied to characterize 67.5PMN-PT bulk ceramics electrical properties such as admittance, dielectric, hysteresis-electrocaloric-strain, and d_{33} analyses. SEM and XRD assisted us to catch a glimpse of the microstructure.

At last, PZT5A-PDMS, PZT5A-PU, and PMN-PT-PU piezo composites were prepared and the same characterization methods were applied. The retrieved results showed us that, 0-3 piezo composite are incomparable to bulk ceramics from an electrical point of view. But, they are flexible and they can be shaped in the desired form, also their density is extremely low. If the amount of ceramic powder is at the limit where it does not cause mechanical integrity problems, electrical properties will be high enough to obtain better results. Generally, the results of PMN-PT and PZT5A were almost the same and sometimes incomparable to each other. Their piezoelectric properties were amazing. PZT5A-PDMS could not be tested enough because it would not be poled.

This thesis is offering a starting point if one wants to have a general overview of 0-3 piezo composites and forecast their studies. This thesis can be thought of as a guidebook for whom wants to learn about 0-3 piezo composites, characterization methods, results, and much more.

REFERENCES

[1] Fulay P., Lee J-K., (2017), "Electronic, Magnetic, and Optical Materials", 13: 978-1-4987-0169-3 (hardback), Taylor & Francis Group, LLC.

[2] Hoffmann, P. (2008), "Solid State Physics An Introduction", 978-3-527-40861-0,Wiley-VCH Verlag GmbH &Co GkaA.

[3] Moulson A.J., Herbert J.M., (2003), "Electroceramics", ISBN 0471-49747-9 (hardback), ISBN 0471 49748 7 (paperback), John Wiley & Sons Ltd.

[4] Vlassov S., Oras S., Antsov M., Sosnin I., Polyakov B., Shutka A., Dorogin L. M., (2018), "Adhesion and Mechanical Properties of PDMS-Based Materials Probed with AFM: A Review, Reviews on Advanced Materials Science", 56(1), 62–78.

[5] Sappati K. K., Bhadra S., (2020), "Flexible Piezoelectric 0–3 PZT-PDMS Thin Film for Tactile Sensing", IEEE Sensors Journal, 20(9), 4610–4617.

[6] Akindoyo J. O., Beg M. D. H., Ghazali S., Islam M. R., Jeyaratnam N., Yuvaraj A. R., (2016), "Polyurethane types, synthesis and applications – a review, RSC Advances", 6(115), 114453–114482.

[7] Salhi I., Belhora F., Hajjaji A., Seveyrat L., Jay J., Boughaleb Y., (2021), "PZT volume fraction's impact on electrical and thermal characterization of the piezoelectric composite PU/PZT, Sensors and Actuators A: Physical", 322, 112613.

[8] Yazdani A., Manesh H. D., Zebarjad S. M., (2021), "Piezoelectric properties and damping behavior of highly loaded PZT/polyurethane particulate composites", Ceramics International.

[9] Panda P. K., Sahoo B., (2015), "PZT to Lead Free Piezo Ceramics: A Review, Ferroelectrics", 474(1), 128–143.

[10] Zhang T.-F., Tang X.-G., Ge P.-Z., Liu Q.-X., & Jiang Y.-P., (2017), "Orientation related electrocaloric effect and dielectric phase transitions of relaxor PMN-PT single crystals, Ceramics International", 43(18), 16300–16305.

[11] Jiang H., Zou Y.K., Chen Q., Li K.K., Zhang R., and Wang Y., "Transparent Electro-Optic Ceramics and Devices", Boston Applied Technologies.

[12] Li J., Lin J., Li F., Zhang Y., Zhao G., Zhai J., Li S., (2019), "Temperature-insensitive large electrocaloric effect near room temperature in La3+-doped lead magnesium niobate-lead titanate ceramics", Ceramics International.

[13] Tang G., Yang B., Liu J., Xu B., Zhu H., Yang C., (2014), “Development of high performance piezoelectric d33 mode MEMS vibration energy harvester based on PMN-PT single crystal thick film”, Sensors and Actuators A: Physical, 205, 150–155.

[14] Berksoy-Yavuz A., Mensur-Alkoy, E., (2018), “Enhanced Soft Character of Crystallographically Textured Mn-Doped Binary 0.675[Pb(Mg1/3Nb2/3)O3]–0.325[PbTiO3] Ceramics”, Journal of Electronic Materials.

[15] Khanbareh H., Topolov V.Y, Bowen C.,R., (2019), “Piezo-Particulate Composites Manufacturing, Properties, Applications”, ISBN 978-3-030-19204-4 (eBook), Springer.

[16] Babu I., de With G., (2014), “Enhanced electromechanical properties of piezoelectric thin flexible films”, Composites Science and Technology, 104, 74–80.

[17] Quinsaat J. E. Q., de Wild T., Nüesch F. A., Damjanovic D., Krämer R., Schürch G., … Opris D. M., (2020), “Stretchable piezoelectric elastic composites for sensors and energy generators”, Composites Part B: Engineering, 108211.

[18] Salhi I., Belhora F., Hajjaji A., Seveyrat L., Jay J., Boughaleb, Y., (2021), “PZT volume fraction’s impact on electrical and thermal characterization of the piezoelectric composite PU/PZT”, Sensors and Actuators A: Physical, 322, 112613.

[19] Yazdani A., Manesh H. D., Zebarjad S. M., (2021), “Piezoelectric properties and damping behavior of highly loaded PZT/polyurethane particulate composites”, Ceramics International.

[20] Berksoy-Yavuz A., Mensur-Alkoy E., (2018), “Enhanced Soft Character of Crystallographically Textured Mn-Doped Binary 0.675[Pb(Mg1/3Nb2/3)O3]–0.325[PbTiO3] Ceramics”, Journal of Electronic Materials.

[21] Berksoy-Yavuz A., Mensur-Alkoy E., (2018), “Electrical properties and impedance spectroscopy of crystallographically textured 0.675 [Pb(Mg1/3Nb2/3)O3]-0.325 [PbTiO3] ceramics”, Journal of Materials Science: Materials in Electronics, 29(15), 13310–13320.

[22] Mathers A., Moon K.S., Yi J., (2009), “A Vibration-Based PMN-PT Energy Harvester”, IEEE Sensors Journal, Vol. 9, No. 7.

[23] Liu Y., Scott J. F., Dkhil B., (2016), “Direct and indirect measurements on electrocaloric effect: Recent developments and perspectives”, Applied Physics Reviews, 3(3), 031102.

BIOGRAPHY

He completed the material science and engineering program at Gebze Technical University in 2020 and earned his BSc degree. He started the MSc. program in his department with Ebru Menşur Alkoy and wrote his thesis about 'Development of Stretchable PZT-Based Elastic Composite Structures and Their Electromechanical Characterization' and published his article. He also took part in the AFOSR project with project number FA9550-18-1-0450, as project assistant.

APPENDICES

Appendix A:

International Workshop on Piezoelectric Materials and Applications in Actuators -2022 (IWPMA2022). Synthesize of Lead-Based 67.5PMN-32.5PT Ceramic Powder with Structural/Electrical Characterization of PMN-PT-PU Composites.

XI. Uluslararası Katılımlı Seramik Kongresi-2022 (SERKON). Kurşun Esaslı PZT5A Seramik Tozu ile Hazırlanmış PZT5A-PDMS ve PZT5A-PU Kompozitlerinin Yapısal ve Mekanik Karakterizasyonu.

Gebze Teknik Üniversitesi Lisansüstü Araştırmalar Sempozyumu- 2022. Kurşun Esaslı 67.5PMN-32.5PT Seramik Toz Sentezi ve PMN-PT-PU Kompozitlerinin Elektriksel Karakterizasyonu.